2021

CALCIUM SIGNALING AND ALG-2 IN THE REGULATION OF CONSTITUTIVE SECRETION

John Robert Sargeant

CALCIUM SIGNALING AND ALG-2 IN THE REGULATION OF CONSTITUTIVE SECRETION

By

John Robert Sargeant

Bachelor of Science, University of Utah, Salt Lake City, UT 84112

Dissertation
presented in partial fulfillment of the requirements

for the degree of

Doctor of Philosophy
in Cellular, Molecular, and Microbial Biology

The University of Montana Missoula, MT

November 2021

Scott Whittenburg, Graduate School Dean

Jesse Hay Division of Biological Sciences

Mark Grimes Division of Biological Sciences

Brent Ryckman Division of Biological Sciences

J. Stephen Lodmell Division of Biological Sciences

Michael Kavanaugh Division of Biological Sciences

TABLE OF CONTENTS

Calcium Signaling and ALG-2 in the Regulation of Constitutive Secretion

Chairperson: Jesse Hay

ABSTRACT

The constitutive secretory pathway influences almost every aspect of cellular function: generation and maintenance of subcellular compartments; cell growth and differentiation; and production and deposition of the extracellular matrix. Classically, constitutive trafficking was thought to be continuous and unregulated—in contrast to regulated secretion, wherein vesicles are stored intracellularly until a Ca^{2+} signal causes synchronous membrane fusion. However, early studies demonstrated a Ca^{2+} requirement for endosome fusion, ER to Golgi, and intra-Golgi trafficking, demonstrating that Ca^{2+} is a regulator of constitutive trafficking steps as well. In **Chapter 1,** I review recent evidence for Ca^{2+} involvement and the specific Ca^{2+}-related machinery implicated in trafficking events throughout the constitutive trafficking systems. Notably, I describe a series of Ca^{2+} pumps, channels, and Ca^{2+}-binding effector proteins—and their trafficking machinery targets—that together regulate the flux of cargo in response to genetic alterations or baseline and agonist-dependent Ca^{2+} signals. Of the intracellular constitutive trafficking steps, the ER-to-Golgi transport stage is the busiest, transporting up to one-third of all eukaryotic proteins. However, the potential regulation of these steps by Ca^{2+} signaling events has remained largely uncharacterized. Studies indicated that the PEF protein apoptosis-linked gene 2 (ALG-2) binds Sec31A at ER-exit-sites (ERES) in a Ca^{2+}-dependent manner, but *in vitro* and intact cell methodologies have been unable to adequately explain the specific role of ALG-2 and its PEF protein binding partner, peflin, in secretion. **Chapter 2** describes experimental procedures, while **Chapter 3** significantly expands upon the ALG-2-peflin regulatory machine. I find that although both proteins are fully dispensable for secretion, a peflin-ALG-2 heterocomplex binds to ERES via the ALG-2 subunit and confers a low, buffered transport rate, while peflin-lacking ALG-2 complexes can either enhance or inhibit transport of ER cargoes depending on expression level. This apparent bifurcated response indicates that PEF protein regulatory states may tune transport rates through expression level or Ca^{2+} changes, yet PEF proteins have never been observed regulating transport in response to Ca^{2+}. In **Chapter 4,** I examine the roles of ALG-2 and peflin in response to physiological Ca^{2+}-mobilizing agonists, and find that ALG-2 depresses ER export in epithelial NRK cells and enhances ER export in neuroendocrine PC12 cells. Furthermore, I find that Ca^{2+} signaling in the NRK cell model can produce opposing effects on secretion depending on signaling intensity and duration—phenomena that could contribute to cellular growth and intercellular communication following secretory increases or protection from excitotoxicity and infection following secretory decreases. Mechanistically, ALG-2-dependent depression of secretion involves decreased levels of the COPII outer shell and increased peflin targeting to ERES, while ALG-2-dependent enhancement of secretion involves increased COPII outer shell and decreased peflin at ERES. These data provide insights into how PEF protein dynamics affect secretion of important physiological cargoes such as collagen I and significantly impact ER stress.

ACKNOWEDGEMENTS

I would like to say thank you to:

Jesse Hay – for your patience and encouragement, for the long days you spent making this work possible. I am incredibly grateful to have had you as an advisor. Thank you for believing in me.

My Committee Members – for challenging me and giving your time to make me a better scientist.

Danette Seiler, Tucker Costain, Mariah Rayl and Colin Bingham – for your direct contributions to this work. It was a pleasure knowing each of you.

Aaron Held, and Lauren Foltz – for laughing at my jokes and sharing your lives. You were my steadfast colleagues; thank you for being with me for most of this journey.

Andrei Tabaraa – for our conversations, which kept me going more than you would think. You are my longest friend and ally.

My family – for your love and unwavering support.

Jessica Bailey, Lewis Sherer, Nagashree Avabhrath, John Kaiser and Carly Anderson – for our game nights, grand and small. You made my time here truly entertaining.

Nicholas Day – for being my first friend in graduate school. I will always remember the night we lost my car.

Valery Román-Cruz, Hannah Morgan, Adam Drobish, Pawel Halicki, Annie Adams, and Tom Pridham – for your support and friendship.

Doreen Gash and Bill Mclintock – for being wonderfully kind and hilarious landlords.

Julie and Marvin – for being excited to see me every day, Julie you are a genuine joy. In the case of Marvin, for biting me when I needed it.

Jill Burke – for making sure I never took myself too seriously.

All DBS staff members – for your aid in navigating the bureaucracy of graduate school.

Stephanie Pugmire – My best friend, my wife. There's no chance I'd be here without you.

ABBREVIATIONS	
Acronym	**Description**
Ca^{2+}	Calcium
CADEE	Calcium-activated depression of ER export
CAEEE	Calcium-activated enhancement of ER export
CaM	Calmodulin
ECM	Extracellular matrix
ER	Endoplasmic Reticulum
ERES	ER-exit-sites
IP3	Inositol trisphosphate
KD	Knockdown
NRK	Normal rat kidney cells
OE	Overexpression
PAEC	Porcine aortic endothelial cell
PEF	Penta-EF-hand structural motif/protein family
ROI	Region of interest
SERCA	Sarcoendoplasmic reticulum calcium transport ATPase
TCF	Total cell florescence
UPR	Unfolded protein response

AGONISTS/DRUGS USED	
Agonist/Drug	**Description**
A-beta peptide	Destabilizes intracellular calcium homeostasis
A23187	Divalent calcium ionophore
AP21998	Conditional aggregation domain inhibitor
ATP	Agonist for P2X ligand gates channels and P2Y GPCRs
BAPTA	Cell permeant chelator, highly selective for calcium
BHQ	SERCA inhibitor
Bradykinin (BK)	Inflammation related agonist for B1 & B2 GPCRs
Brefeldin A (BFA)	ER-to-Golgi transport inhibitor
EGTA	Cell permeant chelator, highly selective for calcium. Slower than BAPTA
Histamine	Inflammation related agonist for H1-H4 GPCRs
Ionomycin	Divalent calcium ionophore
Thapsigargin (TG)	Non-completive SERCA inhibitor

LIST OF FIGURES

LIST OF TABLES

CHAPTER 1:

CA^{2+} REGULATION OF CONSTITUTIVE VESICLE TRAFFICKING

(This chapter has been accepted for publication in F1000 Research and is undergoing final edits)

1. 1 INTRODUCTION

Eukaryotic cells are in a constant state of membrane maintenance, renewal, and expansion, accomplished by an interwoven web of constitutive vesicle trafficking pathways connecting the ER, Golgi, plasma membrane and the endolysosomal system (Figure 1). Classically, constitutive secretion is thought to be continuous and unregulated. This contrasts with the highly controlled, regulated secretory pathway in which proteins stored in intracellular granules are released en masse in response to external factors or signals. However, constitutive secretion is also regulated. By way of example, during mitosis in mammalian cells, the Golgi is fragmented for partitioning into progeny cells. This transition from S to M phase necessitates that most, if not all, membrane trafficking pathways are temporarily shut down, only to be resumed later during cytokinesis (Lowe et al., 1998). Alternatively, the differentiation of B cells to plasma cells requires a marked increase in secretory capacity, driven in part by sequential waves of protein expression (Van Anken et al., 2003). However, there is still much to learn about the regulation of constitutive secretion. The milieu of ions, lipids, and proteins that constitutive trafficking externalizes, degrades, or delivers to various organelles affects nearly every aspect of cell metabolism, making dynamic regulation of these pathways of great significance to biomedical research.

While Ca^{2+} is a required factor in evoked exocytosis within the regulated secretory pathway, Ca^{2+} has also been thought to play a role as a regulator of constitutive secretion. An often-cited study showed that VTC-to-Golgi and Golgi-to-ER retrograde trafficking was inhibited by the fast Ca^{2+} chelator 1,2- bis(2-aminophenoxy)ethane-N,N,N',N'-tetraacetic acid (BAPTA), but not the slower chelator of comparable Ca^{2+} affinity, ethylene glycol-bis(2-aminoethylether)-N,N,N',N'-tetraacetic acid (EGTA) (Chen et al., 2002). In addition to illustrating a role for calcium in constitutive secretion, this study also implied tight spatial coupling of the vesicular fusion machinery and Ca^{2+}, wherein the putative fusion site is close to the Ca^{2+} release site. Further evidence continued to mount with various groups implicating Ca^{2+} in the fusion of yeast vacuoles (Peters & Mayer, 1998), the heterotypic fusion of late endosomes with lysosomes, or the reformation of lysosomes from hybrid compartments (Pryor et al., 2000).

In this chapter, I discuss multiple proteins that appear to regulate constitutive trafficking and have direct or indirect ties to Ca^{2+}, focusing mainly on studies after 2007 when my lab published a review on the same topic (Hay, 2007). Prominent example studies from the text are also briefly summarized in Tables 1-3. Organized by the organelle wherein the primary secretory effects spatially occur I discuss a variety of secretory effectors that modulate secretion via their capacity to bind Ca^{2+}. In addition to these Ca^{2+} binding effectors, what has been most obvious in recent years is the rise in the number of calcium pumps or channels that have been found to affect constitutive trafficking. Channels mobilize Ca^{2+} and create a dynamic Ca^{2+} landscape in the cytoplasm (Figure 2), but still must act upstream of Ca^{2+} sensors and trafficking machinery effectors to influence trafficking. Pumps, on the other hand, tend to affect trafficking on the luminal side by providing sufficiently high Ca^{2+} environments for Ca^{2+}-dependent sorting or retention processes. Some of the examples that discuss, such as certain TRP channel family members of non-selective ion channels, have been implicated in secretion changes yet so far have not been matched up with Ca^{2+} sensors that could translate a Ca^{2+} flux into changes in secretion. This may mean that the critical Ca^{2+}-binding effectors or channel binding partners have not been defined yet. Ultimately, this chapter will serve as a broad review of recent evidence in Ca^{2+} involvement and the specific Ca^{2+}-related machinery implicated in trafficking events throughout the constitutive secretory and endosomal systems.

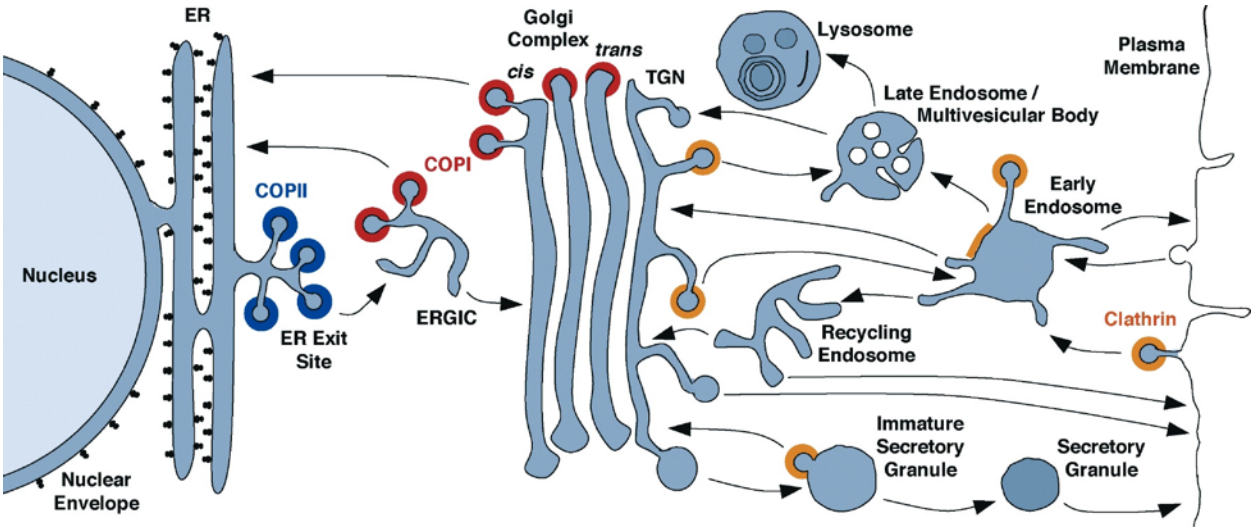

Figure 1: Intracellular vesicle trafficking pathways in the endomembrane system. This diagram depicts critical features of the secretory and endolysosomal pathway. Black arrows indicate vesicle trafficking steps for cargoes. Colored rings indicate the presence of vesicle coats that assist in secretory trafficking: COPII (blue), COP1 (red), and clathirin (orange).

Reproduced with permission from Figure 1, Bonifacino, J. S., & Glick, B. S. (2004). The Mechanisms of Vesicle Budding and Fusion. Cell, 116(2), 153–166.

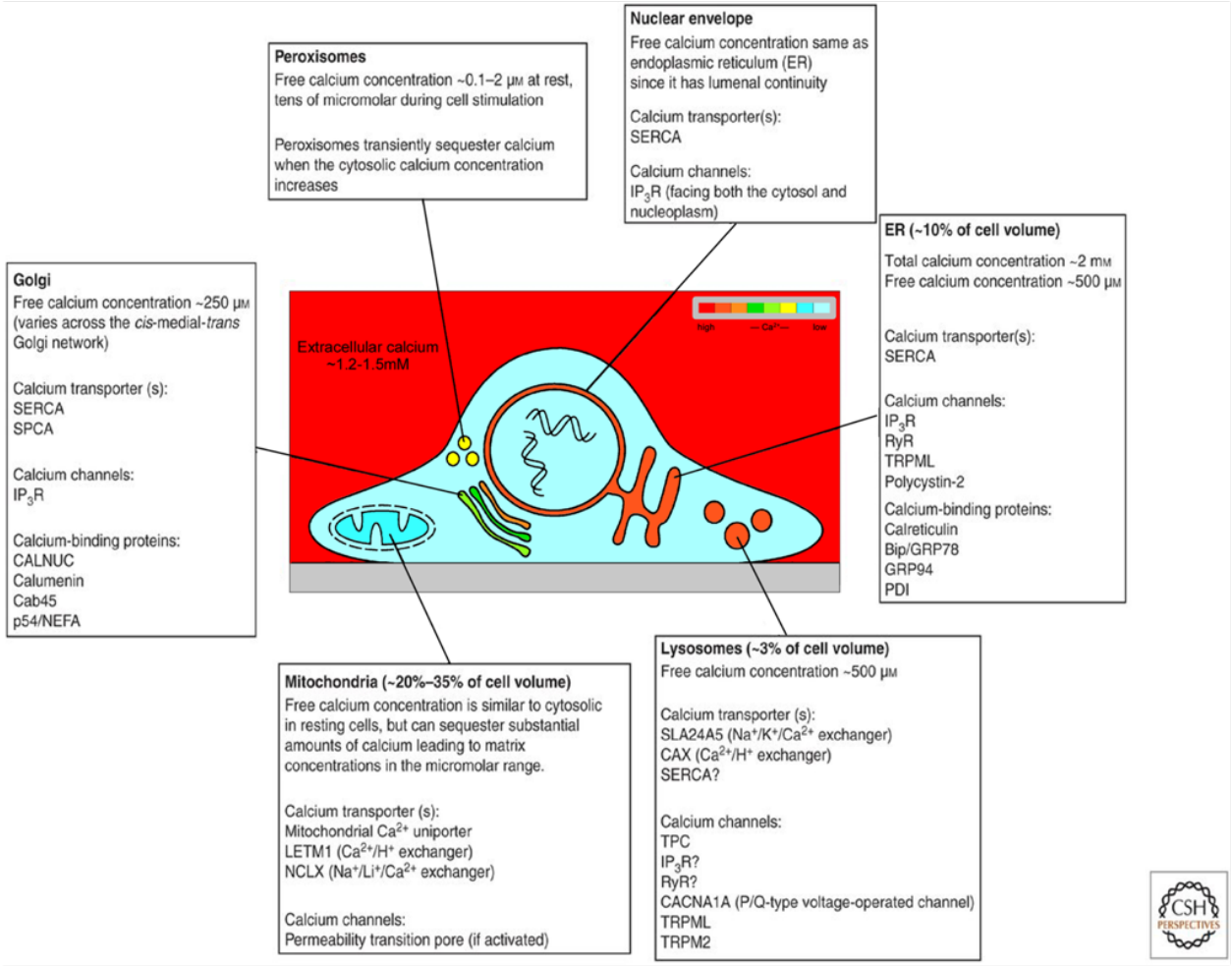

Figure 2: Ca^{2+} sequestering organelles. Infographic detailing Ca^{2+} and Ca^{2+} machinery in intracellular compartments. Cellular Ca^{2+} is stored within several organelles through the action of Ca^{2+} pumps and exchangers. Organelle Ca^{2+} stores, in part, provide a beneficial trafficking environment and imbue organelles with the ability to generate discrete Ca^{2+} signals. Color scale indicates free Ca^{2+} concentration. SERCA, sarcoendoplasmic reticulum Ca^{2+}-ATPase; SPCA, Golgi/secretory pathway Ca^{2+}-ATPase; TPC, two-pore channel; IP3R, inositol 1,4,5-trisphosphate receptor; RyR, ryanodine receptor.

Adapted with permission from Figure 2, Bootman, M. D., & Bultynck, G. (2020). Fundamentals of cellular calcium signaling: A primer. Cold Spring Harb. Perspect. Biol., 12(1).

1.2 CALCIUM AND SECRETION

1.2.1 Endoplasmic Reticulum

Free Luminal Ca^{2+} ~500 µM (Bootman & Bultynck, 2020)

The endoplasmic reticulum (ER) folds and assembles newly synthesized proteins destined for trafficking via the secretory pathway, dysregulation of which leads to the UPR, reviewed elsewhere (Chakrabarti et al., 2011; Hetz et al., 2020) but not covered in this chapter except regarding Ca^{2+}-specific observations. In addition, the ER acts as a principal Ca^{2+} store within cells (Figure 2) facilitating Ca^{2+} signals in the cytosol, or multiple organelles via ER-organelle contact sites (Bootman & Bultynck, 2020; Burgoyne et al., 2015; Patel, 2019). In this section, I describe effects on secretion via ER-localized Ca^{2+} channels or their cytosolic effectors, and finally, I note ways in which luminal Ca^{2+} has been described to affect secretion.

Originally studied for its role in polycystic kidney disease, TRPP2 was suggested to have a role in altered ECM integrity. TRPP2 localizes, in part, to the ER membrane and like all TRP family members functions as a cation channel, principally directing the flow of Ca^{2+} into the cytosol. TRPP2 KD caused enhanced accumulation of type II collagen in the zebrafish notochord sheath (Le Corre et al., 2014), a trait reversed by expression of an ER-retained mutant of TRPP2 (X. Fu et al., 2008). This implied that TRPP2 activity in the ER could directly or indirectly affect collagen translation or vesicle trafficking. Indeed, TRPP2 depletion led to an increase in the mRNAs of inner COPII coat components Sec23B, Sec24C, and Sec24D (Le Corre et al., 2014), factors predicted to increase rates of ER-to-Golgi trafficking. It is unclear whether TRPP2 depletion itself increased secretion since the increased coat expression could also be a compensation mechanism for loss of TRPP2. However, COPII coat protein KD or chemical inhibition of ER-to-Golgi transport via low-level brefeldin A (BFA) treatment were sufficient to reverse the enhanced collagen and aberrant morphology in the notochord sheath. This implies that the secretory pathway was an important target for manifesting the ECM abnormalities. Ultimately, in this study, a specific effector mechanism was not implicated nor were Ca^{2+} dynamics monitored, but previous work had shown that TRPP2 significantly decreased ER Ca^{2+} (Wegierski et al., 2009), and increased ER agonist-stimulated release of Ca^{2+} (Sammels et al.,

2010) or reduced it in the case of mutant TRPP2 (Aguiari et al., 2004). These findings are reminiscent of another study focusing on a separate ER Ca^{2+} channel, inositol trisphosphate receptor-3 (IP3R-3). Held et al. showed that IP3R3 depletion produced an increase in ER-to-Golgi trafficking of a VSV-G transmembrane cargo (Held et al., 2021). It's possible that the two channels, IP3R and TRPP2, may regulate trafficking via the same mechanism, possibly mediated in part by TRPP2's demonstrated ability to bind to IP3R and potentiate its activity (Sammels et al., 2010).

Changes in local Ca^{2+} concentrations, mediated by changes in channel expression, as described above, or signaling events, likely affect secretion via direct binding/unbinding of Ca^{2+} to effectors. At the ER, no effectors may be more important than the PEF protein family. Common features of this family include: (i) five serial Ca^{2+}-binding EF-hand motifs; (ii) capacity to dimerize via EF-hand domains; and (iii) Ca^{2+}-dependent effector binding, often at membrane sites. Of this family, the most studied is apoptosis-linked gene-2 (ALG-2). ALG-2 has more than 20 Ca^{2+}-dependent binding partners and two binding sites (ABM-1 and ABM-2) which can bind up to two proteins in response to Ca^{2+}-induced conformational changes (Maki et al., 2002). Furthermore, in mammalian cells, ALG-2 is also present in two splice forms that have a different spectrum of interaction partners (Tarabykina et al., 2000). Early research on ALG-2 in secretion indicated that it principally localizes with Sec31 at ERES in a manner concomitant with intracellular calcium oscillations (la Cour et al., 2007; Shibata et al., 2007; Yamasaki et al., 2006), suggesting a role for ALG-2 in affecting ERES function in response to a Ca^{2+} signal. To define this role several groups started to study ALG-2. Some work reported that recombinant ALG-2 inhibited homotypic COPII vesicle budding and/or fusion in vitro (Bentley et al., 2010; Cour et al., 2013), implying an inhibitory role for ALG-2 in trafficking. Yet cellular studies showed that recombinant ALG-2 bound to Sec31 was able to stabilize ERES (Shibata et al., 2007, 2010), while dominant-negative ALG-2 (Helm et al., 2014) and ALG-2 depletion (Rayl et al., 2016) also indicated a positive regulatory role. This duality in the regulatory role of ALG-2 may come down to multiple partners it can bind under different circumstances. In this chapter, I will discuss multiple ALG-2-protein complexes that can or do affect secretion. Furthermore, in Chapters 3

and 4, I will present evidence that the extent or pattern of Ca^{2+} signaling can alter ALG-2 activity directly and/or extend the subset of ALG-2 binding partners and, in this way, dictate distinct ALG-2-dependent secretion activities.

In the basal state, or in other words, in the absence of significant cytosolic Ca^{2+} oscillations, ALG-2 binds to the outer COPII coat subunit Sec31 (Shibata et al., 2007; Yamasaki et al., 2006), where it colocalizes with another PEF protein, peflin ((McGourty et al., 2016) and Chapter 3) Likely the colocalized peflin and ALG-2 at ERES is comprised of the earlier reported 1:1 heterodimer, observed in vitro to dissociate in response to Ca^{2+} (Kitaura et al., 2001). Interestingly, depletion of peflin in NRK cells produced increased ALG-2 at ERES and an increase in ER-to-Golgi trafficking of VSVG (Rayl et al., 2016), a situation reminiscent of ALG-2 binding to ERES in response to intracellular Ca^{2+} oscillations (la Cour et al., 2007), indicating a straightforward positive and negative role for ALG-2 and peflin at ERES, respectively. Furthermore, double KD of ALG-2 and peflin did not decrease transport below control levels, indicating that neither are actually required for secretion, and are purely regulatory in this context (Rayl et., al 2016, and Chapter 3). Importantly, this result is in partial contrast to another study. McGourty et al. showed that the ubiquitin ligase CUL3 and its adaptor KLHL12 required both peflin and ALG-2 together for recognition and ubiquitination of Sec31, and further that both PEF proteins were positively required for collagen I secretion (McGourty et al., 2016). In this study, treatment of cells with histamine or ionomycin caused enlargement of COPII membrane sites or vesicles in an ALG-2- and peflin-dependent manner, suggesting activation of collagen export in response to surges in cytoplasmic Ca^{2+}.

Other binding partners for ALG-2 continue to support a regulatory role for ALG-2, for example, annexin A11 (Anxa11). The role of the annexin family of Ca^{2+}- and lipid-binding proteins in trafficking is long and complex; a recent review discussed the potential involvement of annexins in a variety of plant membrane trafficking steps (Konopka-Postupolska & Clark, 2017). Briefly, there is very strong evidence that annexin A2 is involved in regulated exocytosis of chromaffin granules (Chasserot-Golaz et al., 2005), as well as several annexins being involved in Ca^{2+}-dependent plasma membrane repair (Bouter et al., 2011; Lennon et al., 2003) but

Anxa11's role in ER-to-Golgi transport seems to be a unique example of an annexin playing a regulatory role at a constitutive trafficking step. At ERES, Anxa11, like ALG-2 has a role in stabilizing Sec31A (Shibata et al., 2015). There, Anxa11 likely anchors the ALG-2-Sec31A complex directly to the phospholipid bilayer, stabilizing the Sec31A interaction with ALG-2 rather than competing with it. Additionally, studies testing specific mutants that disrupt ALG-2-Anxa11 binding but not Sec31A binding suggest that one ALG-2 molecule can bind Sec31A and Anxa11 *at the same time,* potentially through different binding sites (Figure 3). If this is true, then Anxa11 would not exactly be an additional ALG-2 target but rather an ALG-2 "co-effector" of Ca^{2+}, since Anxa11 is itself a Ca^{2+} binding protein whose interactions with phospholipids could be independently modulated by Ca^{2+}, separately from the Ca^{2+} modulation of ALG-2 binding to Anxa11 and Sec31A. This dual Ca^{2+}-sensing unit could create complex functional responses, as has been observed in ALG-2's Ca^{2+}-dependent changes in ER-to-Golgi transport. Also in support of more complex functions of ALG-2, ALG-2 has been reported to bind trk-fused gene (TFG) Ca^{2+}-dependently at ERES in a Sec31A independent manner (Kanadome et al., 2017) (Figure 3). This further indicates the possibility for ALG-2 to have divergent functions through mutually exclusive interactions with Sec31A or TFG. GFP-MAPK1-interacting and spindle-stabilizing like (GFP-MISSL) also colocalized with ALG-2 in response to increased Ca^{2+} (Takahara et al., 2017). The effector complex responsible for this targeting phenomenon appeared to be distinct from the Sec31A-ALG-2-Anxa11 or ALG-2-TFG complexes and was comprised of ALG-2 bound to both MISSL and MAP1B (microtubule-associated protein 1B), but not Sec31A (Figure 3). These interactions occurred at a subset of ERES, as well as at non-ERES sites. MISSL itself appeared to have a positive role in secretion as its KD attenuated secretion of SEAP (secretory alkaline phosphatase), possibly via sequestration of MAP1B, KD of which reversed the secretion defect. Furthermore, since the MISSL-ALG-2-MAP1B effector complex does not contain a member of the transport machinery, its effects on transport could be indirect, for example by buffering ALG-2 availability for the Anxa11-ALG-2-Sec31A complex. It is also worth pointing out that in the Anxa11 study (Shibata et al., 2015) and in the MSSL/MAP1B study (Takahara et al., 2017), ALG-2 KD had opposite effects on ER-to-Golgi transport (stimulatory and inhibitory,

respectively). Collectively these studies indicate that ALG-2 has the capacity to serve multiple roles in secretion through binding to an array of target proteins (Figure 3).

A completely different line of research has also focused on modification of the COPII subunit Sec31A in response to Ca^{2+} —and also relates to ALG-2. This work examined the effect of Ca^{2+} dysregulation on the O-GlcNAcylation and membrane targeting of Sec31A (Cho & Mook-Jung, 2020). *O*-GlcNAc transferase (OGT) is an enzyme responsible for this newly appreciated cytosolic post-translational modification. OGT was found in a previous paper to interact directly with Sec31A and mediate O-GlcNAcylation at position S964 (Cho & Mook-Jung, 2018). In the more recent paper, extremely high Ca^{2+} for 24 h (brought about with A23187 or A-beta peptide) caused disruption of Sec31A targeting to membranes, while 24 h exposure to EGTA caused enhanced Sec31A targeting. The low-Ca^{2+}, Sec31A targeting-promoting condition was accompanied by increased O-GlcNACylation of Sec31A and less ALG-2 association, while the high-Ca^{2+}, Sec31A targeting-inhibiting condition was accompanied by decreased O-GlcNACylation and increased ALG-2 association. An S694A mutation of Sec31A that cannot be O-GlcNACylated was not subject to the targeting regulation by Ca^{2+} flux, suggesting that O-GlcNACylation is a powerful determinant of Sec31A targeting. One interesting speculation is that since the ALG-2 binding site on Sec31A (residues 839-851 (Shibata et al., 2010)) is relatively close to S694, ALG-2 binding and OGT binding could be mutually exclusive, in which case Ca^{2+} could regulate Sec31A O-GlcNACylation through Ca^{2+}-dependent ALG-2 binding. However, the role of Sec31A O-GlcNACylation in Sec31A function is still relatively unexplored, and it remains to be seen whether it is modulated by physiologically realistic Ca^{2+} fluctuations.

The locus of action of Ca^{2+} in the preceding examples is presumed to be the cytoplasm, where released Ca^{2+} regulates the trafficking machinery, such as vesicle coats. However, Ca^{2+} inside the lumen of organelles can also affect trafficking by altering the function of receptors or other vesicle components that influence whether luminal cargo is recruited to a budding vesicle. Substantial depletion of ER Ca^{2+} has been associated with the abnormal secretion of ER-resident proteins normally retained in the ER (Booth & Koch, 1989; Henderson et al., 2013, 2014). This abnormal ER exit has been demonstrated to affect proteins containing a C-terminal

KDEL retrieval sequence, and their exit can be suppressed by over-expression of KDEL receptors (Trychta et al., 2018). While the mechanism of retrieval via the KDEL receptor is well established, it is not known how luminal Ca^{2+} contributes to the retention of ER proteins, a phenomenon first noted for the ER chaperone calreticulin in 1994 (Sonnichsen et al., 1994). Several putative mechanisms have been proposed to explain this departure including (i) proteins with KDEL sequences such as ER chaperones BiP or GRP94 bind Ca^{2+} with low affinity and interact both with each other and with misfolded proteins, possibly forming a kind of retention matrix. A decrease in Ca^{2+} could reduce their interactions and cause them to be secreted. Or (ii) the ER environment may exist as a dynamic hydrogel due to a high concentration of Ca^{2+} and Ca^{2+}-interacting proteins, with the hydrogel properties limiting access of resident proteins to ERES. A decrease in the Ca^{2+}concentration could thereby decrease the hydrogel viscosity, allowing ER-resident proteins to escape and overwhelm the KDEL retrieval pathway. The precise mechanism for Ca^{2+}-dependent ER protein retention remains to be explored and will have medical significance to the many diseases whose pathologies involve severe disruption of homeostasis, for example, ischemia (Ludhiadch et al., 2021).

Another protein modulated by luminal Ca^{2+} is the cargo receptor ERGIC-53 (also called LMAN1). ERGIC-53 Ca^{2+} dependently binds soluble glycoprotein cargoes in the ER lumen (Appenzeller et al., 1999; Velloso et al., 2003) Example cargoes include coagulation factor V (FV) and factor VIII (FVIII) (Cunningham et al., 2003; Zhang et al., 2005), cathepsins C and Z (Appenzeller et al., 1999; Nyfeler et al., 2006), α1-antitrypsin (Nyfeler et al., 2008), and serotonin neuroreceptors (Y. L. Fu et al., 2019). Previously, ERGIC-53 bound to cargo was thought to assemble in the ER lumen before dissociating in the ERGIC/Golgi in a manner dependent upon Ca^{2+} release facilitated by decreasing pH between organelle compartments (Appenzeller-Herzog et al., 2004). However, a more recent study found that the carbohydrate-binding domain (CRD) of ERGIC-53 bound to Ca^{2+} was insensitive to the changes in pH predicted to occur between the ER and Golgi (Zheng et al., 2013). Importantly, this study also showed that CRD-ERGIC-53 had very little binding to a glycan-like moiety below 0.4mM $CaCl_2$. It remains

unresolved whether differences in pH between the ER and Golgi, or differences in Ca^{2+} concentration, play a more significant role in regulating ERGIC-53 cargo loading and release.

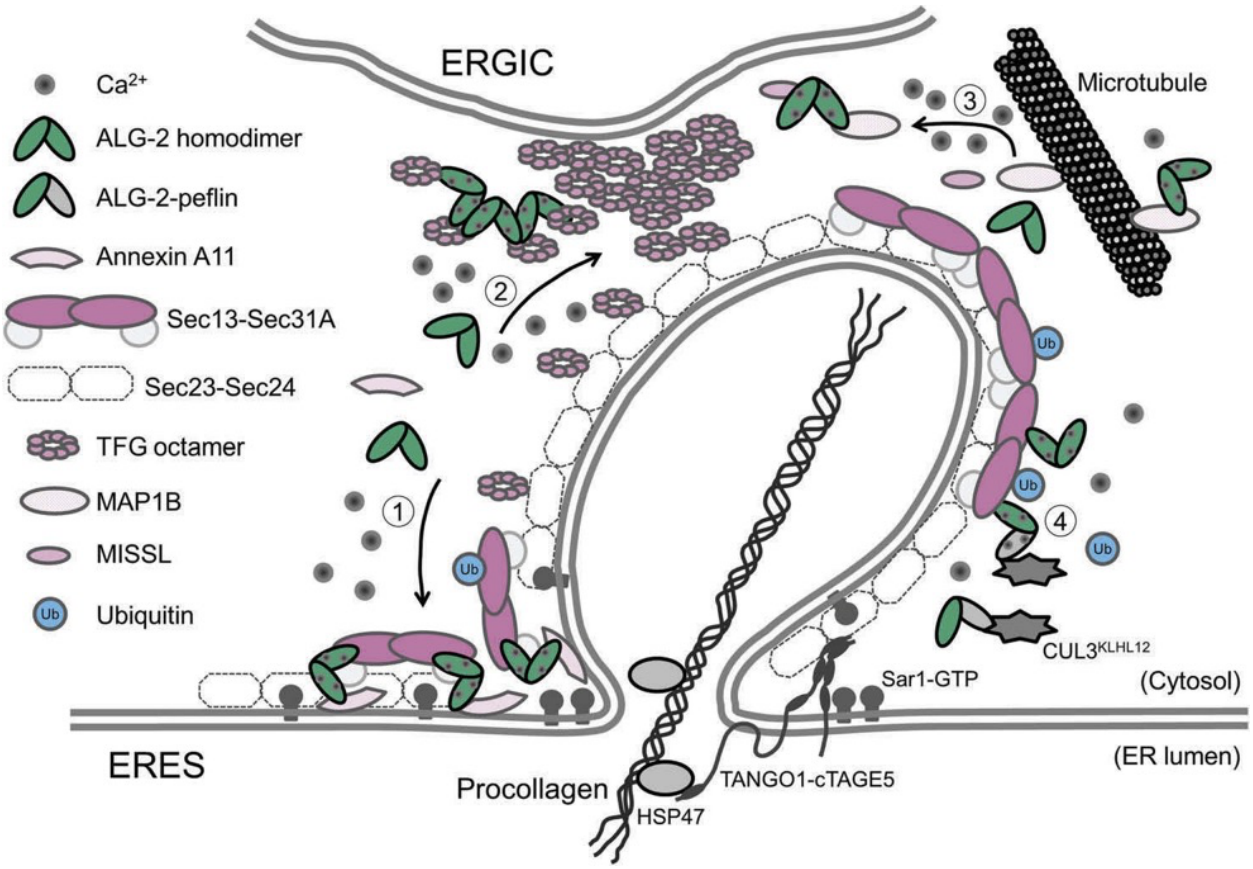

Figure 3: ALG-2 and its adaptor proteins. Schematic representation of an ERES, with potential models for adaptor functions of ALG-2. An ALG-2 homodimer couples the following combinations of target proteins with the following presumed roles: 1) Sec31A and Anxa11: stabilization of Sec31A at ERES 2) two TFG octamers: polymerization of TFG, 3) MISSL and MAP1B: sequestration of ALG-2. Conversely, 4) the ALG-2-peflin heterodimer binds Sec31A attenuating trafficking or alternatively bridges between Sec31A and $CUL3^{KLHL12}$ in a Ca^{2+} -dependent manner leading to monoubiquitylation of Sec31A.

Reproduced with permission from Figure 3, Shibata, H. (2019). Adaptor functions of the Ca^{2+}-binding protein ALG-2 in protein transport from the endoplasmic reticulum. Biosci. Biotechnol. Biochem., 83(1), 20–32.

1.2.2 Golgi Apparatus

Free Luminal Ca^{2+} ~250 µM (Bootman & Bultynck, 2020)

The Golgi apparatus plays a central role in the trafficking and sorting of secretory cargo. Like the ER, the Golgi holds a vast reservoir of Ca^{2+} and is similarly endowed with Ca^{2+} pumps, Ca^{2+} release channels, and Ca^{2+} binding proteins (Pizzo et al., 2011) (Figure 2). However, the Golgi has received comparatively less attention than the ER in facilitating the spatiotemporal complexity of Ca^{2+} signals within the cell.

Many studies have implicated Golgi Ca^{2+} channels and Ca^{2+} effectors in regulating trafficking. To begin, I discuss Sly41, an SLC-family solute transporter that constitutively cycles between the ER and Golgi in *Saccharomyces cerevisiae*. Although the substrate for the transporter remains unknown, genetic interactions with the PMR1 Golgi Ca^{2+} pump led to the discovery that Sly41 over-expression generated elevated cytosolic Ca^{2+} (Mukherjee & Barlowe, 2016). This was an important trafficking discovery since Sly41 was originally identified in a screen for genes whose over-expression suppressed COPII dependent membrane tethering deficiencies (SLY = suppressor of lethality of ypt1). Mechanistically, this meant that raising the cytosolic Ca^{2+} concentration through Sly41 over-expression compensated for the loss of an ER-to-Golgi vesicle tethering factor (Uso1; p115 in mammals) that is essential for intracellular transport pathways and efficient SNARE assembly (Chia & Gleeson, 2014; Mukherjee & Barlowe, 2016). These findings on their own suggest that Ca^{2+} promotes membrane fusion between COPII vesicles and the Golgi. Curiously, while the addition of Ca^{2+} in the absence of maximal vesicle tethering factors did indeed stimulate membrane fusion, it did nothing when saturating levels of vesicle tethering factors were present. A Ca^{2+} effector protein such as ALG-2 or CaM that, for example, interacts with SNAREs or tethers and mediates the stimulation of transport, was not identified. However, some Ca^{2+} effects on membrane fusion could instead be due to the fusion-promoting properties of Ca^{2+} itself, without the requirement for a Ca^{2+} effector (to be discussed later).

A recent study investigated the effect of high cytosolic Ca^{2+} concentrations on Golgi structure (Ireland et al., 2020). The authors exposed HeLa cells to the Ca^{2+} agonist histamine or

the SERCA inhibitor thapsigargin for 0.5-2 h. They noted morphological fragmentation of Golgi stacks via a mechanism that involved PKCα-mediated phosphorylation of Golgi reassembly stacking protein 55 (GRASP-55). The fragmentation response appeared to be independent of ER stress and UPR activation. Satisfyingly, in this example, we have both an established Ca^{2+} effector, PKCα, and the trafficking machinery impacted, GRASP-55. However, the trafficking purpose for the effect is less clear. The authors suggested it was part of a Golgi stress adaptive mechanism or signaling pathway. Cargo trafficking effects through the Golgi were regarded as mild, however, there was measurable acceleration that could have contributed to increased secretion. It would be interesting to know whether the PKCα-mediated response to Ca^{2+} signaling in the Golgi works in concert with changes in ER export mediated by ALG-2 that were discussed above.

Like TRPP2 in the ER, the Golgi also possesses resident TRP channels that appear to affect secretion. The TRPC (transient receptor potential canonical) sub-family of TRP channels are nonselective cation channels that are known to open in response to phospholipase C activation, though their precise ligands (IP3, diacylglycerol, etc.) vary (M. Miller et al., 2011). Human TRPC3 and 7 are localized on the plasma membrane but are also found in intracellular pools at the trans-Golgi network (TGN) and Golgi stack (Lavender et al., 2008). Furthermore, over-expression of either of these channels was found to increase constitutive secretion of secretory alkaline phosphatase (SEAP) by 2-4-fold (Lavender et al., 2008). The precise locus of the secretion effects observed in this study was not elucidated, and it cannot be eliminated that the over-expressed channels mobilized ER Ca^{2+} in addition to Golgi Ca^{2+} and that ER Ca^{2+} was the functional site, possibly via ALG-2's effects on COPII targeting, as discussed earlier. However, it is tempting to speculate that what occurred was local stimulation of intra-Golgi cargo transport, a process conventionally thought to be facilitated, through the process of cisternal maturation, by COPI-coated vesicles (though a competing hypothesis is intra-Golgi tubules, discussed below). Interestingly, two groups have presented evidence that COPI targeting to membranes, like COPII targeting, is Ca^{2+}-dependent (Ahluwalia et al., 2001; Bentley et al., 2010) but that ALG-2 did not affect COPI targeting (Bentley et al., 2010). It would be very

exciting if the COPI coat had a separate Ca^{2+} effector regulating its own dynamics; furthermore, this putative effector could be the key to understanding TRPC effects on secretion.

A prominent Golgi Ca^{2+} effector is the cytosolic phospholipase A_2 alpha (cPLA$_2\alpha$). cPLA$_2\alpha$ is a member of the superfamily of phospholipase A_2 enzymes (PLA_2) reviewed extensively elsewhere (Burke & Dennis, 2009). In general, PLA_2 hydrolyze the fatty acid from the sn-2 position of membrane phospholipids creating a lysophospholipid and a free fatty acid. An inverted-cone-shaped lipid, lysophospholipids favor positive curvature of lipid membranes and thereby promote membrane tubule formation. Tubule-mediated (as opposed to vesicle-mediated) trafficking is gaining recognition for its contributions to intra-Golgi transport as well as Golgi-to-plasma membrane transport of certain cargoes (M. E. Bechler et al., 2012). Three specific PLA_2 enzymes have been implicated in tubule regulation at the Golgi (M. Bechler et al., 2010; M. E. Bechler et al., 2012; Ben-Tekaya et al., 2010) including cPLA$_2\alpha$ (Pietro et al., 2009). While cPLA$_2\alpha$ is Ca^{2+} activated, the other two Golgi-associated PLAs are not, but could instead be activated by G protein βγ complexes (M. E. Bechler & Brown, 2014). Notably, cPLA2α is specifically recruited to the Golgi complex, likely via its C2 domain (J. H. Evans et al., 2004), in response to transient increases in Ca^{2+} initiated by the arrival of secretory cargo (Pietro et al., 2009). There it was required for intra-Golgi transport of VSV-G through the Golgi, apparently via induction of small, inter-stack tubules. In the study by Pietro, depletion of cPLA2α specifically inhibited transport through the Golgi and did not impair ER-to-Golgi transport of VSV-G nor delivery of VSV-G from the TGN to the plasma membrane, nor retrograde Golgi-to-ER transport of the KDEL receptor (Pietro et al., 2009). In another paper, it was shown that cPLA$_2\alpha$ contributes to the delivery of transmembrane proteins to junction complexes in endothelial cells. This point was demonstrated by noting the inhibition or RNAi-mediated KD of cPLA2α prevented delivery of VE-cadherin, occludin, and claudin-5 to cell-to-cell contacts. Instead, these proteins accumulated in the Golgi, indicating that either transport through the Golgi or transport from it was inhibited (Regan-Klapisz et al., 2009). The evidence for cPLA2α in the regulation of intra-Golgi transport is thus quite strong, while the Ca^{2+} signaling that activates cPLA2α on the Golgi is less clear. One report suggested that Ca^{2+} is released from the Golgi

itself (Micaroni et al., 2010) when a bolus of secretory cargo enters the Golgi, though specific channels and/or pumps and their mode of activation were not identified.

Secretory pathway Ca^{2+}-ATPase (SPCA1), is a Golgi-localized Ca^{2+} ATPase, which along with the ER SERCA pump, is responsible for the maintenance of Golgi Ca^{2+} levels. Mutations in SPCA1 (Gene name: ATP2C1) manifest, usually, as a decrease in expression, and elicit the autosomal dominant skin disorder Hailey-Hailey disease (Missiaen et al., 2004). As we will see in the following examples, the role of SPCA1 in secretion seems to be mainly in providing the lumen of the Golgi and associated organelles with high Ca^{2+} that is used in sorting and processing of secretory cargoes en route to their final destinations. SPCA1's role in trafficking was first demonstrated in yeast, where its medial Golgi-localized ortholog PMR1 transports both Ca^{2+} and Mn^{2+} into secretory compartments (Dürr et al., 1998). In this early study, *pmr1* mutants are both unable to sort carboxypeptidase properly to the vacuole and unable to degrade misfolded carboxypeptidase, a luminal ER protein—a trait that was later found to be reversible via addition of external Ca^{2+} (D'hooge et al., 2015). This suggested that low luminal calcium in secretory organelles is the primary cause of these sorting defects. Further studies reinforce this idea. For example, SPCA1 inhibition also produced a decrease in insulin-like growth factor receptor (IGF1R) at the cell surface, a phenotype caused by defective proteolytic processing and accumulation of previously undetectable TGN-localized pro-IGF1R (Grice et al., 2010). One putative effector for SPCA1s sorting role in secretion arose later when it was discovered that the luminal, secreted Ca^{2+}-binding protein Cab45 preferentially accumulates near SPCA1, where it oligomerizes with secretory cargoes in response to the presumably high local concentration of Ca^{2+} (Deng et al., 2018). Cab45 does not play a general role in secretion, but rather binds a few, select secretory cargoes including lysozyme C and cartilage oligomeric matrix protein (COMP), and presumably assists their secretion by forming condensates (Blume et al., 2012; Deng et al., 2018). Curiously, Cab45 is secreted along with its client cargos.

Nucleobindin-1 (NUCB1, also called CALNUC or NUC) appears to be a multi-functional soluble EF-hand-containing Ca^{2+} effector protein. NUCB1 is widely distributed within the cell. The protein contains both an ER signal sequence and an ER export signal, and displays

prominent localization to the cis Golgi (Aradhyam et al., 2010; Lin et al., 1998, 1999) while a fraction gets constitutively secreted as well(Lavoie et al., 2002). Surprisingly, NUCB1 is also present in the cytoplasm (Brodeur et al., 2009). In the cytoplasm it has been suggested to, among other things, undergo Ca^{2+}-dependent interactions with Gαi subunits on Golgi membranes (Garcia-Marcos et al., 2011; Lin et al., 2009). Importantly, cytoplasmic NUCB1 acts as a regulator of endosomal recycling of lysosomal receptors such as the mannose-6-phosphate receptor and sortilin, which capture cargo at the TGN and ferry it to late endosomes for ultimate deposition in the lysosome (Brodeur et al., 2009; Larkin et al., 2016). In these studies, NUCB1 appeared to act in the cytosol and as a regulator of rab7 activation to bring about recruitment of the retrograde coat, retromer, that mediates return of the lysosomal receptors to the TGN. The role of Ca^{2+} in NUCB1 function here was not investigated.

Moving on to NUCB1 that is targeted to the luminal cellular domain, some reports have suggested a chaperone-like activity due to its ability to bind Alzheimer's amyloid precursor protein (APP) and assist in its folding and biogenesis (Kanuru & Aradhyam, 2017; Lin et al., 2007). In the Golgi, NUCB1 may function as a regulator of Golgi Ca^{2+} homeostasis since its over-expression increased Golgi Ca^{2+} storage (Lin et al., 1999) while NUCB1 KO induced a loss of Golgi luminal Ca^{2+} (Pacheco-Fernandez et al., 2020). Furthermore, the authors of the new study also noted that NUCB1 KO and NUCB1 with mutant EF hands produced a delay in the trafficking of ECM constituents MMP2 and MMT1-MMP at the cis-to-trans Golgi stage. Again, like Cab45 or even ERGIC-53, NUCB1 appeared to regulate the trafficking of only a subset of cargoes, for example NUCB1 KO had no effect on the trafficking of lysozyme C (Pacheco-Fernandez et al., 2020). Importantly, this described trafficking defect was a delay and not a block, possibly due to compensatory mechanisms mediated by other Ca^{2+} binding proteins. The trafficking function of NUCB1 was presumed to be mediated by direct interactions with specific cargoes, but a more detailed mechanism of how NUC1B facilitates anterograde transport while remaining in the cis-Golgi remains speculative. Finally, NUCB1 is reported to, after a long period in the Golgi, be constitutively secreted into the extracellular space (Lavoie et al., 2002) where it may have

signaling functions via its capacity to bind Ca^{2+}, such as in bone matrix maturation (Petersson et al., 2004).

1.2.3 Late Endosome/Lysosome

Free Luminal Ca^{2+} ~500 µM (Bootman & Bultynck, 2020)

The late endosome/lysosome (LEL) are central organelles responsible for macromolecule recycling. Importantly, they are also intracellular stores for Ca^{2+}, reaching concentrations that approach that of the ER lumen (Feng & Yang, 2016) (Figure 2). It has been known for quite some time that LEL trafficking requires luminal Ca^{2+} and that CaM is an important Ca^{2+} effector for this (Colombo et al., 1997; Peters & Mayer, 1998; Pryor et al., 2000). Resident in the lysosome is the TRPML1 channel that is critical in Ca^{2+}-dependent lysosome trafficking; lack of TRPML1 activity causes the genetic disorder Mucolipidosis and enlarged vacuole-like lysosomes (Di Paola et al., 2018). TRPML1 belongs to the mucolipin subgroup of the TRP ion channel family whose members I've discussed in the sections on trafficking in the ER and the Golgi. Like other TRP channels, TRPML1 acts as a non-selective ion channel permeable to Ca^{2+}. Some work has indicated that TRPML1 is an activator of lysosome-MVB (multivesicular body) fusion. In this context, TRPML1 was suggested to regulate exosome release, since this process is inhibited when lysosomes fuse with MVB's, the source of exosomes (G. Li et al., 2019; Wong et al., 2012) Other work, however, has implicated TRPML1 in LEL fission (Cao et al., 2017). TRPML1 has been shown to be regulated by pH (Feng & Yang, 2016) and activated by the rare LEL phospholipid $PI(3,5)P_2$. Deficiency of either TRPML1 or $PI(3,5)P_2$ produced enlarged LEL, while OE of TRMPL1 both attenuated the defect observed with $PI(3,5)P_2$ deficiency and enhanced vacuolar calcium release (Dong et al., 2010). This local increase in juxta-organellar calcium could serve to recruit cytosolic complexes necessary for membrane fusion and fission. In fact, CaM was implicated as the specific Ca^{2+} effector for TRPML1's role in LEL fission(Cao et al., 2017), with the mammalian target of rapamycin 1 (mTORC1) serving as a required downstream target (Yang et al., 2019). ALG-2, discussed above in the ER section, has also been implicated as an effector of Ca^{2+} released by TRPML1, since it binds to TRPML1 in a Ca^{2+}-dependent manner (Vergarajauregui et al., 2009). Furthermore, activation of TRPML1 via

$PI(3,5)P_2$ caused ALG-2 to Ca^{2+} dependently couple dynein-dynactin with the N-terminus of TRPML1 (X. Li et al., 2016). This ALG-2-mediated adaptor system ultimately permitted migration of lysosomes to the perinuclear region in response to Ca^{2+} signals. Distinct from CaM's proposed role in LEL fission, this dynein-mediated trafficking implicates Ca^{2+} and ALG-2 in autolysosome formation, which occurs when the migrated lysosomes fuse with autophagosomes.

Also localized to LEL, purinergic receptor P2X4 is a Ca^{2+} release channel activated by luminal ATP in a pH-dependent manner. In a recent article, it was shown that P2X4 promotes LEL fusion in a cell-free assay and that this effect was blocked by various inhibitions of P2X4-mediated Ca^{2+} release (Cao et al., 2015). Though inhibition of P2X4 activity by the low pH of LEL was overcome pharmacologically in these experiments, it is unknown if and how this inhibition is overcome in cells. This study also showed that P2X4 activation recruits CaM and that together they form a complex at the LEL membrane. Finally, P2X4's fusion effect was shown to be suppressed by inhibiting CaM (Cao et al., 2015). The authors do not specifically identify the downstream targets for CaM in this instance, though it may be relevant that CaM interacts with LEL SNARE proteins in a Ca^{2+}-dependent manner (Luzio et al., 2007). It is interesting to note that the same research group also implicated CaM as the effector for TRPML1-mediated LEL fission (Cao et al., 2017), but how two distinct channels could mediate opposing trafficking phenomena (fusion vs. fission) via the same Ca^{2+} effector was not resolved.

1.2.4 Baseline Exocytosis of Secretory Granules

Specialized epithelial goblet cells secrete gel-forming mucins, the first line of defense against pathogens or allergens. Following biogenesis at the Golgi, mucin granules undergo maturation and eventually release their contents at the plasma membrane. While mucin granules undergo stimulated exocytosis in response to agonists such as ATP, it was recently discovered that baseline secretion of mucins, which requires an order of magnitude lower intracellular Ca^{2+} than agonist-stimulated release (Rossi et al., 2004), can exceed stimulated release over long periods (Zhu et al., 2015). A high-affinity Ca^{2+} sensor for baseline mucin secretion is proposed to be K^+ channel interacting protein 3 (KChIP3), a member of the neuronal

Ca^{2+} sensor (NCS) family of EF-hand-containing proteins (Cantero-Recasens et al., 2018). KChIP3 inhibits baseline exocytosis, which was evinced by an increase in baseline mucin secretion during KChIP3 KD and a decrease in baseline secretion during KChIP3 OE. This effect was demonstrated to be entirely dependent on intracellular Ca^{2+} oscillations, as increased intracellular calcium oscillations abrogated the inhibitory effect of KChIP3 OE. Finally, this Ca^{2+} dependent control of KChIP3 activity was discovered to be dependent on the ryanodine receptors, activity of which caused KChIP3 to dissociate from mucin granules (Cantero-Recasens et al., 2018). While this process sounds more akin to regulated secretion, it was able to proceed without stimulation by external agonists and did not require synaptotagmin, thus blurring the distinction between the regulated and constitutive secretory pathways. *In vivo*, the Ca^{2+} oscillations may be driven by fluid flow over the epithelium, as goblet cells were found to increase Ca^{2+} oscillations and mucin secretion in response to cell perfusion (Zhu et al., 2015).

1.3 CALCIUM AND MEMBRANES

Secretory pathway organelles harbor significant stores of calcium. The ER is reported to be the highest with a total Ca^{2+} of up to 2 mM, equivalent to the extracellular Ca^{2+} concentration, while its free Ca^{2+} store is ~500 µM (Bootman & Bultynck, 2020). Meanwhile, the Golgi apparatus sits at an average of 250 µM free Ca^{2+} (Bootman & Bultynck, 2020), although this number varies, with Ca^{2+} steadily diminishing from the cis to the trans-Golgi compartments(Micaroni, 2012). Finally, lysosomes' average free Ca^{2+} is comparable to the ER at ~500 µM(Bootman & Bultynck, 2020; X. Li et al., 2016) (Figure 2). While I've so far discussed the influence of these stores primarily in the context of their capacity to regulate Ca^{2+} binding proteins that in turn regulate vesicle trafficking, here I discuss the possibility that Ca^{2+} directly modulates trafficking by influencing the structural and functional properties of membrane lipids. Indeed, experimental and theoretical work has shown that Ca^{2+} can quickly and concentration-dependently tighten and order lipid bilayers, primarily via coordination with anionic Oxygens of acidic phospholipids such as phosphatidylinositol-4,5- bisphosphate [PI(4,5)P2] (Graber et al., 2015; Sarmento et al., 2014) and phosphatidylserine (PS) (Mao et al.,

2013; Pedersen et al., 2006; Sinn et al., 2006). Together these studies suggested a role for cytosolic Ca^{2+} in promoting membrane fusion, possibly by masking the negative charge of anionic lipids and more readily allowing close association of membranes. Ca^{2+} concentrations on the order of 200-400 μM overcame DOPS (dioleoyl phosphatidylserine) inhibition of lipid or content mixing in prepared vesicles (Tarafdar et al., 2012). Importantly, this Ca^{2+} concentration is on the order one might expect for focal Ca^{2+} signals near release sites (Bootman et al., 2001; Duan et al., 2019).I note that in a previously discussed study, elevations in cytosolic Ca^{2+} were observed to overcome a block in membrane tethering to allow fusion (Mukherjee & Barlowe, 2016). Since no Ca^{2+} effector was evident in this study it could indicate that Ca^{2+} alone may have promoted membrane fusion in a physiological system.

In addition to putative direct effects on fusion, Ca^{2+} may have additional roles in vesicular trafficking. Studies have shown, for example, induction of membrane tubulation in lipid vesicles in response to local Ca^{2+} addition at concentrations above 1 mM (Ali Doosti et al., 2017). The authors of this study note that the observed inward spontaneous curvature and membrane bending is likely due to a large, Ca^{2+}-facilitated reduction in the surface charge density of one membrane leaflet causing stress asymmetry and ultimately bending of the membrane. Meanwhile, another study using a giant unilamellar vesicle transfer assay demonstrated that Ca^{2+} can trigger deformation of membranes containing PS or PI(4,5)P2 in a direction that points away from the ion source (Graber et al., 2017), in a manner reminiscent of vesicle budding. It is important to note that the concentration of Ca^{2+} required to manifest the induced curvature of membranes appears to be on the order of a few hundred micromolar. While this number falls well within the bounds of free luminal Ca^{2+} for secretory pathway organelles, it is highly unlikely that high levels of free Ca^{2+} alone could lead to a membrane budding event. Instead, it is much more plausible that luminal Ca^{2+} stores support induction of membrane curvature by working in concert with other proteins such as the annexins, which also preferentially bind anionic lipids (Boye et al., 2018). Finally, in support of a system wherein Ca^{2+} can facilitate membrane budding, I note that the membranes of organelles most enriched

in the Ca^{2+} binding lipid PS are the luminal leaflets of the ER, Golgi, and mitochondria (Hullin-Matsuda et al., 2014) two of which are critical organelles for constitutive secretion.

1.4 CONCLUSIONS

Since the Hay lab's last review of this topic (Hay, 2007), examples of Ca^{2+} regulation of constitutive trafficking has expanded: from mostly *in vitro* systems using Ca^{2+} addition or chelation into complex systems wherein specific Ca^{2+}-related gene products, many implicated in human pathologies, fundamentally alter trafficking steps throughout secretory and LEL trafficking. It is now clear that Ca^{2+} is a fundamental regulator of the cell's trafficking toolkit, but that each case is also mechanistically unique rather than following a universal pattern. Overall, constitutive trafficking appears significantly more Ca^{2+}-regulated and, therefore, less "constitutive" than once believed.

Of the Ca^{2+}-mediated regulation examples (Table 1) explored in this chapter, the most interesting, and somewhat confounding, is PEF protein ALG-2's (Figure 3) ability to perform multiple, distinct—and occasionally opposing—functions at a variety of cytosolic loci via its capacity to bind with Ca^{2+} and an array of target proteins. Thus, further elucidating ALG-2's role in trafficking is the broad aim of this dissertation. In Chapter 3, I attempt to distill ALG-2's function at ERES under steady-state Ca^{2+} conditions. Then, in Chapter 4, I explore ALG-2's regulation of trafficking in the presence of physiologically relevant Ca^{2+} signals.

Table 1: Summary of Ca^{2+} regulation of vesicle trafficking in the Endoplasmic Reticulum, in order of appearance in Chapter 1.

Endoplasmic Reticulum					
Primary reference(s)	**Ca^{2+} channel/pump**	**Ca^{2+} binding effector**	**Links to Ca^{2+} flux/homeostasis**	**Links to trafficking machinery**	**Observed trafficking effects**
Le Corre (2014); Sammels (2010)	TRPP2	—	TRPP2 KD increased releasable Ca^{2+}	TRPP2 KD upregulated COPII expression	TRPP2 KD increased collagen secretion
La Cour (2013)	—	ALG-2	Ca^{2+}-bound ALG-2 binds Sec31	Ca^{2+}-bound ALG-2 potentiated binding of Sec31 to Sec23	Ca^{2+}-bound ALG-2 inhibited COPII vesicle budding
Shibata (2015)	—	ALG-2/ AnxA11	ALG-2 binds AnxA11 Ca^{2+}-dependently	ALG-2 couples AnxA11 to Sec31A	AnxA11 or ALG-2 KD increased ER-to-Golgi transport of VSV-G
Takahara (2017)	—	ALG-2/MISSL /MAP1B	MISSL colocalizes with ALG-2 in response Ca^{2+}	MISSL-ALG-2-MAP1B may sequester ALG-2	KD of MISSL or ALG-2 decreased SEAP secretion
McGourty(2016)	—	ALG-2/peflin /$CUL3^{KLHL12}$	Ca^{2+}-dependent assoc. of KLHL12 with Sec31	$CUL3^{KLHL12}$ monoubiquitinated sec31A	ubiq. complex required for collagen I secretion
Chapters 3-4; Sargeant (2021)	IP3R	ALG-2/peflin	pulse of Ca^{2+} signaling	increased Sec31 targeting to ERES	increased ER-to-Golgi transport
Chapters 3-4; Sargeant (2021)	IP3R	ALG-2/peflin	continuous Ca^{2+} signaling	decreased Sec31 targeting to ERES	decreased ER-to Golgi transport
Held (2021)	IP3R	ALG-2/peflin	IP3R-3 KD increased Ca^{2+} signaling	IP3R-3 KD increased ALG-2 and COPII coat at ERES	IP3R-3 KD increased ER-to-Golgi transport
Cho (2018); (2020)	—	—	24 h extremes of low or high Ca^{2+}	Sec31 S694 O-GlcNACylated/de-acylated, respect.	Golgi structure modulated by Sec31 acylation
Trychta (2018)	—	—	24 h TG, depleted luminal Ca^{2+}	overwhelmed & upregulated KDEL receptors	secretion of ER-resident proteins
Zheng (2013)	—	ERGIC-53/LMAN-3	Ca^{2+}-dependent binding/release of luminal cargo	ERGIC-53/LMAN-3 is a COPII client membrane protein	req. for trafficking of coag. factors, neurorec. & others

Table 2: Summary of Ca^{2+} regulation of vesicle trafficking in the Golgi Apparatus, in order of appearance in Chapter 1.

Golgi Apparatus					
Primary Reference(s)	**Ca^{2+} Channel/Pump**	**Ca^{2+} binding effector**	**Links to Ca^{2+} flux/homeostasis**	**Links to trafficking machinery**	**Observed trafficking effects**
Lavender(2008)	TRPC3/TRPC7	—	presumed change of steady-state Ca^{2+}	—	TRPC3,7 OE increased SEAP secretion 2x-4x
Ireland (2020)	—	PKCα	Ca^{2+} agonist or TG for up to 2 h	PKCα-mediated phosphorylation of GRASP55	Golgi fragmentation and increased intra-Golgi transport
San Pietro (2009)	—	cPLA2α	presumed cargo-dependent Ca^{2+} release at Golgi	cPLA2α KD or inhibition reduced inter-cisternal tubules	cPLA2α KD inhibited intra-Golgi transport of VSV-G
Regan-Klapisz (2009)	—	cPLA2α	presumed Ca^{2+} release from Golgi	cPLA2α KD changed Golgi morphology	KD accumulated junctional proteins in the Golgi
Mukherjee (2016)	pmr1 (SPCA1 homolog)	possible direct effect of Ca^{2+}	sly41 OE increased cytoplasmic Ca^{2+}	bypassed lack of p115 homolog Uso1	increased fusion of COPII vesicles with Golgi
Grice (2010)	SPCA1	—	SPCA1 KD decreased Golgi luminal Ca^{2+}	—	blocked IGF1R trafficking/ maturation at the TGN
Deng (2018); von Blume (2012)	SPCA1	cab45	SPCA1 KD decreased Golgi luminal Ca^{2+}	cab45 oligomerized Ca^{2+}-dependently with select cargos inTGN	SPCA1 or cab45 KD blocked sorting of lysozyme C in TGN
Larkin (2016); Brodeur (2009)	—	NUCB1	—	NUCB1 req. for rab7-dep. recruitment of retromer coat to LEs	NUCB1 KD caused lysosomal accum. of Mann-6P receptors
Pacheco-Fernandez (2020)	—	NUCB1	NUCB1 KO reduces cis Golgi luminal Ca^{2+}.	NUCB1 directly bound cargo MMPs in cis-Golgi lumen	NUCB1 KO delays intra-Golgi transport of MMPs

Table 3: Summary of Ca^{2+} regulation of vesicle trafficking in the Endosome/Lysomome, in order of appearance in Chapter 1.

Endosome/Lysosome					
Primary Reference(s)	**Ca^{2+} Channel/Pump**	**Ca^{2+} binding effector**	**Links to Ca^{2+} flux/homeostasis**	**Links to trafficking machinery**	**Observed trafficking effects**
Yang (2019); Cao (2017); Dong(2010)	TRPML1	CaM	TRPML1 OE enhanced LEL Ca^{2+} release	CaM recruited mTORC1 to LEL	TRMPL1 KD produced enlarged LEL
Li (2019)	TRPML1	—	TRPML1 Ca^{2+} release regulated by ceramidase	TRPML1 inhibition blocked lysosome-MVB interactions	TRPML1 inhibition stimulated exosome release
Li (2016)	TRPML1	ALG-2/dynein-dynactin	TRPML1 Ca^{2+} release regulated by PI(3,5)P2,	Ca^{2+} recruited ALG-2 and dynein/dynactin to TRPML1	permits perinuclear positioning of LEL
Cao (2015)	P2X4	CaM	P2X4 released Ca^{2+} from the LEL pH-dependently	CaM presumed to activate fusion machinery	P2X4 OE promotes endolysosome fusion

CHAPTER 2:

METHODS

2.1 Antibody Production and Purification

Rat peflin and mouse ALG-2 were ligated into pGEX expression plasmids and expressed in E.coli as GST fusion proteins. Cultures were grown at 37°C to an A_{600} of 0.4-0.6, prior to an induction with 1 mM isopropyl-1-thio-β-D-galactopyranoside (IPTG) at 37°C for GST-ALG-2, and 15°C for GST-peflin, for 3 h. Harvested cells were subjected to a single round of French Press and centrifuged at 20,000 x g for 20 min. Pellets were collected, dissolved in sample buffer and loaded onto SDS–PAGE gels. Gels were stained with 0.1% Coomassie in H_20, and the resolved bands were excised from the gel and subjected to a 3 h electroelution in 25 mM Tris, 1 mM glycine and 0.1% SDS, on ice. The eluted protein solution was concentrated and injected subcutaneously, using Freund's adjuvant, into a rabbit, for peflin, or a chicken for ALG-2. Three subsequent antigen boost injections were done over an 80-day period. At this stage, the peflin antibody was fully useful as a crude serum. For the ALG-2 antibody, sera were supplemented with an equal volume of 10 mM Tris, pH 7.5, filtered with a syringe filter and passed through a 1 ml CNBr-Sepharose column conjugated with GST as non-specific control. The flow through was then loaded onto another CNBr-Sepharose column conjugated with mouse GST-ALG-2. Columns were washed with 3 x 5 ml of 10 mM Tris, pH 7.5, then washed with the same buffer containing 0.5 M NaCl, once again with 10 mM Tris, pH 7.5 and finally eluted with 0.1 M glycine, pH 2.5. Fractions were neutralized with 2 M Tris, pH 8.0, and quantitated at A280. Peak fractions were pooled and dialyzed into PBS.

2.2 Other Antibodies and Expression Constructs

Monoclonal anti-VSV-G was purchased from Sigma (St. Louis, MO: product V5507, clone P5D4), while monoclonal anti-VSV-G clone I14 antibodies (Lefrancois & Lyles, 1982) were produced in-house from the hybridoma cell line. Mouse monoclonal anti-CHOP antibody was purchased from ThermoFisher Scientific, Waltham, MA (product MA1-250). Rabbit polyclonal anti-collagen I antibody was purchased from Abcam, Cambridge, UK (product ab34710). Mouse monoclonal anti-mannosidase II antibody was purchased from Covance Research Products, Denver, PA (product MMS-110R-200). Green secondary antibodies conjugated to Alexa Fluor

488 were from Invitrogen (Carlsbad, CA: product A11001); Cy3-, or Cy5-conjugated secondary antibodies were purchased from Jackson ImmunoResearch Laboratories (West Grove, PA).

Cargo constructs: for routine ER-to-Golgi transport studies, I used the synchronizeable cargo VSV-G_{ts045}-GFP in pCMV, or more commonly the untagged version of VSV-G_{ts045} in pCMV in conjunction with the P5D4 monoclonal antibody for immunofluorescence detection (the untagged construct has a significantly higher transfection efficiency). Human GFP-Collagen I was from David Stephens via Addgene, Cambridge, MA (construct: pEGFP-N2-COL1A1). The transport cargos retained in the ER until triggered to export with a ligand are based upon the RPD Regulated Secretion/Aggregation Kit from ARIAD Pharmaceuticals. The luminal cargo I here call "GFP-F_M4-GH" is identical to the construct “pC4S1-eGFP-F_M4-FCS-hGH” I described before (Gordon et al., 2010). GFP-F_M4-VSV-G_{tm} was constructed from GFP-F_M4-GH by removing the furin cleavage site and human growth hormone by cleavage with SpeI/BamHI and replacing it with a fragment containing the VSV-G transmembrane domain:
5'-actagtTCATCGTCGAAGAGCTCTATTGCCTCTTTTTTCTTTATCATAGGGTTAATCATTG
GACTATTCTTGGTTCTCCGAGTTGGTATTTATCTTTGCATTAAATTAAAGCACACCAA
GAAAAGACAGATTTATACAGACATAGAGATGAACCGACTTGGAAAGTAAGCGCCCG Cggatcc-3'.
To make GFP-F_M4-GPI was the same procedure except that the SpeI/BamHI- cleaved construct was ligated with a fragment containing the CD55 GPI anchor sequence:
5-actagtACAACCCCAAATAAAGGAAGTGGAACCACTTCAGGTACTACCCGTCTTCTATC
TGGGCACACGTGTTTCACGTTGACAGGTTTGCTTGGGACGCTAGTAACCATGGGCTT
GCTGACTTAGggatcc-3'. This construct is targeted to the plasma membrane where it is sensitive to extracellular PI-PLC treatment (DEG and AAP, unpublished observations). For VSV-G_{ts045} employed in Figure 10 as an ERES marker, I utilized the untagged VSV-G_{ts045}, then immuno-labeled it using monoclonal antibody I14, which only detects mature trimers.

Rat peflin was amplified from a cDNA clone by PCR primers encoding EcoR1/XhoI. This product was ligated into mammalian expression vector pCDNA 3.1(+). Mouse ALG-2 was amplified from a cDNA clone (MGC: 49479) and ligated into mammalian expression vector pME18S using PCR primers encoding XhoI and XbaI. GFP-Sec13 was as described (Hammond &

Glick, 2000). Histamine receptor construct pH1R-P2A-mCherry-N1 was purchased from Addgene (product: 84330). For a plasma membrane marker for use in TCF calculations, pCAG-mGFP was purchased from Addgene (product: 14757).

2.3 siRNA Knockdowns and Transfections

For plasmid transfections, NRK or PC12 cells were transfected using Polyjet (SignaGen Laboratories; Frederick, MD), following the manufacturer's instructions, about 24 h prior to transport assays. For transport experiments involving both plasmid and siRNA transfections, NRK or PC12 cells were transfected with siRNAs using RNAiMax (Invitrogen; Carlsbad, CA) with OpiMEM medium as suggested by the manufacturer, approximately 48 h prior to transport. Then, approximately 24 h prior to transport, they were transfected with plasmids using Polyjet as just described. Cells were equilibrated at 41 ^{o}C for 6-12 h prior to transport. Control siRNA had the following sense strand sequence: 5'-AGGUAGUGUAAUCGCCUUGdTdT-3'. Peflin siRNA 0975 had the following sense strand sequence: 5'-GCCUCAUGAUGAUAAACAUdTdT-3'. In a previous manuscript, my lab established that three distinct, non-overlapping peflin siRNA sequences – including 0975 - produced the phenotype of elevated ER-to-Golgi transport ((Rayl et al., 2016), Figure S1). ALG-2 siRNA 8567 had the following sense strand sequence: 5'-GGAGCGGAGUGAUUUCAGAdTdT-3'. In a previous manuscript,my lab established that three distinct, non-overlapping ALG-2 siRNAs - including 8567 - produced consistent, mild effects on ER-to-Golgi transport (Helm et al., 2014)). To demonstrate that multiple distinct sequences also blocked Ca^{2+} effects on transport, I tested the siRNA 8568, which is completely distinct from siRNA 8567, and found that it did (Sargeant et al., 2021) Collagen siRNA had the following sense strand sequence: 5'-GAACUCAACCUAAAUUAAAdTdT-3'. All siRNAs were custom synthesized lacking chemical modifications by Gene Link (Elmsford, NY).

2.4 Cell Culture and Agonist/Drug Treatments

NRK and Rat2 cells were grown in DMEM with 4.5 g/L glucose, 10% FBS (Gibco, qualified grade), and 1% penicillin-streptomycin. For microscopy studies, they were grown directly on

glass coverslips coated with poly-L-lysine. PC12 cells were grown in DMEM with 4.5 g/L glucose, 5% donor horse serum (Hyclone) and 5% iron-supplemented bovine calf serum (Hyclone). PC12 cells were maintained routinely on collagen-I-coated plasticware, while for microscopy they were plated directly on glass coverslips that had been first coated with poly-L-lysine and then coated with collagen I. Porcine aorta endothelial cells were isolated and cultured to P5 as described before (Madreiter-Sokolowski et al., 2019). For agonist/drug treatments NRK or PC12 cells were grown to ~100% confluency in 6-well plates. Histamine (Sigma H7125) was dispensed into glass vials under nitrogen and stored at -20 ^{o}C. Solutions of histamine were prepared fresh each day, while ATP (500 mM in water) and BHQ (100 mM in DMSO) stock solutions were stored frozen and freshly diluted each day. Bradykinin was dissolved at 5 mM in 5% acetic acid, stored in aliquots at -80 ^{o}C, and used immediately after dilution in cell medium.

2.5 PAEC's and RT-PCR

Porcine aorta endothelial cells (PAECs) in an aged state (passage 5), confirmed by positive beta-galactosidase staining and decreased proliferation rate (Madreiter-Sokolowski et al., 2019) were transfected with peflin siRNA using Transfast (Promega Corp., Madison WI, USA) according to manufacturer's instructions. Total RNA was isolated using the PEQLAB total RNA isolation kit (Peqlab; Erlangen, Germany) and reverse transcription was performed in a thermal cycler (Peqlab) using a cDNA synthesis kit (Applied Biosystems; Foster City, CA). mRNA levels were examined by qRT-PCR. A QuantiFast SYBR Green RT-PCR kit (Qiagen; Hilden, Germany) was used to perform real time PCR on a LightCycler 480 (Roche Diagnostics; Vienna, Austria), and data were analyzed by the REST Software (Qiagen). Relative expression of specific genes was normalized to porcine GAPDH as a housekeeping gene. Primers for qRT-PCR were obtained from Invitrogen (Vienna, Austria).

2.6 Calcium Imaging

Prior to imaging, NRK or PC12 cells were loaded by incubation in growth medium containing 20 mM Hepes, 3 µM FURA-2AM and 1.5 mM probenecid for 30 minutes at 37 ^{o}C,

then washed and incubated for 10 min in the same medium lacking FURA-2AM. Coverslips were then placed in a microscope chamber and maintained at 37 ^{o}C using a submerged heating loop. For ATP experiments, cells were maintained in a non-perfusing volume of 1.5 ml growth medium, 20 mM HEPES and probenecid. For BHQ experiments, the medium was continuously perfused with pre-warmed medium at 2 ml/min. Image acquisition was completed by a Nikon TE300 inverted microscope equipped with a Nikon Plan Fluor 20x/0.75 objective, motorized high speed Sutter Lambda filter wheel for emissions, CoolLED pe340 excitation system, and PCO Panda sCMOS camera, all automated with Micro-Manager software. After selecting a suitable field of cells, imaging was carried out for at most 30 min of 10 s imaging cycles capturing separate 340 nm- and 380 nm-excited images collected at 510 nm. Analysis was completed in ImageJ using a custom plugin that determined the ratio of the background-subtracted emissions from 340 and 380 excitation for each individual cell over time (Appendix).

2.7 Immunofluorescence Microscopy

Coverslips were fixed with 4% paraformaldehyde containing 0.1 M sodium phosphate (pH 7) for 30 min at room temperature and quenched three times for 10 min with PBS containing 0.1 M glycine. Fixed cells were treated for 15 min at room temperature with permeabilization solution containing 0.4% saponin, 1% BSA, and 2% normal goat serum dissolved in PBS. The cells were then incubated with primary antibodies diluted in permeabilization solution for 1 h at room temperature. Next, coverslips were washed 3x with permeabilization solution and incubated 30 min at room temperature with different combinations of Alexa Fluor^{TM} 488-, Cy3-, and/or Cy5-conjugated anti-mouse, anti-rabbit, or anti-chicken secondary antibodies. After the secondary antibody incubation, coverslips were again washed 3x using permeabilization solution and mounted on glass slides using Slow Fade Gold antifade reagent (Invitrogen: S36936) and the edges sealed with nail polish. Slides were analyzed using a 40x/1.3 Plan Fluor or 60x/1.4 Plan Apo objective on a Nikon E800 microscope with an LED illumination unit (CoolLED pE 300^{white}), sCMOS PCO.edge 4.2 camera, Prior excitation and emission filter wheels and Z-drive, automated using Micro-Manager software.

For transport assays (see below) typical images collected for each field of cells were VSV-G_{ts045} (green channel) and Golgi marker mannosidase II (cy5 channel). For colocalization assays (see below) typical images collected for each field of cells were Sec13-EGFP (GFP channel), ALG-2 (Cy3 channel), and peflin (Cy5 channel).

2.8 ER-to-Golgi Transport Assay

NRK, PC12, or Rat2 cells were plated on glass coverslips and transfected as described above. For VSV-G_{ts045} and collagen I cargo, cells were shifted to 41 ^{o}C for 6-15 h prior to transport, to accumulate the cargo in the ER. For the transport assay, the cells were either fixed by dropping coverslips directly into 6-well chambers containing fixative or pre- equilibrated 32 ^{o}C medium for 10 min, then fixative. For assays involving collagen I cargo the 32 ^{o}C medium was supplemented with 50 µg/ml ascorbate. Alternatively, for F_M4-containing cargo constructs, transfected cells were kept always at 37 ^{o}C, and the coverslips were fixed either by dropping coverslips directly into fixative or into to 6-well chambers containing 37 ^{o}C media with 500 nM AP21998, also known as D/D solubilizer (TakaraBio, Shiga Japan: 635054), for 10 min prior to transfer to fixative.

Morphological quantitation of ER-to-Golgi transport was accomplished by first collecting images in a consistent manner with regard to cell morphology, protein expression levels and exposure. A single widefield image plane was collected for each color channel for each field of cells randomly encountered; image deconvolution was not performed. Prior to image analysis using a custom ImageJ script (Appendix), files for all experimental conditions were automatically and randomly renamed with a 36- character designation and re-sorted by that identifier, eliminating any way for the user to know their identities. Each image is opened in turn and presented to the user, who at this point only views the cargo image plane. For each image the user first defines an extracellular region for use as a background, after which the user defines the minimal rectangular ROI encompassing the first cell to be analyzed. This ROI is then isolated in a separate window and the Golgi maximum is extracted, which represents the mean intensity of the pixels in the 99.990 percentile and above but excluding the highest pixel. The

user checks that these brightest pixels are in fact within the Golgi as defined on the mannosidase II image planes. The user then sequentially places 3 small circular ROIs within vesicular/reticular regions adjacent to the nucleus but clearly distinct from the Golgi. The ER mean is extracted as the mean of the three mean pixel intensities of these ROIs. Transport index is then extracted for the cell as (Golgi maximum-background) / (ER mean-background). Occasionally intensities of other channels are also collected in tandem using an ROI encompassing the cell, such as in Figure 6B which collected ALG-2 intensities in addition to transport values. The cell is then numbered on the image to avoid re-counting, and all extracted parameters written to an appendable output file along with the cell number, and image title so that the data is fully traceable. The user then defines another cell from the image or opens another image. Using this method, the user quantitates 60-100 cells per hour (Appendix).

Once transport indices have been obtained for all conditions in an experiment, each value is subtracted by the mean transport index value for cells that were fixed directly from 41 ^{o}C without a transport incubation at 32 ^{o}C (typically a value between 1.0 and 1.5) to generate the net transport index. Net transport indices are then normalized to the mean control value for the particular experiment. Each result reported here was obtained in at least three separate experiments on different days.

2.9 Labeling Intensity and Colocalization Assays

Cells were transfected with ERES markers GFP-sec13, or VSV-G_{ts045}. Following immunolabeling as described above, cells such as those shown in Figures 5 and 10 (or quantitated in Figure 10E) were captured as z-stacks in 11 200-nm increments for each channel. These image stacks were deconvolved as a single batch using Huygens Essential Widefield software (Scientific Volume Imaging, Hilversum, The Netherlands) according to the manufacturer's instructions. Final images for display and quantitation represent maximum intensity projections of deconvolved stacks. As before, these deconvolved stacks were each assigned a random 36- character designation and re-sorted by the random name. The intensity of labeled proteins was assessed by a custom ImageJ script (Appendix) performed on individual

cells for which the user manually defines a minimal enclosing ROI. Background labeling was first removed by defining a dark extracellular area of each image channel as background and subtracting that value from every pixel. The specific pixels assessed for intensity were pre-determined using a binary object mask, which was generated by auto-thresholding the desired area of the cell using the Renyi Entropy or Intermodes algorithm, depending upon which most accurately captured the spots of interest (but kept constant for a given marker/protein). Spots on the mask were assessed as ROIs that were used to measure either mean intensity or integrated density (product of area and mean intensity) in relevant channels of the unmodified images. Integrated density measurements are referred to as "total intensity" or "total spot intensity" in the figure legends where relevant, whereas mean intensity measurements are labeled as such. The choice to present total vs. mean intensity was driven by which parameter produced lower variance and thus lower p values when used in t-tests (in no cases did they produce opposing results). In a few cases (Figure 10C and D), the binary mask used was actually the Boolean intersection (see below) of ALG-2 and another ERES marker (sec31A or peflin); this was because the ALG-2 antibody produced suspected background spots that did not co-localize with ERES markers and were not removed by ALG-2-specific siRNAs. In my nomenclature, "ERES intensity" and "spot intensity" are distinguished by whether the mask for interrogation is generated from a distinct ERES marker from that being measured or from the measured marker itself, respectively. Extracted parameters were written to an appendable output file along with the cell number and image title so that the data was traceable. Following re-sorting by experimental conditions, integrated densities and other parameters for each cell were then normalized to the mean control value for the particular experiment. Each result reported here represents combined data from at least three separate experiments that displayed similar trends.

Alternatively, some binary masks were used to assess particle areas or areas of overlap – also referred to as "co-localization". Areas of overlap between two channels were calculated from two auto-thresholded images using the Boolean 'AND' operator in ImageJ's image calculator. This operation generated a mask that contained only spots present in both channels,

permitting a calculation of the total overlap area.

2.10 Total Cell Fluorescence Assay

In Figures 5B and C, TCF of collagen was determined by first transfecting Rat2 cells with the plasma membrane marker pCAG-mGFP (GFP with an N-terminal palmitoylation signal). Endogenous collagen I was labelled in the Cy3 channel. Using pCAG-mGFP, a whole cell ROI was selected via the wand threshold tool in ImageJ. That ROI was then moved into the collagen channel wherein total mean gray values and ROI area were extracted. Separately, a mean background value was extracted by randomly selecting an area without a cell. Total cell fluorescence was calculated as area of selected cell x (mean intensity of cell – mean intensity of background).

CHAPTER 3:

THE EXPRESSION RATIO OF PEFLIN AND ALG-2 DIFFERENTIALLY EFFECT SECRETION

(this chapter has been published: (Sargeant et al., 2021))

3.1 INTRODUCTION

Of the vesicle trafficking steps discussed in Chapter 1, the ER-to-Golgi interface is the busiest, transporting up to one-third of all eukaryotic proteins (Ghaemmaghami et al., 2003). Anterograde cargo is captured into a COPII pre-budding complex containing the inner coat sec23/24 heterodimer, which binds cargo in several distinct pockets on the membrane-proximal surface of sec24 (Bi et al., 2007; Hughes & Stephens, 2008; E. A. Miller & Barlowe, 2010; Stagg et al., 2008). Recruitment of the outer coat layer, comprised of sec13/31, positions a flexible proline rich region (PRR) loop of sec31 across the membrane-distal surface of sec23, potentiating its Sar1 GAP activity required for cargo concentration (Tabata et al., 2009). Together, the inner sec23/24 and outer sec13/31 COPII coat involves polymerization of at least 24 hetero-tetramers (Stagg et al., 2008).

ALG-2 acts as a Ca^{2+} sensor (Figure 3, Table 1) and, while at ERES, stabilizes association of sec31 with ERES via direct binding to a 12-amino acid sequence on the sec31A PRR region (la Cour et al., 2007; Shibata et al., 2007, 2010; Yamasaki et al., 2006). Most ALG-2 in cell extracts exists in a stable heterodimer with peflin, which binds ALG-2 in a Ca^{2+}-inhibited manner (Kitaura et al., 2001, 2002) and has been shown to suppress ER export of the cargo marker VSV-G-GFP, possibly by modulating ALG-2's availability to bind at ERES (Rayl et al., 2016). Despite these observations, a unified model for PEF protein secretion modulation has not emerged. For example, most *in vitro* transport reconstitution results utilizing purified ALG-2 indicate that the protein is an inhibitor of vesicle budding or fusion (Bentley et al., 2010; la Cour et al., 2013). Additionally, recent intact cell trafficking experiments indicate ALG-2 had a suppressive role based upon ALG-2 depletion (Shibata et al., 2015). Despite these studies, I posited a stimulatory role for ALG-2 because peflin antagonized stimulatory ALG-2-sec31A interactions and suppressed transport (Rayl et al., 2016). Furthermore, work on a presumed ALG-2 ortholog in yeast, Pef1p, demonstrated an inverse relationship wherein Pef1p binding to the sec31 PRR was inhibited by Ca^{2+} and delayed coat recruitment to the membrane (Yoshibori et al., 2012). Lastly, a distinct line of investigation suggests that Sec31A function is regulated by mono-ubiquitination and that both ALG-2 and peflin assist in that mono-ubiquitination via recruitment

of the ubiquitin ligase $CUL3^{KLHL12}$ to ERES, all of which was required to elicit collagen secretion from osteosarcoma cells (McGourty et al., 2016).

In this chapter, I significantly expand upon the ALG-2-peflin regulatory machine. Using single and tandem depletion, over-expression studies, and custom antibodies, I found that: (1) both proteins are fully dispensable for secretion; (2) a peflin-ALG-2 heterocomplex binds to ERES through its ALG-2 subunit to confer a low, buffered transport rate; (3) peflin-lacking ALG-2 complexes, depending upon expression level, can either enhance or inhibit transport; and (4) peflin depletion suppresses expression of UPR target genes in highly stressed cells. In summary, my findings indicate the presence of multiple PEF protein regulatory states that tune transport rates through potential expression level or Ca^{2+} changes.

3.2 RESULTS

3.2.1 Peflin Expression Levels Determine ER-to-Golgi Transport Rates Over a Wide Dynamic Range in an ALG-2-Dependent Manner

To investigate the dynamic range and functional interactions of PEF protein regulation of ER export, I forced individual, tandem, or reciprocal expression changes of the two proteins. Endogenous peflin and ALG-2 were either knocked down using transfection with siRNA or over-expressed by transfection with the wt, untagged rodent proteins in NRK cells. After ≥ 24 hours of transfection, the initial rate of ER-to-Golgi transport of the synchronizeable transmembrane protein cargo VSV-G_{ts045}-GFP was determined by incubation for 10 min at the permissive temperature followed immediately by fixation and morphological quantitation of the ratio of VSV-G that has reached the Golgi vs. remaining in the ER, as before (Rayl et al., 2016). Figure 4A columns 1 and 2 show that as previously reported (Rayl et al., 2016), peflin KD significantly increased VGV-G transport above basal by ~84%. On the other hand, over-expression of peflin (column 3) decreased transport by 23% below basal. Interestingly, the same two manipulations of ALG-2 expression (columns 4 and 5) caused little change in transport relative to basal, indicating that at steady state, peflin expression levels are more rate-limiting. Forced peflin over- and under-expression thus defines a dynamic range of peflin regulation of transport at

steady-state Ca^{2+} of ~107% of basal secretory flux (84% above basal and 23% below) in NRK cells.

We next asked whether the effects of peflin over-expression and depletion depended upon the presence of ALG-2. As shown in Figure 4A columns 4 vs. 6 and 7, in ALG-2-depleted cells, forced changes in peflin expression do not change secretion, indicating that peflin is dependent upon ALG-2 to influence transport. This suggests that peflin's effector for secretion is ALG-2. Column 1 vs. 6 also indicates that when both proteins are depleted, secretion is slightly higher than in the presence of both proteins at normal levels. This demonstrates that these PEF proteins are not required for transport and suggests that the two of them together exert a slightly suppressive effect on ER-to-Golgi transport under steady-state conditions.

Using a combination of quantitative Western blotting (Figure 4C and D) and immunofluorescence (Figure 4E), I documented the protein expression levels during the manipulations described above. Notably, and as described before, ALG-2-peflin interactions in the cell stabilize both proteins, such that depletion of one using siRNA resulted in co-depletion of the other (Kitaura et al., 2002; McGourty et al., 2016; Rayl et al., 2016). This complication was not severe for peflin depletion, which resulted in a ~30% reduction in ALG-2 (Figure 4D, column 2). However, depletion of ALG-2 by ~70% using siRNA resulted in a comparable depletion of peflin, essentially creating a double-depletion condition (Figure 4D, column 4). Therefore, determining the effect of peflin when ALG-2 is depleted depended upon the condition in Figure 4D, column 7, in which cells were both depleted of ALG-2 and transfected with a peflin encoding plasmid. The Western analysis indicated that peflin was only slightly restored (Figure 4D, column 7). This particular plasmid, and NRK cells in general, suffered from a low transfection efficiency using lipofection, and especially so when ALG-2 was depleted. However, for transport assays,Iused peflin immunofluorescence intensity as an aid to choose cells for functional analysis. When peflin fluorescence intensities were measured for the included cells, peflin was over-expressed by over 200% in the ALG-2-depleted cells (Figure 4E, right bar). This condition corresponds to column 7 in the transport experiment (Figure 4A), reinforcing the conclusion that dramatic changes in peflin expression when ALG-2 is depleted

do not result in transport changes. Thus, although there were significant peflin co-depletion effects due to ALG-2 siRNA, they did not change the conclusions from Figure 4A that peflin expression levels dramatically affect the secretion rate in an ALG-2-dependent manner, and that the two proteins together are functionally dispensable for baseline levels of ER-to-Golgi transport.

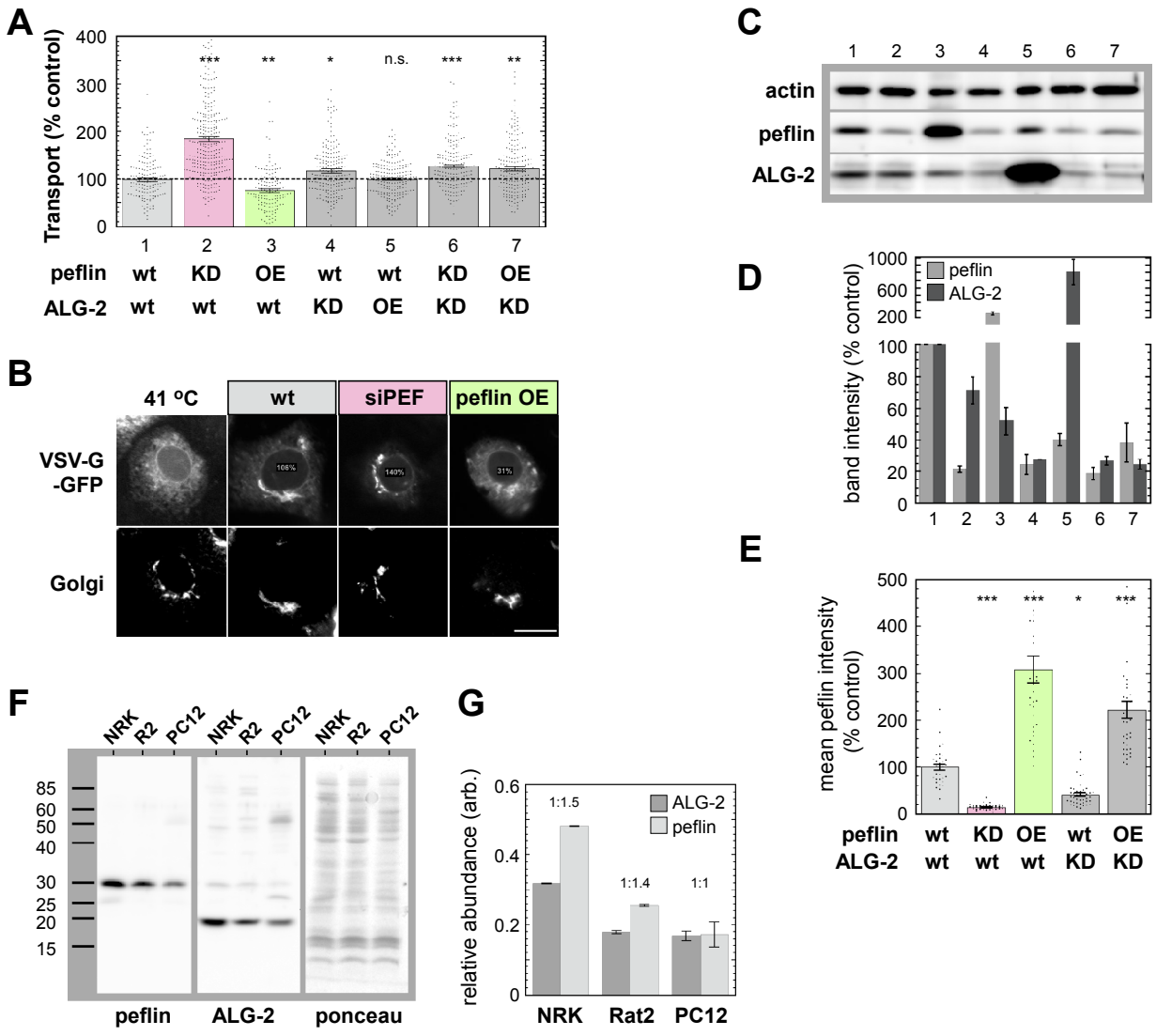

Figure 4. Peflin expression levels define a wide dynamic range of trafficking effects in an ALG-2 dependent manner. (A) NRK cells transfected with VSV-G_{ts045}-GFP were transfected with control or specific siRNAs and untagged over-expression constructs (1 µg DNA) for peflin or ALG-2. Following growth at 41 °C, cells were shifted to 32 °C for 10 min to permit transport prior to fixation. Fixed cells were immuno-labeled with mannosidase II. Each transfected cell was assigned a transport index representing trafficking of VSV-G based upon the ratio of Golgi intensity to peripheral ER fluorescence. The net transport index of each individual cell is plotted following subtraction of the mean transport index of cells kept at 41 °C, and normalization to the mean net transport index of wt cells. Approximately 200 cells were randomly quantified from each condition, and results shown are representative of at least 3 experiments with consistent trends. Asterisks indicate p values for one-way ANOVA using the Dunnet post-hoc test which compares each value to that of the control; *, $p<0.05$; **, $p<.005$; ***, $p<.0005$. Standard error is shown for each plot. **(B)** Example widefield images of individual cells for select conditions with their transport index indicated as percent of control. **(C)** Immunoblot of cell extracts left over from the transport experiment in Figure 4A. **(D)** Quantitation of the blot in part C;

two technical replicates. **(E)** Quantitation of peflin mean cell intensity in a selection of the conditions from part A. One-way ANOVA as for part A. **(F)** Western characterization of whole-cell extracts from 3 cell lines using crude rabbit anti-peflin serum (1:50,000) and affinity-purified chicken anti-ALG-2 (1:200). **(G)** Quantitation of the blot in F; two technical replicates. Side lanes not shown in F contained dilutions of purified GST-peflin and GST-ALG-2 at a ratio that had been determined on Coomassie-stained gels to be equimolar to each other. The y-axis shows the band intensities of ALG-2 and peflin relative to their respective standards on the same exposure. From these values, the relative molar ratio of the two proteins was determined and is listed above each cell type. Image scale bar: 20 micrometers.

3.2.2 Peflin Binds ERES Via ALG-2 and Prevents Its Stimulatory Activity

Previous work reported localization of epitope-tagged peflin to ERES, and deduced using immunoprecipitations that ALG-2 was able to mediate an interaction between peflin and Sec31 (McGourty et al., 2016). However, the interdependence of ALG-2 and peflin for ERES localization, and the subcellular localization of endogenous peflin has not been reported.

We raised a rabbit polyclonal antibody against rat peflin and a chicken polyclonal antibody against mouse ALG-2 to be used for localization studies of the endogenous proteins. Characterization of the antibodies' reactivity toward whole-cell lysates of NRK epithelial cells, Rat2 fibroblasts, and PC12 neuroendocrine cells was documented by Western blot in Figure 4F. The crude anti-peflin serum was high affinity and specific while the affinity-purified ALG-2 antibody was less so. Quantitation of the blots (Figure 4G), relative to stoichiometric purified protein standards of GST-peflin and GST-ALG-2, revealed that NRK cells contained roughly twice the ALG-2 and peflin expression of Rat2 cells. Despite this difference, both cell lines maintained an ALG-2:peflin ratio of approximately 1:1.5. PC12 cells, on the other hand, contained similar amounts of ALG-2 to Rat2 cells but were relatively depleted of peflin, maintaining an ALG-2:peflin ratio of approximately 1:1. These results indicate that distinct cell types maintain significantly different levels and ratios of the two proteins, potentially producing tissue-specific regulation of ER export rates.

To characterize the localization of the proteins in NRK cells, I detected the endogenous proteins using immunofluorescence. I observed diffuse, reticular as well as distinctly punctate labeling for peflin throughout the cytoplasm (Figure 5A, upper right) In addition, endogenous peflin was significantly concentrated in the nucleus. Due to the concentration of peflin in the nucleus, the ratios of ALG-2:peflin noted in Figure 4G are probably significantly higher outside the nucleus, with likely an excess of ALG-2 in the cytoplasm. However, my findings indicated a higher concentration of peflin in the nucleus of NRK cells compared with a previous report in Jurkat cells (Kitaura et al., 2001). Nonetheless, the labeling was specific for endogenous peflin since peflin siRNA transfection reduced all types of labeling (Figure 5A, third row, right column). Peflin cytosolic puncta noticeably co-localized with the ALG-2 cytosolic puncta previously

identified as ERES (la Cour et al., 2007; Shibata et al., 2007; Yamasaki et al., 2006), in these experiments also marked by sec13-GFP. I found that 95% of ERES defined by sec13-GFP were positive for ALG-2 and that the vast majority of ERES (>75%) were positive for both ALG-2 and peflin (supplemental Figure 1, columns 1 and 7). To determine the interdependence of peflin and ALG-2 for localization at ERES, I manipulated their expression levels as in Figure 4 and then quantified the labeling intensity of the two proteins specifically at ERES as defined by a sec13-GFP marker. KD of ALG-2 removed peflin from ERES (Figure 5B, bars 1 vs. 2) as expected due to the co-depletion phenomenon documented in Figure 4. However, when ALG-2 was depleted, over-expression of peflin did not restore it to ERES (Figure 5B, columns 1 vs. 3), though peflin over-expression greatly increased peflin at ERES in the presence of ALG-2 (Figure 5B, columns 1 vs. 5). ALG-2 targeting to ERES, on the other hand, did not depend upon, but yet was buffered by peflin. Peflin depletion greatly enhanced ALG-2 targeting to ERES (Figure 5C, columns 1 vs. 3), and peflin over-expression reduced it (Figure 5C columns 1 vs. 4). Targeting of the outer COPII coat subunit sec13-GFP as indicated by the intensity of accentuated spots (Figure 5D) mirrored the transport effects demonstrated in Figure 4A and extended the result reported earlier for Sec31A (Rayl et al., 2016). That is, KD of peflin increased COPII targeting, potentially causing the observed increased transport, while peflin over-expression reduced COPII targeting, potentially inhibiting transport. While accentuated spots decreased and increased with peflin over-expression and KD the total integrated fluorescence intensity of GFP-sec13 per cell, measured in the same set of cells, did not significantly change (Figure 5E), arguing that the effects were due to coat localization changes rather than significant changes in coat expression.

The targeting data indicates that peflin binds ERES through ALG-2 as part of an ALG-2-peflin complex, most likely the heterodimer species previously described (Kitaura et al., 2001). However, since removal of peflin increases ALG-2 at ERES, ALG-2 must also bind in other states, most likely the previously described homo-dimer for which a crystal structure is available with bound sec31A peptide (Takeshi et al., 2015). The high secretion caused by the lack of peflin and the low secretion caused by excess peflin are approximately equally above and below, respectively, the secretion with depletion of both proteins (Figure 4; height of column 4 or 6 is

about mid-way between that of columns 2 and 3); this suggests that cytosolic peflin does not simply act as an ALG-2 sponge that decreases transport by withdrawing stimulatory ALG-2 from ERES - if this were the case, peflin over-expression could never inhibit transport below the level seen upon depletion of both proteins. Rather, peflin-containing ALG-2 species appear to themselves inhibit transport.

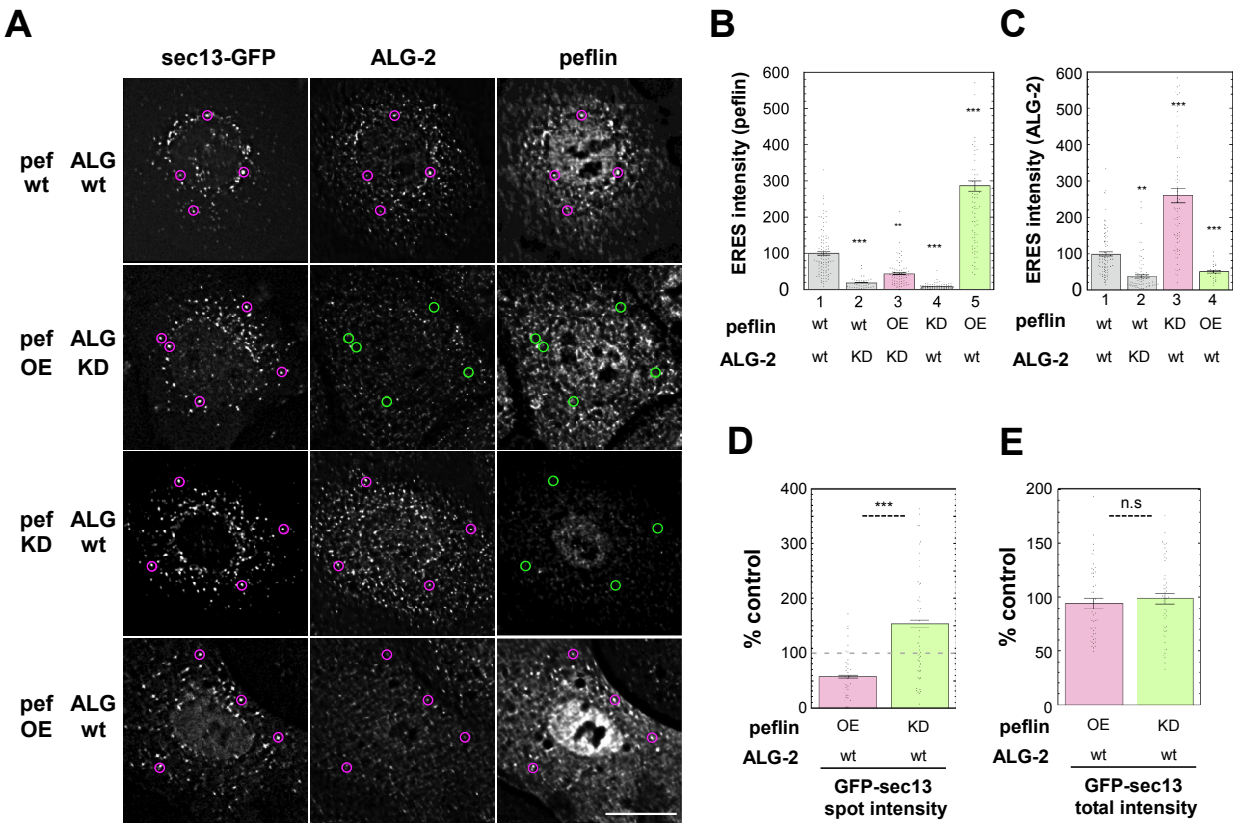

Figure 5. Peflin-ALG-2 complexes localize to ER exit sites via ALG-2, competing with other ALG-2 complexes. NRK cells were transfected with GFP-sec13 and control or specific siRNAs and an untagged rat over-expression construct for peflin (1 µg DNA). **(A)** Deconvolved widefield immunofluorescence images of cells labelled with sec13-GFP, ALG-2 and peflin. Magenta circles highlight ERES containing peflin or ALG-2 that co-localizes with GFP-sec13, while green circles note the absence of co-localization with GFP-sec13. Transfection conditions are specified to the left of images. Image scale bar; 20 micrometers. Note: I believe a subset of ALG-2 spots may be inauthentic, since some bright spots are not reduced by siRNA and these are much less likely to co-localize with Sec13 or peflin. Spots visible in the GFP-sec13 channel were defined as ERES. **(B)** Total intensity values of peflin colocalizing with ERES. Each point represents a single cell. Transfection conditions are specified below the graph and significance levels compared to column 1 are indicated above. Standard error is shown for each condition. **(C)** Total intensity values of ALG-2 colocalizing with ERES. **(B, C)** One-way ANOVA as for Figure 4A. **(D)** Total spot intensity of GFP-sec13 in conditions with increased or decreased peflin expression levels, expressed as percent of control. **(E)** Total fluorescence intensity of GFP-sec13 in the same images as D. **(D, E)** Unpaired Student's T-test with unequal variance; same p-value significance symbols as used in Figure 4A.

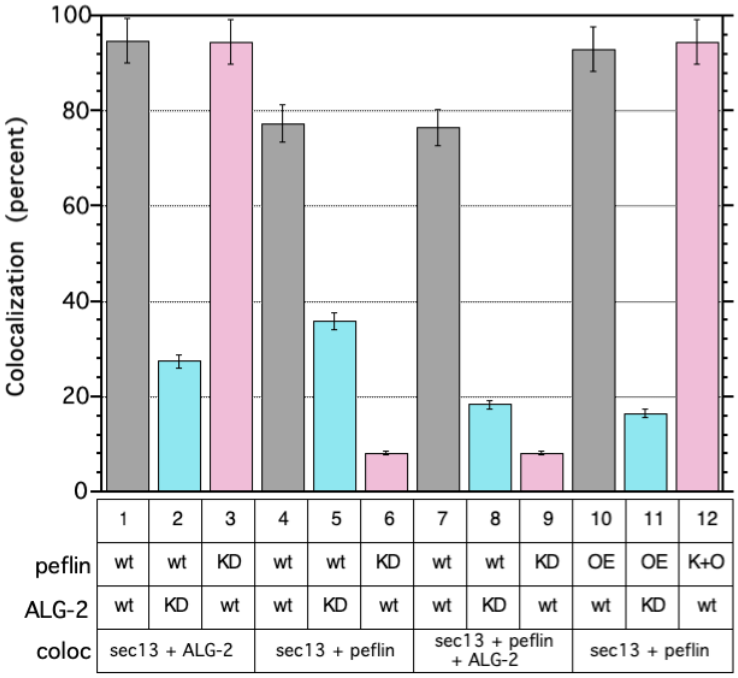

Supplemental Figure 1.Manual co-localization analysis for the experiment shown in Figure 5. Methods: Deconvolved images from ~25 transfected cells containing in focus GFP-Sec13 labeling at ER-exit-sites were randomly selected, and the background labeling was removed by defining a dark extracellular area of the image as zero. A GFP-sec13 object binary image mask was generated in Fiji by auto-thresholding using the Renyi Entropy method, which consistently captured the brightest GFP-sec13 spots. Each of these objects were then tested by eye for co- localization with spots in the ALG-2 and/or peflin channel with overlap scored as positive for co- localization. The percentage of bright ALG-2 and/or peflin objects that overlapped with ERES spots was directly calculated from this analysis for each cell, and the values above represent means of ~25 cells per condition. Mean ± SEM is shown for each condition.

3.2.3 ALG-2 Can Either Stimulate or Inhibit ER-to-Golgi Transport, Activities Buffered by Peflin

Figure 4A, columns 1 vs. 5, indicated that ALG-2 over-expression did not lead to significant changes in the ER export rate. This did not fit with other data. For example, since over-expression of ALG-2 should favor ALG-2 homomeric species over ALG-2-peflin hetero-complexes, as does a peflin KD, I wondered why ALG-2 over-expression did not stimulate transport. Thus, I titrated NRK cell transfections with 0.3, 1, and 3 micrograms of wildtype untagged ALG-2 construct DNA, and as shown in Figure 6A, black circles, these transfections resulted in 8-, 15- and ~25-fold over-expression of ALG-2 relative to control, demonstrating a titration of ALG-2 expression in individual cells. Figure 6B, black circles, then demonstrates that 8-fold over-expression stimulated transport by over 20%, 15-fold over-expression (the dose employed in Figure 4A) had no significant effect, and ~25-fold over-expression inhibited transport by 20%. The same titration performed in cells depleted of peflin (magenta circles) resulted in similar biphasic effects, except that the inhibition was more potent and more severe relative to no over-expression (a drop from ~155% to ~95% of control). This experiment indicates that the relationship between ALG-2 and the secretion rate is complicated by several competing activities. First, it indicates that ALG-2 can both stimulate and inhibit transport, with stimulation giving way to inhibition as fold over-expression increases. Second, it indicates that there is both a stimulatory and inhibitory role for ALG-2 that are independent of peflin, in addition to the inhibitory role of ALG-2-peflin hetero-complexes suggested in Figures 4A and 5D. Third, it indicates that ALG-2-peflin hetero-complexes, though inhibitory, must buffer against the other inhibitory activity of ALG-2, revealed in this experiment, that is independent of peflin. Thus Figures 4-6, completed at steady-state Ca^{2+}, suggest at least three distinct activities for ALG-2 and peflin complexes: an inhibitory but buffering role for ALG-2-peflin hetero-complexes, a stimulatory role for ALG-2 without peflin, and an inhibitory role for ALG-2 without peflin.

Since ALG-2 over-expression in the above experiments could potentially alter Ca^{2+} homeostasis due to ALG-2's ability to bind Ca^{2+} in the micromolar range, or interact with other Ca^{2+}-related proteins, I performed control experiments to examine whether ALG-2 over-

expression was accompanied by measurable changes in Ca^{2+} handling. Here, I used transfection with mRuby2-ALG-2 followed by analysis of equal numbers of transfected and non-transfected cells within the same fields during live Ca^{2+} imaging with FURA-2. Only bright red cells were analyzed as over-expressing cells, and no attempt was made to distinguish effects at different levels of over-expression. I chose 1 mM bradykinin as a Ca^{2+} agonist because it produces simple, immediate, synchronous responses in NRK cells that are readily quantified. As shown in Figure 6D, a very similar range of response strengths and kinetics were observed in both untransfected and ALG-2-transfected cells. Only rarely did any cells of either type produce subsequent Ca^{2+} oscillations. Furthermore, there was no significant difference in the percentage of cells that exhibited an immediate response to agonist between wildtype and ALG-2 OE cells, when results from three experiments were combined (Figure 6E). Furthermore, the quantity of Ca^{2+} released, estimated by peak height minus baseline (DR), was not significantly different between the two types of cells (Figure 6F). Nonetheless, I did detect a slight but significant decrease in the baseline cytosolic Ca^{2+}, demonstrating that ALG-2 over-expression does measurably buffer cytosolic Ca^{2+} (Figure 6G), and could potentially buffer Ca^{2+} transients as well. On the other hand, I conclude that ALG-2 OE did not grossly perturb the releasable Ca^{2+} store or activity of ER Ca^{2+} channels. This information points to caution interpreting the ALG-2 over-expression study and to future studies of Ca^{2+} signaling employing PEF protein over-expression, since effects on secretion per se cannot be completely dissociated from effects on Ca^{2+} buffering.

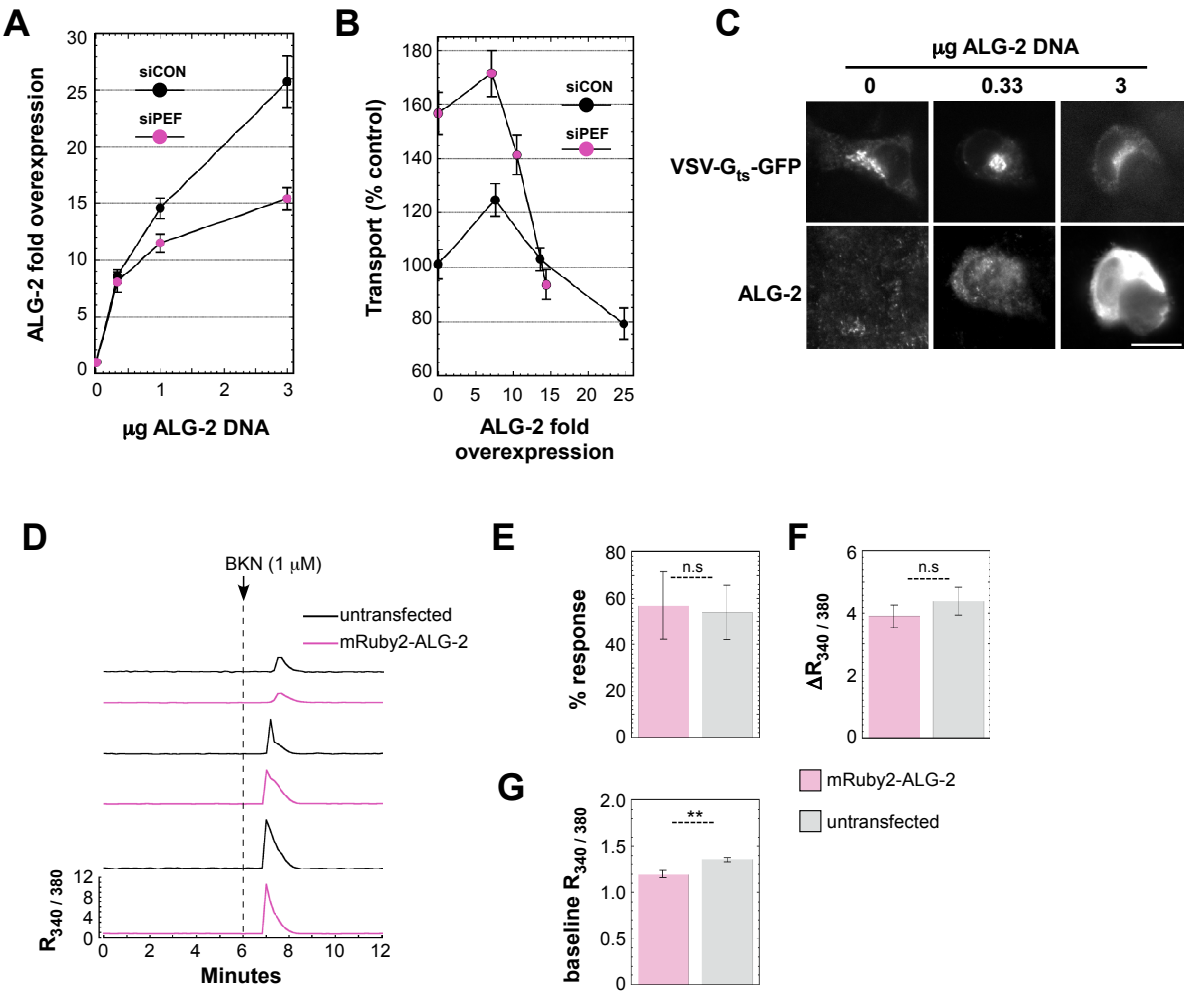

Figure 6. ALG-2 can inhibit or promote ER-to-Golgi transport independently of peflin. NRK cells transfected with control or peflin siRNAs were then re-transfected with VSV-G_{ts045} DNA and differing amounts of ALG-2 DNA. Following immunofluorescence labeling, each condition was assayed for mean ALG-2 florescence and accompanying transport index on a per-cell basis. **(A)** Micrograms of ALG-2 DNA used in transfections versus fold OE determined by immunofluorescence quantitation. Fold OE for each cell was calculated as its own ALG-2 intensity divided by the mean intensity of untransfected cells. Mean ± SEM (N~100) is shown for each point. **(B)** The mean ER-to-Golgi transport value correlated to the mean ALG-2 fold OE level. (**C)** Example widefield images of individual siCON cells for select conditions. **(D)** Representative single-cell cytosolic Ca^{2+} traces measured using FURA-2 in NRK cells. Traces are from the same coverslip, on which both mRuby2-ALG-2-transfected and non-transfected cells were analyzed in parallel. 1 mM BKN was added after 6 min of perfusion in growth medium. Non-responding cells were present but are not shown. **(E)** Quantitation of the percentage of cell traces per coverslip that showed a Ca^{2+} increase within 2 min of adding BKN. N=3 runs, 40 cells per run per condition. **(F)** Quantitation from responding cells only, of maximum peak height minus mean baseline value prior to BKN addition; N=60 cells per condition, combined from 3 runs. **(G)** Mean baseline value for 5 min prior to BKN addition; N=60 cells per condition, combined from 3 runs. **(E-F)** Unpaired Student's T-test with unequal variance; same p-value significance symbols as used in Figure 4A. Image scale bar; 20 micrometers.

3.2.4 Peflin-ALG-2 Complexes Affect ER Export Similarly for Multiple COPII Client Cargos, but not Bulk Flow Cargo, and Influence ER Stress

A recent study reported that in an osteosarcoma cell line, peflin depletion inhibited ER-to-Golgi transport of collagen I, implying that peflin was required for collagen export from the ER (McGourty et al., 2016) (Chapter 1 and Table 1). Since my results have instead suggested a suppressive role for peflin in VSV-G export, I investigated whether peflin may have opposite effects on different actively sorted cargoes. To address this, I expressed different cargoes in NRK cells and tested the effects of peflin depletion. These cargoes are schematized in Figure 7A. As seen if Figure 7B, compared to VSV-G-GFP, export of GFP-collagen I was even more strongly stimulated by peflin depletion (columns 1 and 2 vs. 3 and 4), supporting a suppressive effect of peflin under normal conditions. Since both VSV-G_{ts045}-GFP and collagen export were synchronized by incubation at a restrictive temperature followed by a shift to permissive temperature, I wanted to rule out that the temperature shift was involved in the suppressive effects of peflin. I created novel reporter constructs containing a conditional aggregation domain, F_M4, that aggregates in the ER and prevents export until a small molecule drug, AP21998, is provided (Rivera et al., 2000), causing synchronous ER export. The first construct included GFP as a luminal domain followed by F_M4 and the VSV-G transmembrane domain (GFP-F_M4-VSV-G_{tm}) which contains a di-acidic COPII sorting motif on the cytosolic surface. The second construct was similar but included the GPI anchor from CD55 at the C-terminus instead of a transmembrane domain (GFP-F_M4-GPI). GPI anchors function as an export sequence recognized and sorted in a p24-dependent manner (Bonnon et al., 2010). Both constructs, when triggered by ligand AP21998 were actively transported from the ER to the Golgi over a 10-minute time course. For both constructs, peflin depletion caused a highly significant increase in ER-to-Golgi transport (Figure 7, columns 5-8). A third construct, GFP-F_M4-GH (Gordon et al., 2010), was fully luminal, contained human growth hormone, and lacked any ER export sequence. Peflin depletion caused a significant *decrease* in ER export of this bulk flow construct. This result implies that peflin depletion does not act simply to accelerate vesicle production, but rather stimulates COPII function broadly--including its sorting function. It is also consistent

with a recent study demonstrating that COPII sorting works in part by exclusion of proteins that are not actively included (Ma et al., 2017). In summary, Figure 7 establishes that the stimulatory effects of peflin depletion on transport are not restricted to high temperature-synchronized reporter cargoes, and that four actively sorted cargoes, VSV-G_{ts045}-GFP, GFP-collagen I, GFP-F_M4-VSV-G_{tm} and GFP-F_M4-GPI, containing three distinct ER export signals - but not bulk flow cargo - are exported more efficiently when peflin is depleted in NRK cells. Thus peflin, it appears, is a bona fide suppressor of COPII function.

NRK cells may not be an adequate model for ER-to-Golgi transport for certain cargoes, for example collagen I, which require specific cargo adaptors and modified vesicles for efficient export (McCaughey et al., 2016; Raote et al., 2018; Saito et al., 2009; Wilson et al., 2011). The vast majority of collagen I is secreted by fibroblasts, osteoblasts and chondrocytes. To address whether peflin also suppressed secretion of collagen I in cells whose normal function includes secretion of collagen I in abundance, I tested the effects of peflin depletion on endogenous collagen I secretion in Rat2 embryonic fibroblasts. The collagen I precursor, procollagen I folds inefficiently in the ER and mis-folded procollagen undergoes degradation by non-canonical autophagy at ERES (Omari et al., 2018). To be certain that non-secretory collagen fates potentially affected by peflin expression did not interfere with my assay for ER-to-Golgi transport, I monitored TCF of endogenous collagen I in addition to the ER-to-Golgi transport index. I measured ER-to-Golgi transport and collagen I TCF in the same cells with and without peflin depletion, and found that peflin depletion increased the ER-to-Golgi transport index by 75% (Figure 8A) but had no significant effect on collagen I TCF (Figure 8B). As shown in Figure 8C, collagen I TCF was quantitative and reflected collagen I content since titration of cells with a collagen I-specific siRNA resulted in distinct, decreasing TCF values. Furthermore, Western blotting demonstrated an 83% depletion of peflin in Rat2 cells (Figure 8E). Together these data indicate that peflin depletion dramatically increases transport of endogenous collagen I from the ER to Golgi in fibroblasts and does not appear to affect collagen degradative pathways.

So far I have shown that dramatically increasing the ALG-2 to peflin expression ratio can accelerate secretion of multiple cargoes. This suggests that decreasing peflin expression or

another means of favoring the positive activity of ALG-2 could potentially relieve ER stress. To begin testing this idea, I utilized porcine aortic endothelial cells (PAECs), primary cells that undergo cellular ageing and senescence after passaging five times (P5) *in vitro*. As recently demonstrated (Madreiter-Sokolowski et al., 2019), P5 PAECs display ER Ca^{2+}-driven mitochondrial overload, oxidative stress, as well as profoundly increased UPR signaling and expression of CHOP, a UPR transcription factor involved in the transition from UPR to apoptosis (Hu et al., 2019). Under these Ca^{2+} stress conditions, I found by quantitative reverse-transcription PCR (qRT-PCR) that a 60% KD of peflin, using siRNA, resulted in a specific 45% reduction in expression of the UPR target gene GRP78, and a 55% reduction of CHOP (Figure 8F). This demonstrates that peflin expression exacerbates life-threatening ER stress in aging endothelial cells, and that activation of secretion by ALG-2 can in principle relieve this burden.

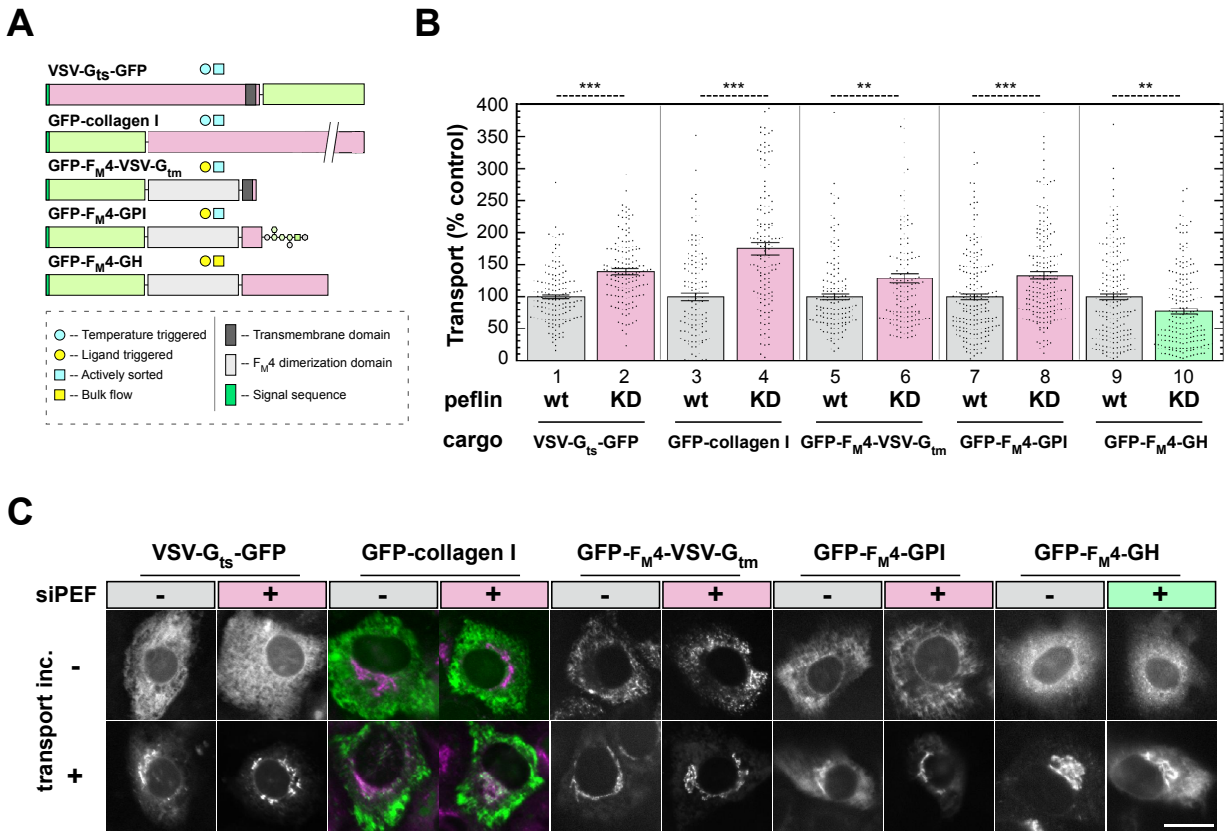

Figure 7. Peflin suppresses ER export of multiple actively exported cargos in NRK cells. (A) Schematic of cargo constructs used in B and C**. (B)** The initial rate of ER-to-Golgi transport was determined as in Figure 4 for NRK cells transfected with the indicated constructs in the presence of control or peflin siRNA. For VSV- G_{ts045}-GFP and GFP-collagen I, transfected cells were placed at 41 ^{o}C to build up cargo in the ER. Transfer of cells to 32 ^{o}C provided a synchronous wave of transport to the Golgi. For GFP-F_M4-VSV-G_{tm}, GFP- F_M4-GPI, and GFP-F_M4-GH, cargo was accumulated in the ER under normal growth conditions at 37 ^{o}C, and transport was initiated by addition of the F_M4-specific ligand. Mean ± SEM is shown for each condition, as well as approximate p values for the indicated unpaired T tests. **(C)** Example widefield images of individual cells for select conditions. For GFP-collagen I, a merge of GFP-collagen I and the Golgi marker Mannosidase II is shown since otherwise it was difficult to identify the Golgi following transport; all other images show the GFP channel only. Image scale bar; 20 micrometers.

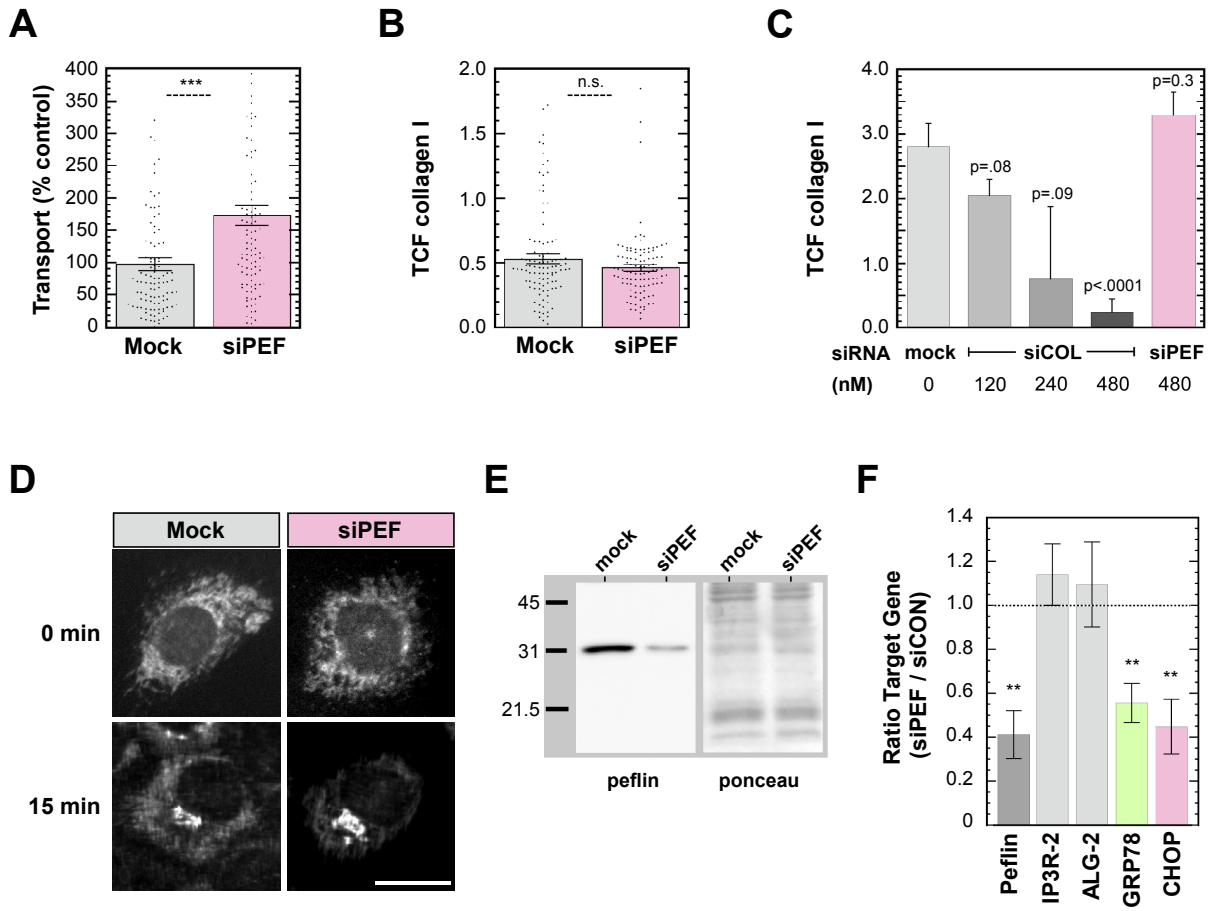

Figure 8. Peflin expression suppresses ER export of endogenous collagen I in Rat2 fibroblasts and facilitates pro-apoptotic UPR signaling in PAECs. Rat2 cells were transfected with the plasma membrane marker pCAG-mGFP in the presence or absence of peflin siRNA. Following growth at 41 °C for 24 h, cells were shifted to 32 °C with ascorbate-supplemented medium for 15 min to allow transport prior to fixation. **(A)** ER-to-Golgi transport assay employing collagen I immunofluorescence intensity in the ER and Golgi. **(B)** The same cells from A were analyzed for TCF of collagen (Chapter 2). **(C)** Validation of immunofluorescence assay for TCF of collagen I. Cells were transfected with different concentrations of collagen I siRNA or an siRNA for peflin. Standard error and p values (vs. mock) is shown for each plot. **(D**) Example widefield images of collagen I immuno-labelling for select conditions in individual cells. **(E)** Western immunoblot on cells from part A and B, demonstrating an 83% depletion of peflin. **(F)** Peflin depletion in P5 PAECs reduces GRP78 and CHOP expression. Senescent P5 PAECs were subjected to control or peflin siRNA transfection and grown under standard conditions for 3 days prior to lysis and analysis by qRT-PCR for expression of several mRNAs as indicated beneath the plot. Results are shown as the ratio of mRNA expression in siPEF cells to that in siCON cells for each mRNA. Bars show mean ± SEM for 3 complete experiments conducted on different days using cells from different donors. p values indicate probabilities that the obtained ratios are equal to 1.0 (the null hypothesis). Image scale bar; 20 micrometers.

CHAPTER 4:

CALCIUM REGULATION OF ER-TO-GOLGI TRANSPORT BY ALG-2

(this chapter has been published: (Sargeant et al., 2021))

4.1 INTRODUCTION

Like many of the vesicle trafficking steps discussed in Chapter 1, preliminary evidence of regulatory roles for Ca^{2+} in ER-to-Golgi transport are prominent. Recent work demonstrates a requirement for luminal Ca^{2+} stores at a stage following cargo folding/assembly, perhaps through the entry of Ca^{2+} into the cytoplasm, where it binds and activates the vesicle budding, docking, and/or fusion machinery (Bentley et al., 2010; Helm et al., 2014). Depletion of luminal Ca^{2+} via SERCA inhibitors leads to significantly reduced transport and to the buildup of budding and newly-budded COPII vesicles and vesicle proteins (Bentley et al., 2010; Helm et al., 2014). The precise way Ca^{2+} actuates these effects continues to be elusive, but part of the answer may lie with the PEF protein Ca^{2+} binding adaptors. We know from Chapter 1 that ALG-2 binds peflin and acts as a Ca^{2+} sensor at ERES, stabilizing association of sec31 with ERES through direct binding to a 12-amino acid sequence on the sec31A PRR region (la Cour et al., 2007; Shibata et al., 2007, 2010; Yamasaki et al., 2006). From Chapter 3, we know that ALG-2 and peflin can produce multiple regulatory states at ERES, promoting or attenuating ER-to-Golgi transport. Therefore, ALG-2 and peflin clearly have the capacity to regulate constitutive vesicle trafficking in response to Ca^{2+} signals—yet this feat has never been observed in response to physiological Ca^{2+} fluxes in a realistic cellular context.

In this chapter, I examine the roles of ALG-2 and peflin in response to cytoplasmic Ca^{2+} signals elicited by calcium-mobilizing agonists in NRK and PC12 cells. I find that, in response to short bursts of agonist-driven Ca^{2+} signaling, ALG-2 increases outer COPII coat targeting to ERES and stimulates transport, a finding supported by a recent report wherein ER Ca^{2+} release stimulated the ER-to-Golgi transport of a bulk flow cargo in HeLa cells (Rauter et al., 2020). This Ca^{2+}-driven response could be imagined to propel stimulated cells to proliferate and/or replenish exhausted endocrine or exocrine secretory vesicles. On the other hand, I also found more persistent Ca^{2+} signalling decreased outer COPII coat targeting to ERES and caused ALG-2 to markedly slow ER export. This novel physiological response could represent a protective mechanism against excitotoxicity or infection. I conclude that Ca^{2+} signals and PEF protein

complexes together represent a true regulatory system of constitutive transport and are able to adjust the secretion rate in response to physiological stimuli.

4.2 RESULTS

4.2.1 In NRK Cells, ALG-2 Depresses ER Export in Response to Sustained Ca^{2+} Agonist Stimulation

Since peflin and ALG-2 are regulated by Ca^{2+} binding in NRK cells, I tested whether their ability to regulate ER-to-Golgi transport was affected by cytoplasmic Ca^{2+} signaling. Histamine receptors present on many cell types activate phospholipase C via G_Q to stimulate Ca^{2+} release by IP3 receptor channels on the ER. As shown in Figure 9A (black circles), 10 minutes of ER-to-Golgi transport initiated after increasing times of exposure to histamine indicated that initially and for up to 30 minutes of exposure, no significant modulation of transport occurred. However, by 60 minutes of exposure, ER-to-Golgi transport was significantly reduced, with continued reduction for up to 150 minutes, wherein transport was reduced by 40% below basal. Thus, NRK epithelial cells respond to sustained Ca^{2+} agonist exposure by sharply curtailing ER secretory output, a new phenomenon I termed Ca^{2+}-activated depression of ER export (CADEE).

We next tested the involvement of PEF proteins in the down-modulation. Significantly, the Ca^{2+}-dependent modulation of transport was entirely dependent upon the presence of PEF proteins, since KD of ALG-2 (which also causes a co-KD of peflin, Figure 4, C and D) prevented any significant change in transport over the same timecourse (Figure 9A, green circles). The PEF protein-dependent activation mechanism, however, did not require peflin, since peflin KD (which leaves at least 70% of ALG-2 intact, and increases its presence at ERES, Figures 1-2) did not prevent a histamine-activated decrease in ER-to-Golgi transport (Figure 9A, magenta circles). When depleted of peflin, however, ER export always remained well above control levels, indicating that although peflin is not the trigger, it still exerts a strong suppressive role throughout the Ca^{2+} signaling effect. Furthermore, Figure 9C demonstrates that over-expression of peflin inhibited transport (Figure 9C, columns 1 vs. 3), as shown earlier, but also protected

against any inhibitory effects of histamine signaling (Figure 9C, columns 3 and 4). Together these results showed that the inhibitory effect of ALG-2-peflin hetero-complexes is an independent inhibitory state that can compete with a distinct, inhibitory ALG-2 activity during histamine signaling. One possibility is that histamine signaling activated the same inhibitory activity of ALG-2 observed when ALG-2 was over-expressed at steady-state Ca^{2+}, which was also independent of peflin yet buffered against by ALG-2-peflin hetero-complexes (Figure 6B).

To investigate the nature of the Ca^{2+} signals that lead to CADEE, I performed FURA-2 Ca^{2+} imaging in wildtype NRK cells. As shown in Figure 9D by 4 representative single-cell traces, 100 mM histamine led to continuing Ca^{2+} oscillations for the duration of the recording period, 19 minutes. Persistent Ca^{2+} oscillations in the same field of confluent NRK cells often display synchronous activity (gray arrows). Since 100 mM histamine, in contrast to 1 mM bradykinin (Figure 9D), led to persistent Ca^{2+} oscillations, perhaps the persistence of Ca^{2+} stimulation is important for the time-dependent induction of CADEE observed in Figure 9A. This is also supported by the observation that bradykinin produces CADEE when applied in very low amounts (100 pM-1nM; not shown), but does not do so when using high concentrations which, as shown in Figure 9D, result in immediate downregulation after an initial response. One caveat to the experiment in Figure 9C is that peflin OE, through over-abundance of cytosolic EF hands, may have dampened the actual Ca^{2+} concentrations somewhat (see Figure 6C-G for ALG-2 OE). Due to the inability to produce a functional fluorescent peflin construct (our experience and (McGourty et al., 2016), this was not directly tested.

While the histamine effect was repeatable numerous times, I found that NRK cells would occasionally respond not at all to histamine, a phenomenon that tended to occur several experiments in a row, perhaps indicating that specific lots of FBS or other unknown environmental factors might be affecting histamine responsiveness. This gave us the opportunity to directly assess the involvement of a single receptor system in the CADEE phenomenon. As shown in Figure 9E, in a single experiment NRK cells that were unable to modulate secretion in response to 50 μM histamine produced significant CADEE when transfected with the wildtype H1 histamine receptor, considered the main histamine receptor

in kidney (Veglia et al., 2015). Furthermore, the self-cleaving mCherry/H1R construct allowed us to distinguish transfected and untransfected H1R cells side-by-side during Ca^{2+} imaging; I found that H1R over-expression dramatically increased the sensitivity of NRK cells to 50 mM histamine (Figure 9F). The experiments in Figures 6E and F defined a receptor system leading to CADEE in NRK cells.

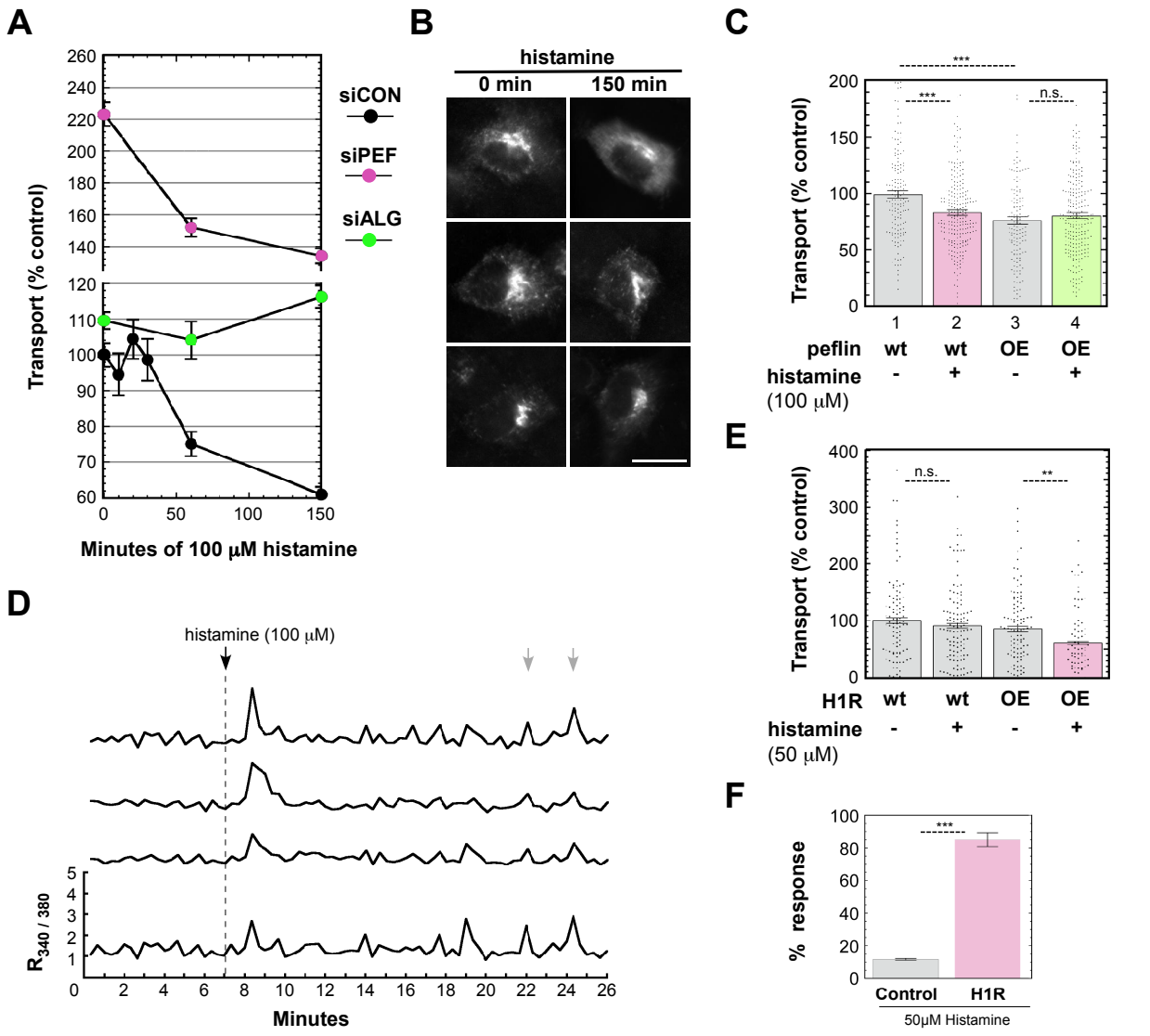

Figure 9. Ca^{2+}-activated depression of ER export is mediated by ALG-2 independently of peflin. (A) NRK cells were transfected with VSV-G_{ts045}-GFP along with control, ALG-2, or peflin siRNAs. Transfected cells were exposed to 100 μM histamine for 0-150 min at the non-permissive temperature prior to shift to the permissive temperature for 10 min, and transport was quantitated as in Figure 4A. Mean ± SEM is shown for each point; N~150 cells per condition. **(B)** Example widefield images of individual cells for select conditions. **(C)** The rate of ER-to-Golgi transport following peflin OE (1 μg DNA) and/or 100 μM histamine exposure for 150 min was determined as in Figure 4. **(D)** Representative single-cell cytosolic Ca^{2+} traces measured using FURA-2 in wildtype NRK cells. Traces are from the same coverslip. 100 mM histamine was added after 7 min of perfusion in growth medium. Non-responding cells were present but are not shown. Gray arrows mark synchronous Ca^{2+} oscillations. **(E)** Transport index for NRK cells transfected with VSV-G alone ("wt") or with VSV-G and a self-cleaving mCherry/H1R construct ("OE"). Only cells with red fluorescence and VSV-G fluorescence were analyzed for transport in the right two bars. Cells were exposed to +/- 50 μM histamine for 150 min prior to transport assay. **(F)** Single-cell cytosolic Ca^{2+} traces were obtained using FURA-2 in NRK cells, either untransfected or transfected with

mCherry/H1R, with 50 mM histamine added half-way through the runs. Shown is quantitation of the percentage of cell traces per coverslip that showed a clear Ca^{2+} increase within 2 minutes of adding histamine. N=4 runs (control) and 2 runs (transfected). Transfected cells were included only if displaying bright red fluorescence. **(C, E, F)**. Unpaired Student's T-test with unequal variance; same p-value significance symbols as used in Figure 4A. Image scale bar; 20 micrometers.

4.2.2 Sustained Ca^{2+} Signaling Decreases Targeting of the COPII Outer Coat and Increases Targeting of Peflin to ERES.

To investigate the mechanism of the Ca^{2+}-activated depression of ER export phenomenon, I monitored: outer coat subunits, peflin, ALG-2, and cargo at ERES by immunofluorescence microscopy in NRK cells with and without histamine treatment. Figure 10 parts A and B show representative images with different markers which, when quantitated revealed several significant changes. Most notably, at ERES containing ALG-2 and peflin, the outer coat labeling decreased in intensity. For example, using spots that contain ALG-2 and peflin to define ERES of interest, we found that GFP-sec13 intensity decreased by 40% at those ERES after histamine treatment (Figure 10C, left). This effect was due to a real change in sec13 intensity and was not a result of a change in the area of the regions of interest interrogated (Figure 10C, right). A similar 35% decrease was observed when measuring endogenous sec31A intensity using ALG-2 and the cargo VSV-G to define the measured ERES (Figure 10D), extending the trend to both subunits of the outer coat. If CADEE involved decreased targeting of outer coat to ERES by ALG-2, one prediction would be decreased co-localization of outer coat and ALG-2. Figure 10E demonstrates that there was a 40% decrease in GFP-sec13/ALG-2 overlap upon histamine treatment. Furthermore, the observed decrease in outer coat/ALG-2 overlap was not due to a detectable decrease in ALG-2 (data not shown), reinforcing the significance of decreased outer coat targeting (Figure 10C and D) as the driver of decreased co-localization. While the presence of ALG-2 under steady-state conditions has been implicated in stabilization of the outer coat (la Cour et al., 2007; Shibata et al., 2007, 2010; Yamasaki et al., 2006), my results may imply a role, under sustained Ca^{2+}-signaling conditions, in which ALG-2 destabilizes the outer coat instead. Interestingly, despite the decrease in outer coat, I did not observe a decrease in GFP-sec13-peflin co-localization in the same cells (data not shown). This unexpected finding appeared to be due to a Ca^{2+}-induced redistribution of peflin that counteracted the effects on co-localization of lost outer coat. Figure 10F, left, shows that cytoplasmic peflin spot intensity increased by 40% in the same cells in which the destabilized outer coat was documented. In these same cells, however, I detected a statistically significant

15% decrease in nuclear peflin spot intensity (Figure 10F, right). It is unknown whether peflin release from the nucleus is a passive result of, as opposed to a driver of, increased peflin targeting to ERES. Note that peflin, per se, is not required for CADEE induction but that during CADEE, peflin contributes substantially to the low transport values observed (Figure 9A). I currently do not know the significance of increased peflin at ERES during CADEE, but note that peflin-bound ALG-2 seems to be a parallel inhibitory state (Figure 9C). In conclusion, the CADEE phenomenon is accompanied by destabilization of the COPII outer coat at ERES and increased peflin localization at these sites, both predicted to decrease the rate of ER export.

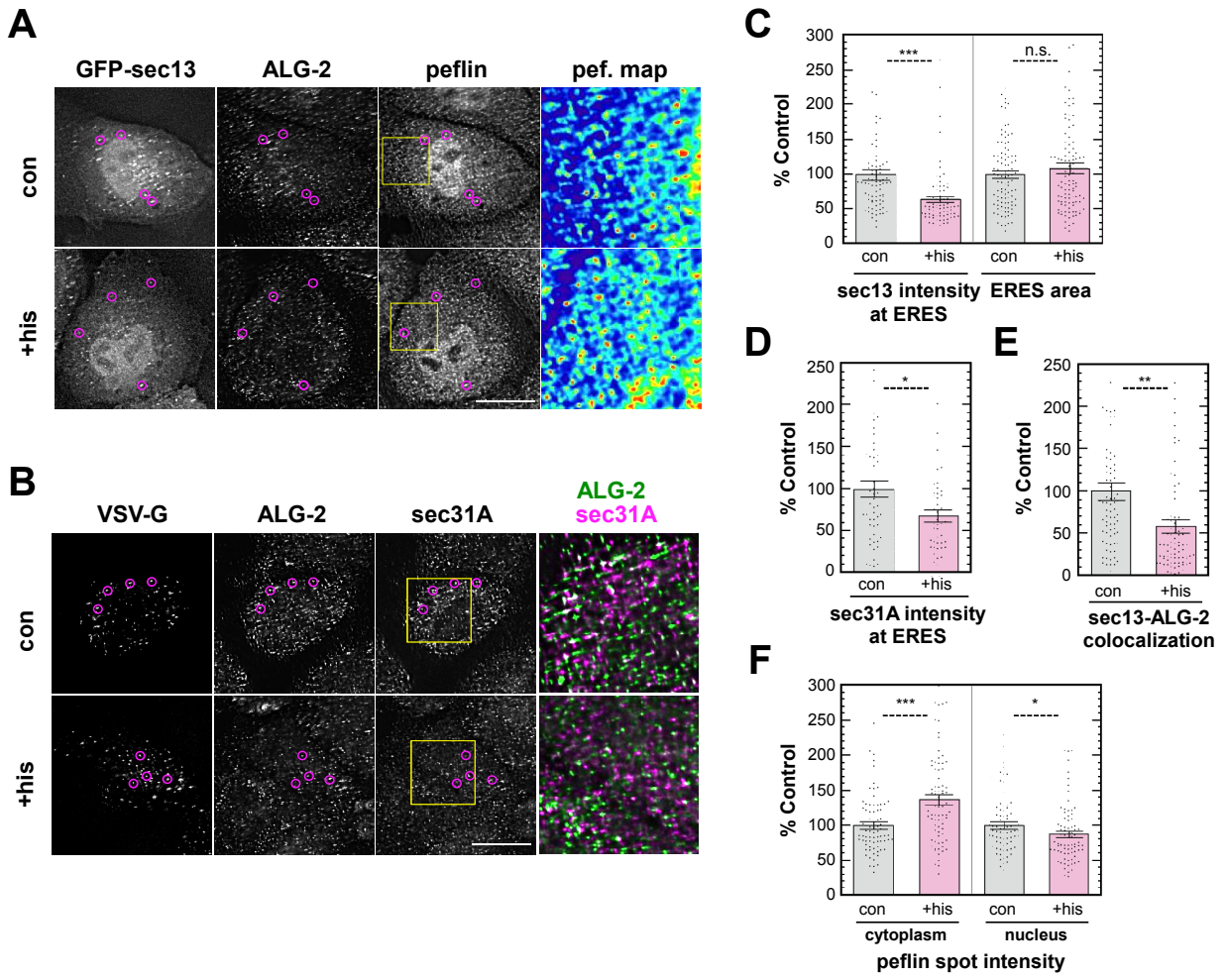

Figure 10. Histamine stimulation decreases outer COPII coat and increases peflin targeting to ERES. (A) NRK cells were transfected with GFP-sec13, treated with or without histamine for 2.5 h, fixed and immuno-labeled for endogenous proteins. Shown are representative deconvolved images. Magenta circles mark several ERES positive for all three markers. GFP-sec13 intensity was lower at ERES in histamine-treated cells, while peflin intensity was higher. Peflin heatmap panels illustrate that there are more yellow/red objects in the cytoplasm following histamine treatment. **(B)** NRK cells were transfected with the transmembrane cargo VSG-G_{ts045}, treated +/- histamine for 150 min at 41 °C, incubated for 45 s at 32 °C, fixed, immuno-labeled and displayed as in A. The conformation-specific VSV-G antibody used only recognizes assembled trimers. Sec31A intensity at ERES decreased upon histamine treatment, producing decreased co-localization with ALG-2, illustrated in the merged panels. Image scale bars; 20 micrometers. **(C)** Left, an ROI was generated using ALG-2/peflin-colocalized spots to mark ERES and used to interrogate mean intensity in the unmodified GFP-sec13 channel. Right, the area of spots that had colocalized ALG-2 and peflin. **(D)** Using an ERES ROI generated from colocalized ALG-2 and VSV-G_{ts045} spots, total intensity of sec31A was measured. **(E)** Shows the total area of spots that had both GFP-sec13 and ALG-2. **(F)** Left, Peflin total spot intensity of cytoplasmic peflin. Right, the same calculation was performed for peflin particles inside the nucleus. In all plots, binary image masks were used to measure intensities on the unmodified images (see Chapter 2 for details). Each dot represents data from a single cell, with the mean and SEM indicated.

4.2.3 ATP Elicits Functionally Distinct Effects on ER Export in NRK and PC12 Cells

Extracellular ATP was used as a Ca^{2+} agonist and found to elicit CADEE similarly to histamine. A dose-response curve for ATP in ER-to-Golgi transport is shown in Figure 11A. CADEE occurred maximally in doses close to 100 nM, while doses of 100 µM - a typical concentration in the literature for induction of Ca^{2+} signaling - resulted in little or no CADEE. This implied that the CADEE secretion response may depend upon on a defined Ca^{2+} signature or pattern during its induction. To investigate what the Ca^{2+} pattern associated with CADEE was, I recorded cytosolic Ca^{2+} signaling over a 40-minute period using FURA-2 cytosolic Ca^{2+} dye; cells were maintained at 37 ^{o}C in their regular medium during imaging. As shown in Figure 11B, which displays representative individual cell traces, 100 nM ATP elicited a small, or sometimes no immediate Ca^{2+} response. During the subsequent 10 minutes following ATP addition, Ca^{2+} oscillations became more frequent and larger. Following a 15-minute break from imaging, cells with oscillations following ATP addition continued to show oscillations, now with even greater frequency and intensity. This experiment demonstrates that once again CADEE was associated with sustained Ca^{2+} oscillations over many minutes.

To examine the generality of these phenomena, I titrated neuroendocrine PC12 cells with the Ca^{2+} agonist ATP using the same cargo and ER-to-Golgi transport assay as in NRK cells. As shown in Figure 12A, PC12 cells responded to ATP with the opposite response to that of NRK cells, constituting a Ca^{2+}-activated enhancement of ER export (CAEEE). The response to ATP involved an approximately 30% increase in ER export (as opposed to a 40% decrease in NRK cells) and was approximately 1 order of magnitude less sensitive to ATP, with a maximum near 1 mM ATP. Higher concentrations of ATP gave smaller effects on secretion as observed in NRK cells. To investigate the role of PEF proteins in the CAEEE response, I used ALG-2 siRNA. As shown in Figure 12B, PC12 cells depleted of PEF proteins did not change secretion in response to ATP, indicating that CAEEE, like CADEE, requires the correct complement of ALG-2 and peflin. Figure 12E demonstrates that the functional effects of depletion were obtained with a somewhat modest 51% depletion of ALG-2, and that as in other cells, there was co-depletion of peflin as well. One possibility to explain the differing responses to ATP between NRK and PC12

cells would be that in different cell types, ALG-2 responds to Ca^{2+} in different ways because of differences in secretory machinery. In support of this idea, as shown in Figure 4G, PC12 cells contain around half as much ALG-2 and are relatively depleted of peflin compared to NRK cells. However, another possibility would be that ATP produces distinct Ca^{2+} signaling intensities or patterns in NRK and PC12 cells, and ALG-2 responds to distinct signaling properties in different ways. To help distinguish these possibilities, I carried out studies of cytoplasmic Ca^{2+} signaling in PC12 cells as I did in Figure 11B for NRK cells. As shown in Figure 12D, 1 µM ATP produced an immediate surge of cytoplasmic Ca^{2+} followed by a significant diminution within a few minutes. Thereafter, clear Ca^{2+} oscillations were rare and widely interspersed. These data suggest that distinct intensities and/or durations of Ca^{2+} signaling may underlie the different ALG-2-dependent secretory responses to ATP in NRK (Figure 11) and PC12 (Figure 12) cells. Sustained Ca^{2+} signals are associated with CADEE while strong responses followed by diminution are associated with CAEEE.

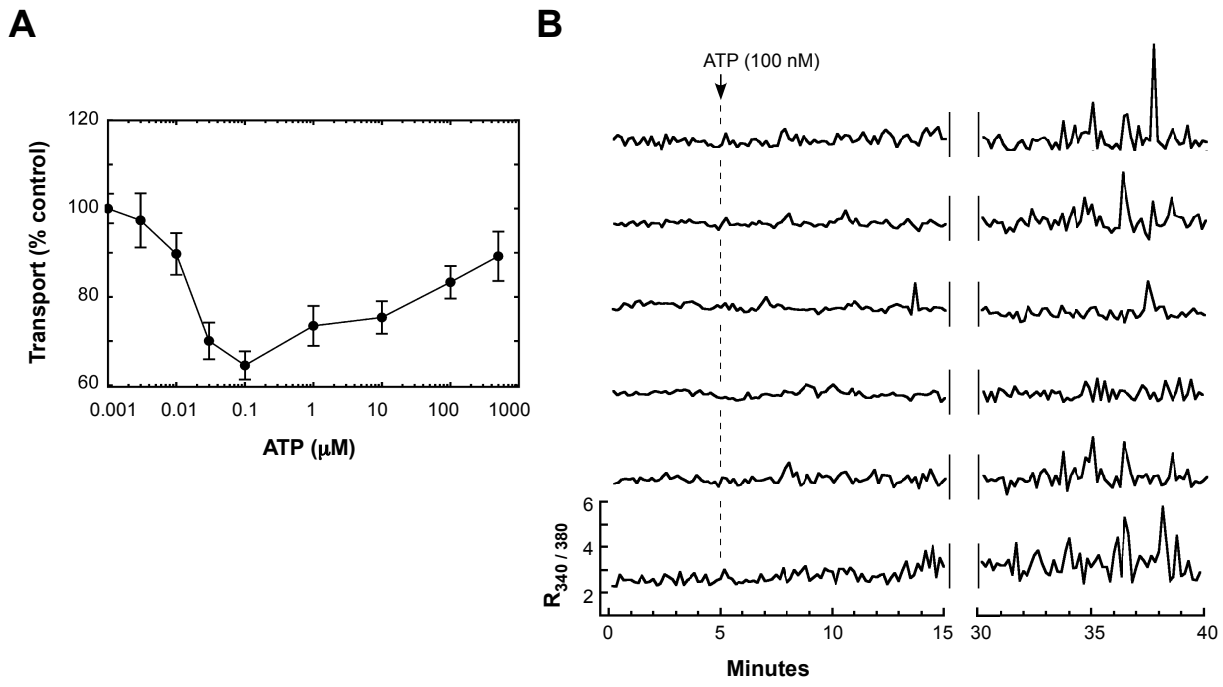

Figure 11. ATP elicits Ca^{2+}-activated depression of ER export and continuing Ca^{2+} oscillations in NRK cells. (A) NRK cells were transfected with VSV-G_{ts045} and treated with a range of ATP concentrations for 2.5 h at the non-permissive temperature prior to shift to the permissive temperature for 10 min, after which transport was quantitated as in Figure 4A. Mean ± SEM is shown for each point; N~100 cells per condition. **(B)** Representative single cell FURA-2 traces. NRK cells were loaded with FURA-2 AM prior to incubation at 37 °C on the microscope stage in their regular medium supplemented with 20 mM Hepes. A first round of imaging every 10 s for 15 min was conducted, with introduction of ATP by pipet at t=5 min. At t=30 min, a second round of imaging every 10 s for 10 min was conducted on the same field of cells.

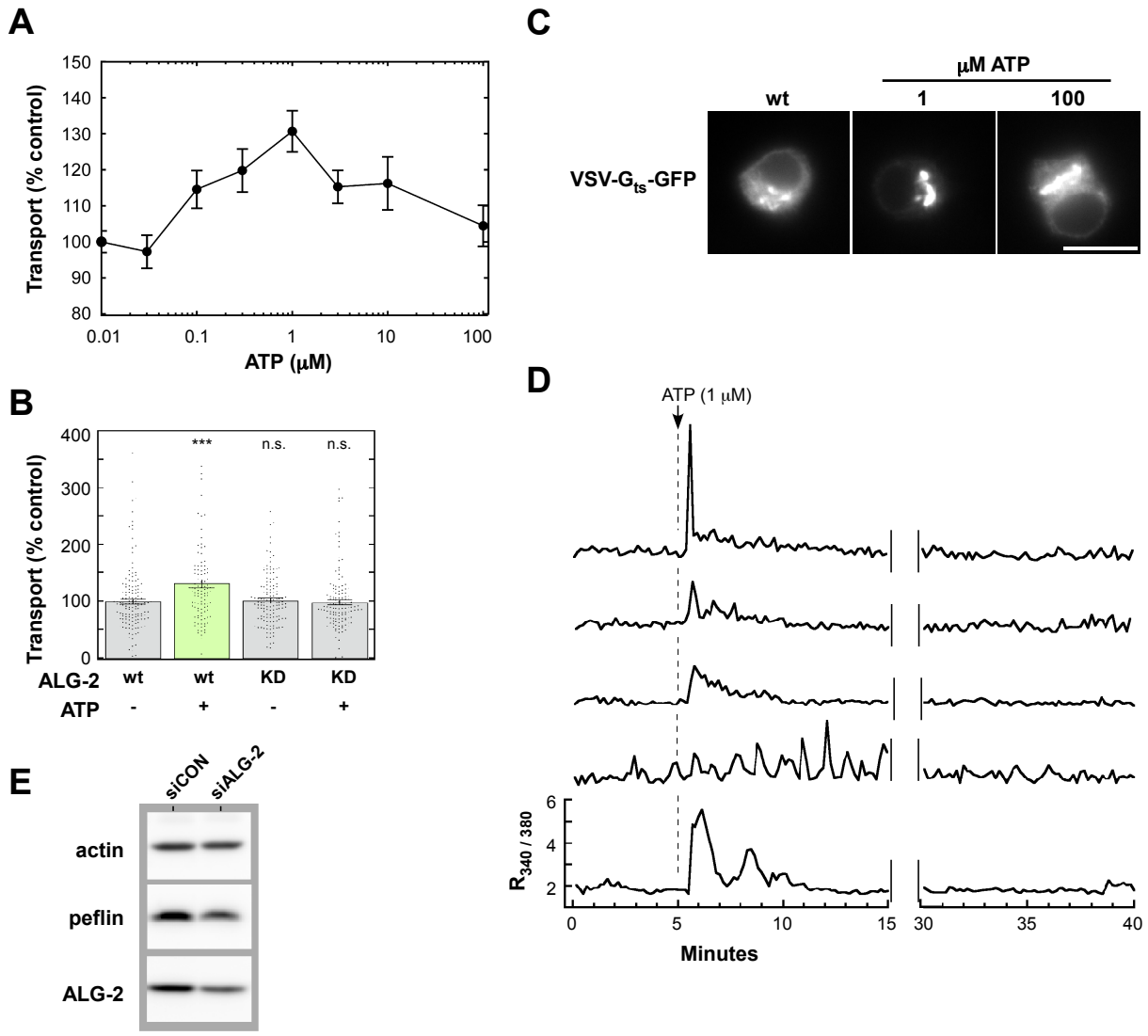

Figure 12. ATP elicits Ca^{2+}-activated enhancement of ER export and discontinuous Ca^{2+} signaling in PC12 cells. (A) PC12 cells were transfected with VSV-G_{ts045} and treated with a range of ATP concentrations for 2.5 h at the non-permissive temperature prior to shift to the permissive temperature for 10 min, after which transport was quantitated as in Figure 4. Mean ± SEM is shown for each point; N~100 cells per condition. One-way ANOVA as in Figure 4A. (B) PC12 cells were transfected with VSV-G and control or ALG-2 siRNA. Cells were exposed to 1 μM ATP for 2.5 h prior to the shift to a permissive trafficking temperature and quantitation of VSV-G transport. (C) Example widefield images of individual cells from A for select conditions. (D) In PC12 cells, exposure to 1 μM ATP produces immediate Ca^{2+} signaling that fades in strength and frequency over time. Shown are individual cell traces representative of this effect. The conditions used were identical to in Figure 11B. (E) Western blot on leftover cell extracts from part B, demonstrating a 51% depletion of ALG-2 with siRNA, as well as a co-depletion of peflin. Image scale bar; 20 micrometers.

4.2.4 In NRK Cells, Distinct Ca^{2+} Mobilization Patterns Determine Whether ALG-2 Enhances or Depresses ER Export

Since the opposing secretory responses of NRK and PC12 cells to ATP were associated with distinct Ca^{2+} signaling patterns, it seemed likely that spatiotemporal signaling properties, rather than a difference in secretory machinery, accounted for the distinct functional outcomes between the cell types. If this were the case, then NRK cells, given an appropriate Ca^{2+} stimulus, could respond with enhanced secretion like PC12 cells. Since an abrupt, discontinuous Ca^{2+} pattern was associated with CAEEE in PC12 cells (Figure 12), I tested the SERCA inhibitor 2,5-Di-(t-butyl)-1,4-hydroquinone (BHQ) in NRK cells, which invokes a surge of cytoplasmic Ca^{2+} for a few minutes until extrusion and other mechanisms restore the cytoplasm to near-basal levels (see below). A similar idea using a combination of ATP and BHQ produced an increase in ER-to-Golgi transport of GFP-F_M4-GH in HeLa cells, though a mechanism was not pursued further (Rauter et al., 2020). As shown in Figure 13A, at low micromolar concentrations for 2.5 hours, BHQ stimulated ER-to-Golgi transport by 50% or more, while by 10 µM, the compound caused no significant effect on transport (and in many cells, caused visible cytopathic effects). As shown in Figure 13B, the Ca^{2+}-activated enhancement of ER export elicited by 4 µM BHQ was entirely PEF protein-dependent, since ALG-2 siRNA rendered cells unresponsive to BHQ. Representative individual cell traces of Ca^{2+} dynamics elicited by BHQ are presented in Figure 13C. BHQ produced a surge of Ca^{2+} that then diminished and stabilized. Compared to the 100 nM dose of ATP in NRK cells (Figure 11B) and the 1 µM dose of ATP in PC12 cells (Figure 12D), the 4 µM dose of BHQ more closely resembled the discontinuous pattern for ATP in PC12 cells that resulted in CAEEE. Together, these experiments indicate that ALG-2 responses to Ca^{2+} signaling can produce CADEE or CAEEE - even within the same cell type - based upon the signaling pattern and/or duration, with continuous, tonic elevations associated with the former and large surges followed by significant diminution associated with the latter.

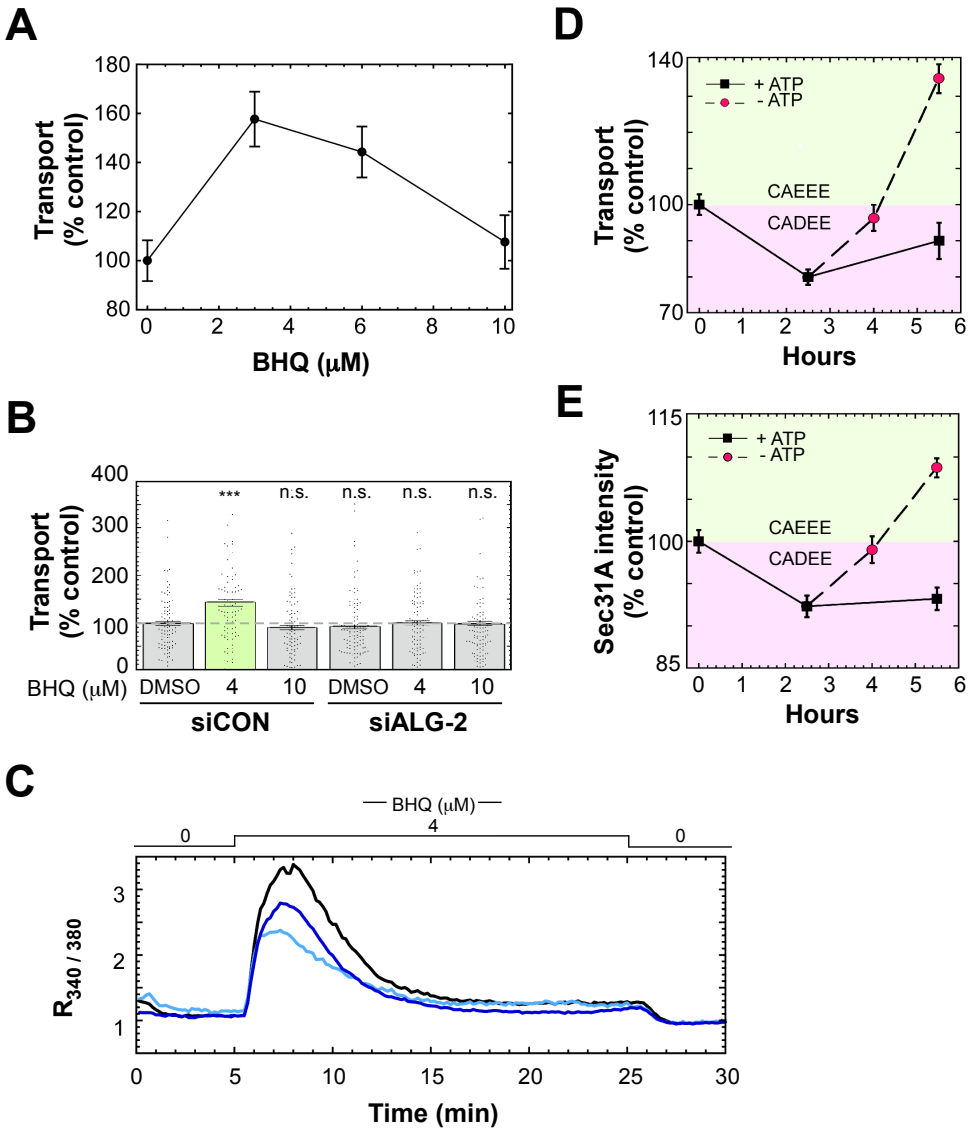

Figure 13. NRK cells possess both Ca^{2+}-activated depression and enhancement of ER export, dependent upon the stimulation pattern and duration. (A) NRK cells transfected with VSV-G were exposed to a range of BHQ doses for 2.5 h after which transport indices were calculated for ~100 cells as for Figure 4A. The mean transport index for each BHQ condition is plotted as a single black dot. **(B)** NRK cells transfected with VSV-G and control, or ALG-2-specific siRNAs were treated with specific BHQ doses or a DMSO control for 2.5 h prior to determination of transport indices. One-way ANOVA as in Figure 4A. **(C)** Example FURA-2 traces of NRK cells exposed to 4 μM BHQ. Methods similar to Figure 11B except that the cells were recorded during perfusion with media successively lacking, containing, and then lacking BHQ. **(D)** NRK cells were treated with 100 nM ATP and either maintained (black squares) for up to 5.5 h, or the ATP was removed by washing at 2.5 h and the cells were incubated for up to 3 h further (red circles). Transport relative to control was plotted for several timepoints. **(E)** Using cells from D, mean sec31 spot intensity was calculated from deconvolved images as in Figure 5D.

4.2.5 ALG-2-Dependent Depression of Transport is Succeeded by the Enhancement of Transport Upon Agonist Removal

Since both the ATP depressive effect and the BHQ enhancing effects in NRK cells depended upon Ca^{2+} and ALG-2, I doubted that they were mechanistically completely distinct. Instead, it seemed plausible that they were both part of a more uniform ALG-2 response that proceeded in consecutive phases, but that the relative intensity and timing of the phases could differ between different Ca^{2+} protocols or cell types. If this were the case, it should be possible to produce both CADEE and CAEEE using just ATP in NRK cells. Figure 13D black squares shows ATP- dependent CADEE over 5.5 hours in NRK cells. As with the response to histamine (Figure 9), the CADEE effect of ATP is strong at 2.5 hours. After this initial induction, the depression may diminish somewhat but persists for an additional three hours. On the other hand as shown in the red circles, if ATP is removed after the initial 2.5 hours, the secretion rate rebounds, achieving its initial rate 1.5 hours following ATP removal. Strikingly, by 3 hours following ATP removal (t = 5.5 h in Figure 13D), secretion has accelerated well beyond its initial, basal rate, an increase reminiscent of the enhancement of secretion caused by 2.5 hours of ATP treatment in PC12 cells (Figure 12A).While my results do not explain the molecular changes that result in the reversal of CADEE to cause CAEEE, it suggests that CADEE is not an off-pathway state but rather a state associated with ongoing signaling, while CAEEE may be a response to the cessation of signaling. In other words, both CADEE and CAEEE constitute a regulatory sequence controlled by the intensity and length of signaling episodes. This experiment using only ATP in NRK cells also rules out the possibility that potential signaling crosstalk between distinct signaling pathways determine whether CADEE or CAEEE manifests.

Given that changes in outer coat targeting to ERES would be a sufficient mechanistic basis for ALG-2- and peflin-dependent transport activities, I wondered whether the cycle of decreased and then increased transport induced by ATP incubation and removal (Figure 13D) would be reflected in parallel decreases followed by increases in outer coat targeting. Indeed, when sec31 spot intensity was quantified from the transport experiment shown in Figure 13D, I found that sec31A targeting closely correlated with CADEE, the release from CADEE by ATP

removal, and subsequent induction of CAEEE by 5.5 hours (Figure 13E). These results support the hypothesis that ALG-2-dependent modulation of outer coat targeting drives all the ALG-2-dependent transport phenotypes characterized herein.

CHAPTER 5:

CONCLUSION

5.1 DISCUSSION

5.1.1 ALG-2, Peflin and Effectors Comprise a Hetero-Bifunctional Regulator of ER Export

In this chapter, I discuss the main features of a model for PEF protein regulation of transport (Figure 14) that emerges from Chapters 3 and 4. In this model I present the idea that ALG-2, peflin and their effectors exist in several activity states correlating with distinct compositions of ER exit sites. These states result in either up-regulation (Figure 14B) or down-regulation (Figure 14C) of the basal ER export rate (Figure 14A) with potentially important consequences for cell physiology and pathology, including ER stress. The activity states are purely regulatory since neither peflin nor ALG-2 are essential for secretion. By experimentally adjusting the ALG-2:peflin ratio at steady-state Ca^{2+} I determined that a peflin-ALG-2 hetero-complex bound to ERES and inhibited ER-to-Golgi transport, and that a peflin-lacking ALG-2 species bound there to stimulate transport. Mechanistically, these states correlate with decreased and increased, respectively, targeting of the COPII outer coat to ERES, presumably mediated by the well-characterized interaction between ALG-2 and its binding site in the proline-rich region or loop of Sec31a that connects the inner and outer coats (Takeshi et al., 2015). Though my studies did not define the subunit makeup or stoichiometry of ALG-2 complexes, it is likely that the inhibitory ALG-2-peflin complex targeted to ERES by ALG-2 is at least in part the 1:1 heterodimer characterized earlier to occupy the majority of ALG-2 in the cell and is dissociated by high Ca^{2+} (Kitaura et al., 2001, 2002). The peflin-lacking ALG-2 complex is most likely comprised at least in part of the Ca^{2+}-stimulated ALG-2 homodimer whose crystal structure was determined in complex with Sec31A peptide (Takeshi et al., 2015). my schematic depicts them as a heterodimer and homodimer as the simplest explanation comprised of known species. The ALG-2 homodimer has been described generally as a Ca^{2+}-dependent adaptor because of its ability to engage two co-effectors at once and link them (Maki & Shibata 2007, and Figure 3). In my schematic, one of the ALG-2 co-effectors is always Sec31A, since that interaction is required for ALG-2 localization to ERES (Shibata et al., 2007; Yamasaki et al., 2006). For the stimulatory activity of ALG-2 (Figure 14, part B), the simplest model would be that the other co-effector would be a second molecule of Sec31A, as this could result in

cooperative coat assembly, more outer coat, and higher transport. Indeed, ALG-2-dependent inner-outer coat interactions have been demonstrated in solution without inclusion of other proteins (la Cour et al., 2013). However, there may be other ALG-2 effectors involved that my work does not address, several of which I identified in Chapter 1 to be at ERES (Figure 3), including annexin A11 (Shibata et al., 2015), MISSL, MAP1B (Takahara et al., 2017), and KLHL12 (McGourty et al., 2016). I have not ruled out, for example, the possibility that ALG-2 and peflin interactions with KLHL12 contribute to the Sec31A increases and decreases I observe at ERES during CADEE and CAEEE, through a mechanism involving Sec31A ubiquitination (Jin et al., 2012; McGourty et al., 2016). Another post-translational modification that could play a role as directed by ALG-2 and peflin is O-GlcNAcylation of Sec31A (Cho & Mook-Jung, 2018,2020;Table 1).

Ca^{2+} signaling can result in either a stimulatory or inhibitory activity of ALG-2, as can over-expression of ALG-2, that is independent of peflin. This stimulatory state is assumed in my model to be the same state just discussed and ascribed to the homodimer (Figure 14, part B). The Ca^{2+}-induced inhibitory state could also be mediated by ALG-2 alone or could involve a distinct, inhibitory co-effector that is recruited by ALG-2 during sustained Ca^{2+} elevation (Figure 14, part C, red pause button). ALG-2 homodimers alone could be inhibitory because if the positive function of ALG-2 homodimers is to cross-link sec31A molecules, then over-saturation by homodimers should prevent that crosslinking. Though the cross-linking/over-saturation model to explain both influences is the simpler model, the distinct, inhibitory cofactor model actually fits my data better since it explains why depletion of ALG-2, or ALG-2 and peflin, does not per se inhibit secretion. I do not know what the putative inhibitory co-effector might be, but as just mentioned, ALG-2 has a number of Ca^{2+}-dependent client proteins. By whichever mechanism, the inhibitory state is experimentally distinct from that containing peflin since it does not require peflin (Figures 3B, 6A) and is buffered against by the presence of peflin (Figures 3B, 6C).

Questions remain about how transitions occur between the identified activity states. For example, why does cessation of long-term Ca^{2+} stimulation lead to the stimulatory state (Figure

14, "Ca^{2+} ceases" blue arrow)? Perhaps during long-term Ca^{2+} signaling, ALG-2 homodimers accumulate at ERES, such that once the inhibitory co-effector is released, the stimulatory state mediated by homodimers automatically ensues. Another hole in my understanding is whether all Ca^{2+}-induced secretion changes include at least a short, transient inhibitory state. An alternative possibility is that certain Ca^{2+} intensities and durations directly induce positive regulation of secretion (Figure 14 "discontinuous Ca^{2+}" blue arrow). Unfortunately, this question is currently difficult to address given the lags before measurable secretion changes occur.

Another aspect to my model is that it only addresses the export of actively-sorted COPII client cargo. I have no data about whether vesicle budding rates, per se, increase and decrease in concert with the export rates of the measured cargos. It cannot be ruled out, for example that increases in VSV-G transport are actually caused by slower vesicle budding but more stringent sorting of client cargos. The fact that bulk flow cargo export slows as client cargo accelerates (Figure 7B) implies that client cargo sorting is so stringent as to exclude non-client cargo. What effect this has on vesicle budding remains unexplored.

An unexpected discovery was that peflin is concentrated in the nucleus (Figure 5A). ALG-2 has also been reported to localize to the nucleus, and has been implicated in Ca^{2+}-regulated splicing reactions there (Sasaki-Osugi et al., 2013). While I cannot rule out the possibility that nuclear function of either ALG-2 or peflin could contribute to their transport effects, their presence and intensity ratios at ERES during expression studies (Figure 5) correlates extremely well with their functional impacts on ER-to-Golgi transport (Figure 4A). I still do not understand, however, how Ca^{2+} changes result in the ERES targeting and functional changes I observed. For example, ALG-2 binding/unbinding to ERES occurs unitemporally with every single Ca^{2+} oscillation ((la Cour et al., 2007), and my own unpublished observations), yet ALG-2-dependent changes in ERES structure/function caused by Ca^{2+} changes take ≥ 30 minutes. The unitemporal binding/unbinding may contribute to a longer-term change, perhaps involving the entire cellular balance of ALG-2 homodimers vs. heterodimers, that actually drives the functional changes. Alternatively, the ERES functional changes may involve something more akin to ERES

biogenesis and disassembly, rather than merely changes in the content of outer coated located at ERES. One possibility I have largely ruled out involves the transcriptional response to ER stress. KD's of peflin in unstressed cells under basal conditions did not detectably affect the UPR as indicated by intensities of bands on Westerns with the following antibodies: anti-phospho-IRE1, anti-phosho-EIF2 alpha, anti-ATF4 and anti-CHOP (data not shown). This excludes the mechanism wherein peflin depletion could cause ER stress which would increase transcription of COPII machinery to build ERES and accelerate secretion. Based upon all available evidence, I conclude that PEF protein effects on ER-to-Golgi transport are mediated directly through, or triggered by, their interactions with Sec31A at ERES.

The long-term Ca^{2+} signaling required for CAEEE or CADEE does have precedence in other aspects of cellular regulation. For example, fertilized mammalian eggs initiate development by generating regular Ca^{2+} spikes that persist for ~2 h (Santella et al., 2004)—about the time required for CAEEE or CADEE. Additionally, the strengthening of neural connections (long-term potentiation) and the weakening of neural connections (long-term depression) both require extended elevations of intracellular Ca^{2+} (R. C. Evans & Blackwell, 2015)—an example of Ca^{2+}'s bifunctionality similar to CAEEE or CADEE. Finally, long-term histamine signaling has been observed to regulate trafficking by promoting intra-Golgi VSV-G transport in manner that involved a distinct Ca^{2+} effector and trafficking machinery target (Ireland et al., 2020) (Table 2)—an observation reminiscent of my finding that ATP induced Ca^{2+} signaling in PC12 cells causes ALG-2 to accelerate ER-to-Golgi transport (CAEEE) (Figure 12). My findings build upon these reports, as I have shown that the opposite effects on transport could be dictated by specific Ca^{2+} signals and patterns in a manner dependent upon ALG-2.
There are many reasons cells regulate constitutive trafficking: inter-cellular communication between secretory cells or neurons; resource consumption; cell growth; ER stress; and to limit viral replication. My model appears to contain two inhibitory states, one peflin-dependent and another peflin-independent. The peflin-containing state is present at steady state, which may allow cells to permanently change secretion rates by adjusting the relative peflin expression level. On the other hand, the Ca^{2+}-activated inhibitory state could "choke" secretion quickly

during transient excitotoxic circumstances or viral infection. Though the consequences of secretion reduction could be protective to otherwise healthy cells, I speculate that it may be maladaptive to highly stressed cells (Genereux et al., 2015). Along these lines I depleted peflin in a cellular model of ageing wherein primary porcine aorta endothelial cells become senescent, display mitochondrial Ca^{2+} excitotoxicity, elevated ROS production, chronic ER stress signaling in the absence of chemical inducers, and eventual apoptosis (Madreiter-Sokolowski et al., 2019). I found that peflin depletion drastically reduced pro-apoptotic UPR signaling (Figure 8F), consistent with its suppressive role in secretion being relevant to damage-inducing ER stress.

Areas of future study range from the relatively narrow to the more comprehensive. The former may, for example, include potential identification of an inhibitory co-effector recruited by ALG-2 during continuous Ca^{2+} signaling, discovery of a role for peflin at other loci including the nucleus, or a better understanding of the transition states between distinct ALG-2 activity states and the calcium signals that elicit them. The latter may, for example, involve understanding the regulatory roles PEF proteins and their Ca^{2+} regulation in specific physiological contexts, such as in regulating pools of readily-releasable vesicles and synapse formation/strengthening in neurons, or in regulating extracellular matrix deposition in kidney cells where dysregulation of Ca^{2+} homeostasis and collagen secretion contribute to polycystic kidney disease (Le Corre et al., 2014).

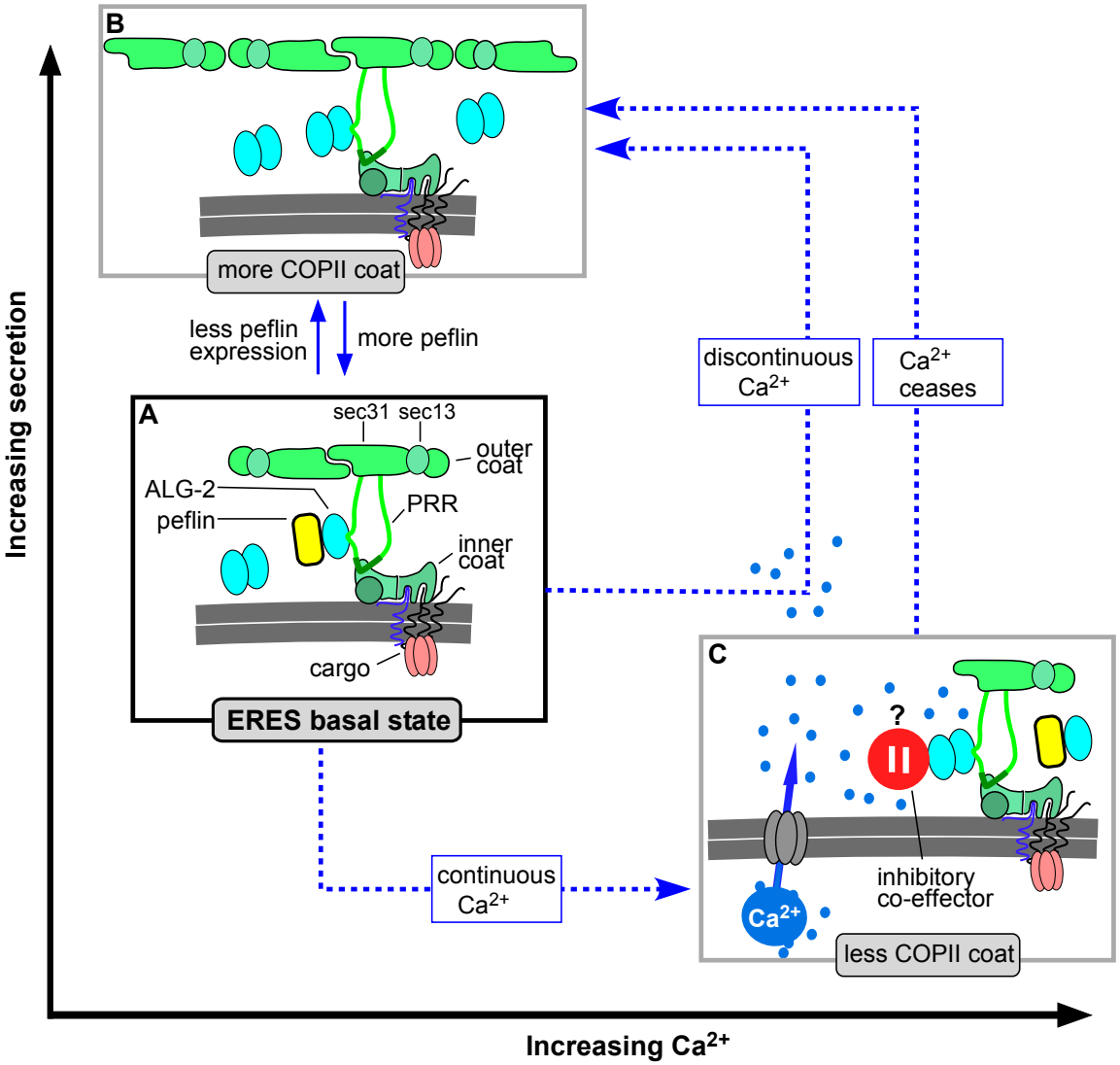

Figure 14. Model of PEF protein and Ca^{2+} regulation of ER export. (A) Under steady-state conditions, ALG-2 binds ERES in two distinct functional states that compete with each other. An ALG-2 homodimer binds sec31A to stimulate transport, while a peflin-ALG-2 complex binds sec31A via ALG-2 and inhibits transport. **(B)** Increases in the ALG-2:peflin expression ratio or discontinuous agonist-driven Ca^{2+} signaling comprised of high Ca^{2+} followed by low Ca^{2+}, leads to more ALG-2 homodimers at ERES, greater outer coat recruitment, and greater export of COPII client cargo. **(C)** Continuous Ca^{2+} signals such as persistent agonist-driven oscillations leads to an ALG-2-dependent reduction of COPII targeting and decreased export of COPII client cargoes. Though peflin binding to ERES also increases during this state, it is not required for the response, leading us to posit either a distinct, unknown inhibitory Ca^{2+}-activated ALG-2 effector (red pause button) or alternatively an inhibitory effect of ALG-2 produced by saturation of Sec31A (see Chapter 5). State C persists for hours if signaling persists, however, abrupt cessation of Ca^{2+} signaling leads directly to state B.

APPENDIX:

FIJI PLUGINS

a.1 PLUGIN COLLECTION

For use cases of FIJI (ImageJ) plugins, see Chapter 2. All code is written in Python and is available to the public at: https://github.com/JohnSargeant-rgb. Plugins are presented in the expected order of use.

a.1.1 File Mover:

Description: searches and copies a group of files, based on file extension, from one directory to another. This is useful for aggregating all files from a specific experiment into one directory.

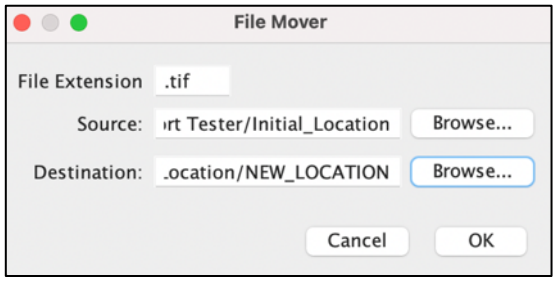

File Extension: file type
Source: location of the source directory containing groups of files to be moved
Destination: destination location of all copied files from the source directory. File Mover will create a new folder called “Moved Images” in the specified destination. *Note: if left blank, the default destination is the same as the source directory.*

Pre-File Mover:

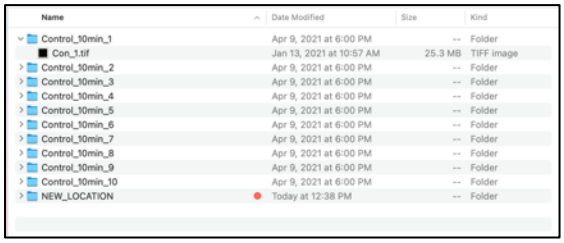

Post-File Mover:

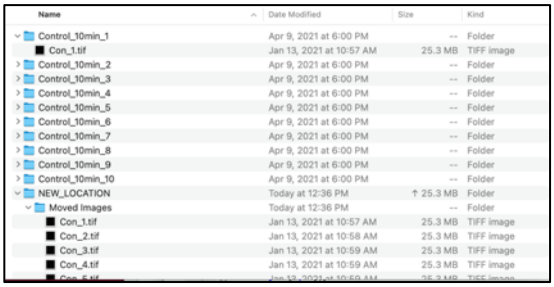

a.1.2 File Randomizer:

Description: renames files to a randomly-generated, 36-character name consisting of characters (a-f, 0-9, -). Document key matching old file names with randomized names are stored as a .csv ("key.csv") in the directory folder. This is useful for blinding a researcher from file names during image analysis. *Note: for tool to function, directory must contain no subdirectories.*

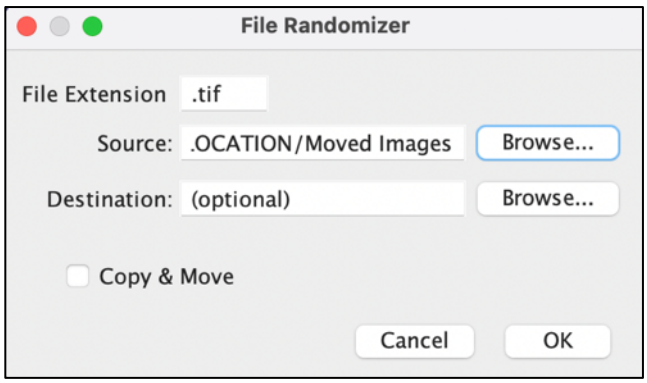

File Extension: file type.
Source: location of the source directory containing files to be randomized
Destination *use only if "Copy & Move" is checked*: destination location of randomized files
Copy & Move: makes a copy of the source directory prior to randomizing file names

Pre-File Randomizer:

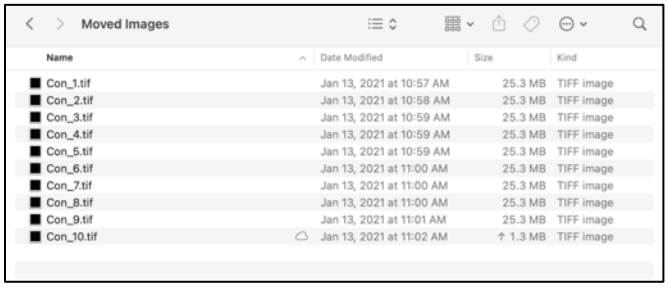

Post-File Randomizer: Source Directory:

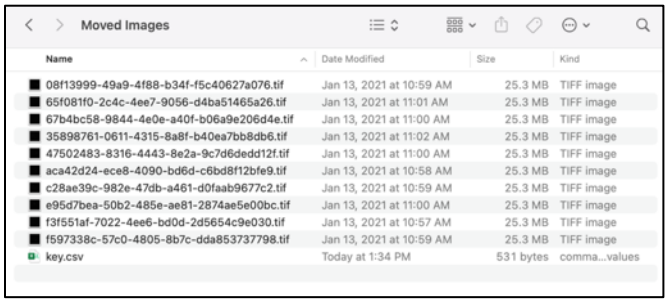

Post-File Randomizer: key.csv:

	A	B
1	Con_9.tif	65f081f0-2c4c-4ee7-9056-d4ba51465a26.tif
2	Con_8.tif	47502483-8316-4443-8e2a-9c7d6dedd12f.tif
3	Con_1.tif	f3f551af-7022-4ee6-bd0d-2d5654c9e030.tif
4	Con_3.tif	c28ae39c-982e-47db-a461-d0faab9677c2.tif
5	Con_2.tif	aca42d24-ece8-4090-bd6d-c6bd8f12bfe9.tif
6	Con_6.tif	67b4bc58-9844-4e0e-a40f-b06a9e206d4e.tif
7	Con_7.tif	e95d7bea-50b2-485e-ae81-2874ae5e00bc.tif
8	Con_5.tif	08f13999-49a9-4f88-b34f-f5c40627a076.tif
9	Con_4.tif	f597338c-57c0-4805-8b7c-dda853737798.tif
10	Con_10.tif	35898761-0611-4315-8a8f-b40ea7bb8db6.tif

a.1.3 ER-Golgi Transport Assay:

(Base code written by Mariah Rayl

Description: Determines a series of intensity data based upon ROI's Principally, this assay calculates the ratio of maximum intensity over average intensity. This is useful for determine transport rates of synchronizeable cargo and gathering associated corollary data.

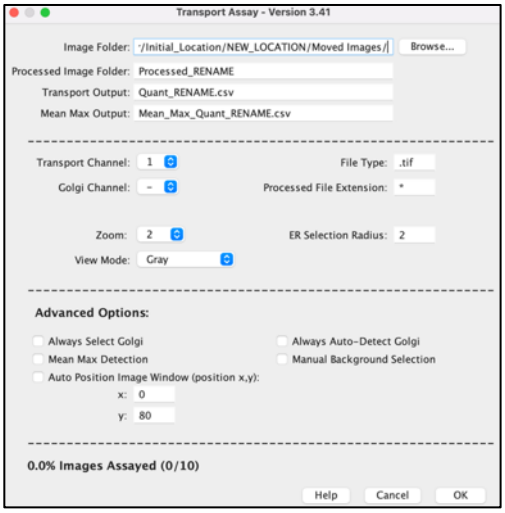

Image Folder *(assigned automatically)*: location of the image file to be assayed
Processed Image Folder: name of folder containing a copy of each processed image
Transport Output: name of .csv file containing ratiometric output data

---

Mean Max Output *(optional)***:** name of .csv file containing channel intensity output data
Transport channel *(optional)***:** channel where the ratio of maximum intensity over average intensity is determined
Golgi channel *(optional)***:** channel in which the Golgi Apparatus is visible
Zoom: the level of zoom after selection of an image ROI
View Mode: Look Up Table (LUT) selection
File Type: extension of the image file type
Processed File Extension: character added to the start of an image filename after its been processed
ER Selection Radius: radius of the circular ROI's used to determine average intensity of the ER

Advanced Options (will occur if checked):
Always Select Golgi: forces the user to manually determine the region from which maximum intensity is derived
Mean Max Detection: generates .csv file that records area, mean, and max intensity of a selected ROI for all channels
Auto Position Image Window: positions image window at the specified coordinates
Always Auto-Detect Golgi: automatically determines the maximum intensity of an ROI in the transport channel

Manual Background Selection: forces the user to manually assign a background value. *Note: if unchecked, lowest pixel intensities will be assigned automatically*

ER-to-Golgi Transport Assay: ER selection phase of selected ROI:

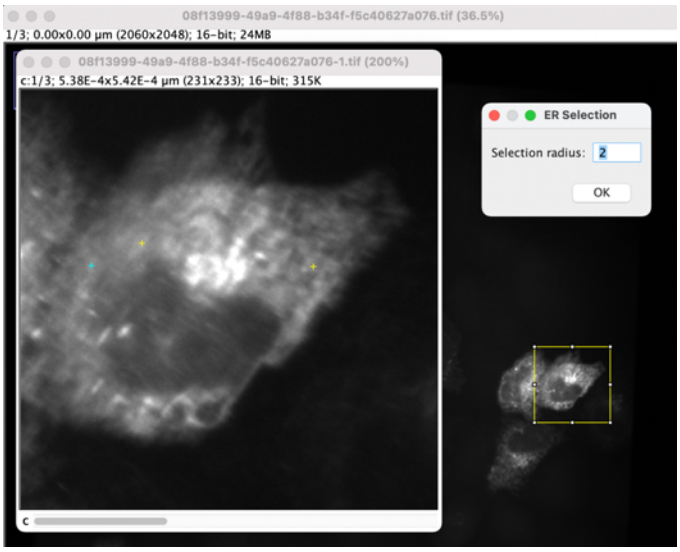

ER-to-Golgi Transport Assay: Transport Output .csv:

	A	B	C	D	E	F	G	H	I	J	K	L	M	N
1	Cell	AVG_Max	bck_auto	bck	ER1	ER2	ER3	net_ER	net_golgi	T_Index	Image_title			
2	1	18328.2	493	0	6467.75	7427.66667	8245.16667	6887.19444	17835.2	2.58961761	08f13999-49a9-4f88-b34f-f5c40627a076.tif			
3	2	13892.625	438	0	2266.16667	3701.16667	4018.91667	2890.75	13454.625	4.6543717	67b4bc58-9844-4e0e-a40f-b06a9e206d4e.tif			
4	3	15520.6	795	0	5271.83333	4811.5	5396.66667	4365	14725.6	3.37356243	aca42d24-ece8-4090-bd6d-c6bd8f12bfe9.tif			
5	4	19718.7692	724	0	5691.25	4394.16667	6032.66667	4648.69444	18994.7692	4.08604383	e95d7bea-50b2-485e-ae81-2874ae5e00bc.tif			
6	5	16339.8182	491	0	4481.91667	3591.41667	4588.25	3729.52778	15848.8182	4.24955092	65f081f0-2c4c-4ee7-9056-d4ba51465a26.tif			
7	6	12838.1	753	0	5067.16667	4837.83333	5126.5	4257.5	12085.1	2.83854375	47502483-8316-4443-8e2a-9c7d6dedd12f.tif			
8	7	14225.5455	462	0	3780.75	3546.41667	3082.08333	3007.75	13763.5455	4.57602708	f3f551af-7022-4ee6-bd0d-2d5654c9e030.tif			
9	8	10773.5	832	0	3190.91667	3110	3690.08333	2498.33333	9941.5	3.97925284	35898761-0611-4315-8a8f-b40ea7bb8db6.tif			
10	9	20089.5455	851	0	3000.25	2733.83333	3324.5	2168.52778	19238.5455	8.8717081	f597338c-57c0-4805-8b7c-dda853737798.tif			
11	10	16952.75	245	0	5529.08333	4404.75	4341.41667	4513.41667	16707.75	3.7017965	c28ae39c-982e-47db-a461-d0faab9677c2.tif			
12														

Cell: ROI number assayed
AVG_Max: average of the top 0.01% of pixels in selected ROI.
bck_auto: average of the bottom 0.1% of pixels in selected ROI.
bck: manually selected background
ER1: average pixel intensity in the first selected circular ROI
ER2: average pixel intensity in the second selected circular ROI
ER3: average pixel intensity in the third selected circular ROI
net_ER: average of ER regions 1-3.
net_golgi: AVG_Max-bck_auto
T_index: net_golgi/net_ER
Image_title: image that a particular ROI was derived from

ER-to-Golgi Transport Assay: Mean Max Output .csv:

	A	B	C	D	E	F	G	H	I	J	K	L	M	N	O	P	Q	R
1	Cell	Cell Area	ch1_Backgro	ch1_avg	ch1_Maximu	ch2_Backgro	ch2_avg	ch2_Maximu	ch3_Backgro	ch3_avg	ch3_Maximu	ch4_Backgro	ch4_avg	ch4_Maximu	Image_title			
2	1	1.28E-07	670	5058.7766	17972.1429	459	1162.21316	2512.71429	427	1247.19992	3749.42857	0	0	0	08f13999-49a9-4f88-b34f-f5c40627a076.tif			
3	2	1.67E-07	650	2313.18333	14401.3333	582	1420.63669	3015.33333	515	1490.94779	4430.66667	0	0	0	67b4bc58-9844-4e0e-a40f-b06a9e206d4e.tif			
4	3	1.58E-07	801	2649.12357	15409	742	1517.54996	2742.125	783	1712.93732	3725.375	0	0	0	aca42d24-ece8-4090-bd6d-c6bd8f12bfe9.tif			
5	4	2.22E-07	749	4038.82134	20311.5	587	1221.34476	2879.25	592	1457.24223	5111.25	0	0	0	e95d7bea-50b2-485e-ae81-2874ae5e00bc.tif			
6	5	1.82E-07	667	2950.41188	16973.3333	540	1503.58523	3709.66667	531	1919.89932	4643.33333	0	0	0	65f081f0-2c4c-4ee7-9056-d4ba51465a26.tif			
7	6	2.25E-07	772	3004.01377	13031.25	587	1569.86592	3834	540	1931.89587	5827	0	0	0	47502483-8316-4443-8e2a-9c7d6dedd12f.tif			
8	7	2.48E-07	534	2508.00533	14710.75	488	1174.24538	2047	425	1239.39119	3193	0	0	0	f3f551af-7022-4ee6-bd0d-2d5654c9e030.tif			
9	8	1.78E-07	866	2718.23863	11089.6667	885	1512.34401	3308.66667	1060	1637.83792	5639.66667	0	0	0	35898761-0611-4315-8a8f-b40ea7bb8db6.tif			
10	9	2.37E-07	860	3598.34921	20456.5	729	1623.09406	3247.25	827	1760.25501	4533.5	0	0	0	f597338c-57c0-4805-8b7c-dda853737798.tif			
11	10	2.09E-07	718	3379.24868	17507.6667	665	1294.26286	3149.33333	759	1454.80458	3206.66667	0	0	0	c28ae39c-982e-47db-a461-d0faab9677c2.tif			

Cell: ROI number assayed

Cell Area: area of selected ROI, determined by FIJI's measure function

***ch1_Background:** minimum of selected ROI in channel 1. Determined by FIJI's measure function

ch1_avg: mean of selected ROI in channel 1. Determined by FIJI's measure function

ch1_Maximum: maximum of selected ROI in channel 1. Determined by FIJI's measure function

*Repeats from * for all channels in an image*

Image_title: image that a particular ROI was derived from

a.1.4 FRET/FURA Assay:

Description: Calculates the net intensity ratio of multiple user defined ROIs from a dual channel hyperstack (width, height, channels and time frames). In myexperiments the two channels are usually, C1: 435nm and C2: 513nm for FRET, while for FURA, the two channels are C1: 340nm and C2: 380nm.

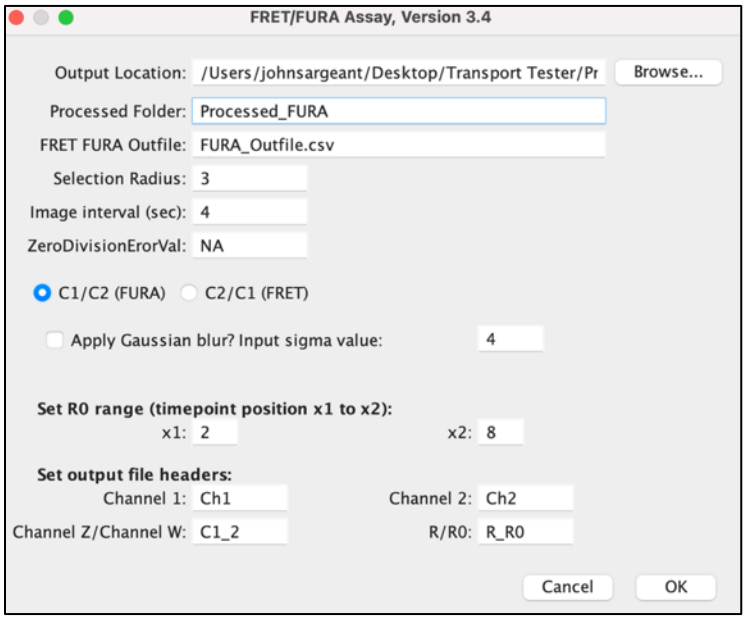

Output Location: location of data output
Processed Folder: name of folder containing processed image (saves ROI overlay)
FRET FURA Outfile: name of file containing ratio data for each ROI
Selection Radius: radius of ROI's generated using the multi point tool
Image Interval (sec): number of seconds between each image interval
ZeroDivisionErrorVal: output when dividing by zero
C1/C2(FURA): if checked ROI ratio is channel 1 /channel 2
C2/C1(FRET): if checked ROI ratio is channel 2 /channel 1
Apply Gaussian blur? Input sigma value: apply a gaussian blur function prior to data acquisition.
Set RO range (timepoint position x1 to x2): range of channels used to determine the baseline ratio (R0)
Set Output file headers: headers printed onto a .csv file

FRET FURA: ROI selection phase:

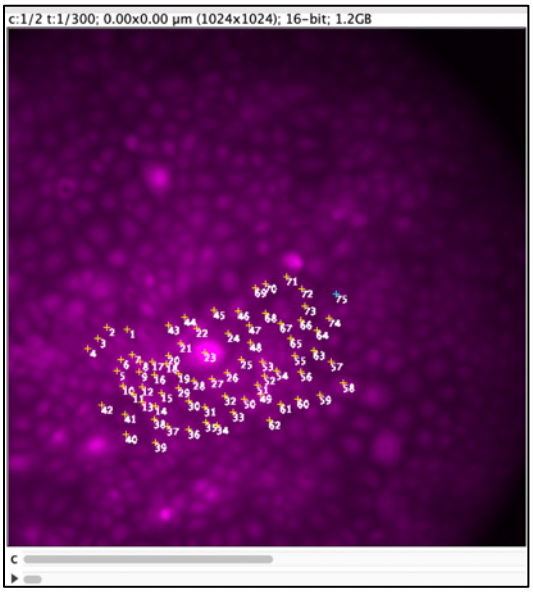

FRET FURA: Output:

	A	B	C	D	E	F	G	H	I	J	K	L
1	Image_Title	Time_min	ch1_bck	ch2_bck	Ch1_1	Ch2_1	C1_C2_1	R_R0_1	Ch1_2	Ch2_2	C1_C2_2	R_R0_2
2	AH3-66_FURA	0.07	497.657025	527.460744	1058.46798	688.758006	1.53677774	1.00489481	1147.06173	695.726756	1.64872447	1.00228807
3	AH3-66_FURA	0.13	500.539256	528.068182	1061.33574	681.244318	1.55793702	1.0187308	1149.30449	690.963068	1.66333708	1.01117133
4	AH3-66_FURA	0.2	499.619835	530.002066	1065.41142	685.935434	1.55322405	1.01564901	1149.69267	692.747934	1.65961183	1.00890669
5	AH3-66_FURA	0.27	500.733471	529.510331	1058.54778	689.552169	1.53512356	1.00381314	1141.42278	691.427169	1.65082142	1.00356284
6	AH3-66_FURA	0.33	499.479339	527.336777	1049.52066	686.381973	1.5290621	0.99984957	1148.86441	694.600723	1.65399254	1.00549062
7	AH3-66_FURA	0.4	500.5	526.799587	1038.84375	683.106663	1.5207636	0.9944232	1139.4375	692.137913	1.64625789	1.0007886
8	AH3-66_FURA	0.47	498.820248	528.254132	1039.17975	680.183368	1.52779354	0.99902006	1132.586	693.777118	1.63249259	0.99242043
9	AH3-66_FURA	0.53	499.394628	528.820248	1032.91787	684.148502	1.50978606	0.98724502	1133.26162	696.711002	1.62658781	0.98883082
10	AH3-66_FURA	0.6	499.107438	528.006198	1028.54881	682.212552	1.50766621	0.98585886	1133.67381	692.775052	1.63642413	0.99481049
11	AH3-66_FURA	0.67	500.43595	528.964876	1028.2828	675.285124	1.52273871	0.99571472	1135.62655	691.160124	1.64307302	0.99885246
12	AH3-66_FURA	0.73	500.714876	527.221074	1020.25387	680.841426	1.49851909	0.97987758	1127.25387	696.310176	1.61889617	0.98415493
13	AH3-66_FURA	0.8	497.913223	526.863636	1024.55553	683.886364	1.49813709	0.97962779	1131.18053	694.480114	1.6288163	0.99018555
14	AH3-66_FURA	0.87	500.247934	529.099174	1021.03332	685.338326	1.48982375	0.97419172	1123.28332	694.057076	1.61843075	0.983872
15	AH3-66_FURA	0.93	498.258264	526.018595	1028.49174	690.137655	1.49027042	0.9744838	1128.67924	699.700155	1.61308988	0.98062519
16	AH3-66_FURA	1	499.008264	527.528926	1026.86674	685.408574	1.49818192	0.97965711	1126.46049	698.377324	1.6129683	0.98055128

Image_title: image that all ROI's were derived from
Time_min: time in minutes after acquisition of repeating sets of dual channels
ch1_bck: background of channel 1
ch2_bck: background of channel 2
Ch1_(n): average intensity of pixels within ROI 'n' in channel 1
Ch2_(n): average intensity of pixels within ROI 'n' in channel 2
C1_C2_(n): Ch1_(n) / Ch2_(n)
R_R0_(n): **(**Ch1_(n) / Ch2_(n)) / average intensity of pixels of ROI 'n' amassed from positions defined by the R0 range (above)

a.1.5 File Derandomizer:

Description: Returns randomized filenames to their original name based upon a key (generated by *File Randomizer* plugin)

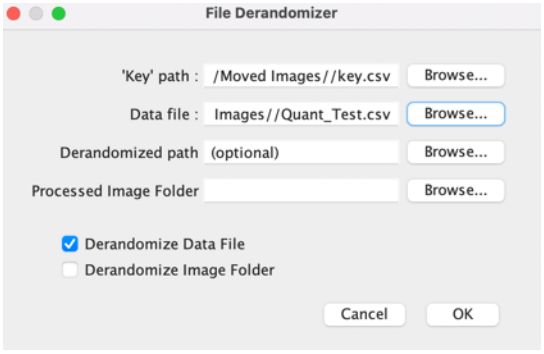

Key path: path to key.csv file
Data file: path to the data file that includes randomized names
Derandomized path: path for *File Derandomizer* output. Default is the path to *Data file*.
Processed Image Folder: path to processed image folder generated in *Transport Assay* plugin
Derandomize Data File: if checked, will derandomize the selected data file and generate a copy with unscrambled filenames
Derandomize Image Folder: if checked, will derandomize files in the selected directory

Pre-File Derandomizer: Output from *Transport Assay* plugin:

	A	B	C	D	E	F	G	H	I	J	K	L	M	N
1	Cell	AVG_Max	bck_auto	bck	ER1	ER2	ER3	net_ER	net_golgi	T_Index	Image_title			
2	1	18328.2	493	0	6467.75	7427.66667	8245.16667	6887.19444	17835.2	2.58961761	08f13999-49a9-4f88-b34f-f5c40627a076.tif			
3	2	13892.625	438	0	2266.16667	3701.16667	4018.91667	2890.75	13454.625	4.6543717	67b4bc58-9844-4e0e-a40f-b06a9e206d4e.tif			
4	3	15520.6	795	0	5271.83333	4811.5	5396.66667	4365	14725.6	3.37356243	aca42d24-ece8-4090-bd6d-c6bd8f12bfe9.tif			
5	4	19718.7692	724	0	5691.25	4394.16667	6032.66667	4648.69444	18994.7692	4.08604383	e95d7bea-50b2-485e-ae81-2874ae5e00bc.tif			
6	5	16339.8182	491	0	4481.91667	3591.41667	4588.25	3729.52778	15848.8182	4.24955092	65f081f0-2c4c-4ee7-9056-d4ba51465a26.tif			
7	6	12838.1	753	0	5067.16667	4837.83333	5126.5	4257.5	12085.1	2.83854375	47502483-8316-4443-8e2a-9c7d6dedd12f.tif			
8	7	14225.5455	462	0	3780.75	3546.41667	3082.08333	3007.75	13763.5455	4.57602708	f3f551af-7022-4ee6-bd0d-2d5654c9e030.tif			
9	8	10773.5	832	0	3190.91667	3110	3690.08333	2498.33333	9941.5	3.97925284	35898761-0611-4315-8a8f-b40ea7bb8db6.tif			
10	9	20089.5455	851	0	3000.25	2733.83333	3324.5	2168.52778	19238.5455	8.8717081	f597338c-57c0-4805-8b7c-dda853737798.tif			
11	10	16952.75	245	0	5529.08333	4404.75	4341.41667	4513.41667	16707.75	3.7017965	c28ae39c-982e-47db-a461-d0faab9677c2.tif			
12														

Post-File Derandomizer:

	A	B	C	D	E	F	G	H	I	J	K
1	Cell	AVG_Max	bck	bck_auto	ER1	ER2	ER3	net_ER	net_golgi	T_Index	Image_title
2	1	18328.2	493	0	6467.75	7427.66667	8245.16667	6887.19444	17835.2	2.58961761	Con_5.tif
3	2	13892.625	438	0	2266.16667	3701.16667	4018.91667	2890.75	13454.625	4.6543717	Con_6.tif
4	3	15520.6	795	0	5271.83333	4811.5	5396.66667	4365	14725.6	3.37356243	Con_2.tif
5	4	19718.7692	724	0	5691.25	4394.16667	6032.66667	4648.69444	18994.7692	4.08604383	Con_7.tif
6	5	16339.8182	491	0	4481.91667	3591.41667	4588.25	3729.52778	15848.8182	4.24955092	Con_9.tif
7	6	12838.1	753	0	5067.16667	4837.83333	5126.5	4257.5	12085.1	2.83854375	Con_8.tif
8	7	14225.5455	462	0	3780.75	3546.41667	3082.08333	3007.75	13763.5455	4.57602708	Con_1.tif
9	8	10773.5	832	0	3190.91667	3110	3690.08333	2498.33333	9941.5	3.97925284	Con_10.tif
10	9	20089.5455	851	0	3000.25	2733.83333	3324.5	2168.52778	19238.5455	8.8717081	Con_4.tif
11	10	16952.75	245	0	5529.08333	4404.75	4341.41667	4513.41667	16707.75	3.7017965	Con_3.tif
12											

REFERENCES:

Aguiari, G., Banzi, M., Gessi, S., Cai, Y., Zeggio, E., Manzati, E., Piva, R., Lambertini, E., Ferrari, L., Peters, D., Lanza, F., Harris, P., Borea, P., Somlo, S., & Senno, L. Del. (2004). Deficiency of polycystin-2 reduces Ca2+ channel activity and cell proliferation in ADPKD lymphoblastoid cells. *FASEB J.*, *18*(7), 884–886.

Ahluwalia, J. P., Topp, J. D., Weirather, K., Zimmerman, M., & Stamnes, M. (2001). A Role for Calcium in Stabilizing Transport Vesicle Coats. *J. Biol. Chem.*, *276*(36), 34148–34155.

Ali Doosti, B., Pezeshkian, W., Bruhn, D., Ipsen, J., Khandelia, H., Jeffries, G., & Lobovkina, T. (2017). Membrane Tubulation in Lipid Vesicles Triggered by the Local Application of Calcium Ions. *Langmuir*, *33*(41), 11010–11017.

Appenzeller-Herzog, C., Roche, A.-C., Nufer, O., & Hauri, H.-P. (2004). pH-induced Conversion of the Transport Lectin ERGIC-53 Triggers Glycoprotein Release. *J. Biol. Chem.*, *279*(13), 12943–12950.

Appenzeller, C., Andersson, H., Kappeler, F., & Hauri, H.-P. (1999). The lectin ERGIC-53 is a cargo transport receptor for glycoproteins. *Nat. Cell Biol. 1999 16*, *1*(6), 330–334.

Aradhyam, G. K., Balivada, L. M., Kanuru, M., Vadivel, P., & Vidhya, B. S. (2010). Calnuc: Emerging roles in calcium signaling and human diseases. *IUBMB Life*, *62*(6), 436–446.

Bechler, M., Doody, A., Racoosin, E., Lin, L., Lee, K., & Brown, W. (2010). The phospholipase complex PAFAH Ib regulates the functional organization of the Golgi complex. *J. Cell Biol.*, *190*(1), 45–53.

Bechler, M. E., & Brown, W. J. (2014). Gβ1γ2 activates phospholipase A 2 -dependent Golgi membrane tubule formation. *Front. Cell Dev. Biol.*, *2*(FEB), 4.

Bechler, M. E., De Figueiredo, P., & Brown, W. J. (2012). A PLA1-2 punch regulates the Golgi complex. In *Trends in Cell Biology* (Vol. 22, Issue 2, pp. 116–124). NIH Public Access.

Ben-Tekaya, H., Kahn, R., & Hauri, H. (2010). ADP ribosylation factors 1 and 4 and group VIA phospholipase A_2 regulate morphology and intraorganellar traffic in the endoplasmic reticulum-Golgi intermediate compartment. *Mol. Biol. Cell*, *21*(23), 4130–4140.

Bentley, M., Nycz, D. C., Joglekar, A., Fertschai, I., Malli, R., Graier, W. F., & Hay, J. C. (2010). Vesicular calcium regulates coat retention, fusogenicity, and size of pre-Golgi intermediates. *Mol. Biol. Cell*, *21*(6), 1033–1046.

Bi, X., Mancias, J. D., & Goldberg, J. (2007). Insights into COPII Coat Nucleation from the Structure of Sec23•Sar1 Complexed with the Active Fragment of Sec31. *Dev. Cell*, *13*(5), 635.

Blume, J. von, Alleaume, A.-M., Kienzle, C., Carreras-Sureda, A., Valverde, M., & Malhotra, V. (2012). Cab45 is required for Ca2+-dependent secretory cargo sorting at the trans-Golgi network. *J. Cell Biol.*, *199*(7), 1057.

Bonnon, C., Wendeler, M. W., Paccaud, J.-P., & Hauri, H.-P. (2010). Selective export of human GPI-anchored proteins from the endoplasmic reticulum. *J. Cell Sci.*, *123*(10), 1705–1715.

Booth, C., & Koch, G. L. E. (1989). Perturbation of cellular calcium induces secretion of luminal ER proteins. *Cell*, *59*(4), 729–737.

Bootman, M. D., & Bultynck, G. (2020). Fundamentals of cellular calcium signaling: A primer.

Cold Spring Harb. Perspect. Biol., *12*(1).
Bootman, M. D., Collins, T. J., Peppiatt, C. M., Prothero, L. S., MacKenzie, L., De Smet, P., Travers, M., Tovey, S. C., Seo, J. T., Berridge, M. J., Ciccolini, F., & Lipp, P. (2001). Calcium signalling—an overview. *Semin. Cell Dev. Biol.*, *12*(1), 3–10.
Bouter, A., Gounou, C., Bérat, R., Tan, S., Gallois, B., Granier, T., D'Estaintot, B. L., Pöschl, E., Brachvogel, B., & Brisson, A. R. (2011). Annexin-A5 assembled into two-dimensional arrays promotes cell membrane repair. *Nat. Commun.*, *2*(1), 1–9.
Boye, T. L., Jeppesen, J. C., Maeda, K., Pezeshkian, W., Solovyeva, V., Nylandsted, J., & Simonsen, A. C. (2018). Annexins induce curvature on free-edge membranes displaying distinct morphologies. *Sci. Reports 2018 81*, *8*(1), 1–14.
Brodeur, J., Larkin, H., Boucher, R., Thériault, C., St-Louis, S. C., Gagnon, H., & Lavoie, C. (2009). Calnuc Binds to LRP9 and Affects its Endosomal Sorting. *Traffic*, *10*(8), 1098–1114.
Burgoyne, T., Patel, S., & Eden, E. R. (2015). Calcium signaling at ER membrane contact sites. *Biochim. Biophys. Acta - Mol. Cell Res.*, *1853*(9), 2012–2017.
Burke, J. E., & Dennis, E. A. (2009). Phospholipase A2 structure/function, mechanism, and signaling. *J. Lipid Res.*, *50*(Suppl), S237.
Cantero-Recasens, G., Butnaru, C. M., Valverde, M. A., Naranjo, J. R., Brouwers, N., & Malhotra, V. (2018). KChIP3 coupled to Ca2+ oscillations exerts a tonic brake on baseline mucin release in the colon. *Elife*, *7*.
Cao, Q., Yang, Y., Zhong, X., & Dong, X. (2017). The lysosomal Ca 2+ release channel TRPML1 regulates lysosome size by activating calmodulin. *J. Biol. Chem.*, *292*(20), 8424–8435.
Cao, Q., Zhong, X. Z., Zou, Y., Murrell-Lagnado, R., Zhu, M. X., & Dong, X. P. (2015). Calcium release through P2X4 activates calmodulin to promote endolysosomal membrane fusion. *J. Cell Biol.*, *209*(6).
Chakrabarti, A., Chen, A. W., & Varner, J. D. (2011). A Review of the Mammalian Unfolded Protein Response. *Biotechnol. Bioeng.*, *108*(12), 2777.
Chasserot-Golaz, S., Vitale, N., Umbrecht-Jenck, E., Knight, D., Gerke, V., & Bader, M.-F. (2005). Annexin 2 Promotes the Formation of Lipid Microdomains Required for Calcium-regulated Exocytosis of Dense-Core Vesicles. *Mol. Biol. Cell*, *16*(3), 1108.
Chen, J. L., Ahluwalia, J. P., & Stamnes, M. (2002). Selective effects of calcium chelators on anterograde and retrograde protein transport in the cell. *J. Biol. Chem.*, *277*(38), 35682–35687.
Chia, P. Z. C., & Gleeson, P. A. (2014). Membrane tethering. *F1000Prime Rep.*, *6*.
Cho, H. J., & Mook-Jung, I. (2018). O-GlcNAcylation regulates endoplasmic reticulum exit sites through Sec31A modification in conventional secretory pathway. *FASEB J.*, *32*(9), 4641–4657.
Cho, H. J., & Mook-Jung, I. (2020). Amyloid beta regulates ER exit sites formation through O-GlcNAcylation triggered by disrupted calcium homeostasis. *Biol. Cell*, *112*(12), 439–451.
Colombo, M., Beron, W., & Stahl, P. (1997). Calmodulin regulates endosome fusion. *J. Biol. Chem.*, *272*(12), 7707–7712.
Cour, J. M. la, Schindler, A. J., Berchtold, M. W., & Schekman, R. (2013). ALG-2 Attenuates COPII Budding In Vitro and Stabilizes the Sec23/Sec31A Complex. *PLoS One*, *8*(9), e75309.

Cunningham, M. A., Pipe, S. W., Zhang, B., Hauri, H.-P., Ginsburg, D., & Kaufman, R. J. (2003). LMAN1 is a molecular chaperone for the secretion of coagulation factor VIII1. *J. Thromb. Haemost.*, *1*(11), 2360–2367.

D'hooge, P., Coun, C., Van Eyck, V., Faes, L., Ghillebert, R., Mariën, L., Winderickx, J., & Callewaert, G. (2015). Ca2+ homeostasis in the budding yeast Saccharomyces cerevisiae: Impact of ER/Golgi Ca2+ storage. *Cell Calcium*, *58*(2), 226–235.

Deng, Y., Pakdel, M., Blank, B., Sundberg, E. L., Burd, C. G., & von Blume, J. (2018). Activity of the SPCA1 Calcium Pump Couples Sphingomyelin Synthesis to Sorting of Secretory Proteins in the Trans-Golgi Network. *Dev. Cell*, *47*(4), 464-478.e8.

Di Paola, S., Scotto-Rosato, A., & Medina, D. L. (2018). TRPML1: The Ca(2+)retaker of the lysosome. *Cell Calcium*, *69*, 112–121.

Dong, X. P., Shen, D., Wang, X., Dawson, T., Li, X., Zhang, Q., Cheng, X., Zhang, Y., Weisman, L. S., Delling, M., & Xu, H. (2010). PI(3,5)P2 controls membrane trafficking by direct activation of mucolipin Ca2+ release channels in the endolysosome. *Nat. Commun.*, *1*(4).

Duan, J., Navarro-Dorado, J., Clark, J. H., Kinnear, N. P., Meinke, P., Schirmer, E. C., & Evans, A. M. (2019). The cell-wide web coordinates cellular processes by directing site-specific Ca2+ flux across cytoplasmic nanocourses. *Nat. Commun.*, *10*(1), 1–12.

Dürr, G., Strayle, J., Plemper, R., Elbs, S., Klee, S. K., Catty, P., Wolf, D. H., & Rudolph, H. K. (1998). The medial-Golgi ion pump Pmr1 supplies the yeast secretory pathway with Ca2+ and Mn2+ required for glycosylation, sorting, and endoplasmic reticulum-Associated protein degradation. *Mol. Biol. Cell*, *9*(5), 1149–1162.

Evans, J. H., Gerber, S. H., Murray, D., & Leslie, C. C. (2004). The Calcium Binding Loops of the Cytosolic Phospholipase A2 C2 Domain Specify Targeting to Golgi and ER in Live Cells. *Mol. Biol. Cell*, *15*(1), 371.

Evans, R. C., & Blackwell, K. T. (2015). Calcium: Amplitude, duration, or location? *Biol. Bull.*, *228*(1), 75–83.

Feng, X., & Yang, J. (2016). Lysosomal Calcium in Neurodegeneration. *Messenger (Los Angeles, Calif. Print)*, *5*(1–2), 56.

Fu, X., Wang, Y., Schetle, N., Gao, H., Pütz, M., Gersdorff, G. von, Walz, G., & Kramer-Zucker, A. G. (2008). The Subcellular Localization of TRPP2 Modulates Its Function. *J. Am. Soc. Nephrol.*, *19*(7), 1342–1351.

Fu, Y. L., Zhang, B., & Mu, T.-W. (2019). LMAN1 (ERGIC-53) promotes trafficking of neuroreceptors. *Biochem. Biophys. Res. Commun.*, *511*(2), 356.

Garcia-Marcos, M., Kietrsunthorn, P. S., Wang, H., Ghosh, P., & Farquhar, M. G. (2011). G Protein Binding Sites on Calnuc (Nucleobindin 1) and NUCB2 (Nucleobindin 2) Define a New Class of Gαi-regulatory Motifs. *J. Biol. Chem.*, *286*(32), 28138.

Genereux, J. C., Qu, S., Zhou, M., Ryno, L. M., Wang, S., Shoulders, M. D., Kaufman, R. J., Lasmézas, C. I., Kelly, J. W., & Wiseman, R. L. (2015). Unfolded protein response-induced ERdj3 secretion links ER stress to extracellular proteostasis. *EMBO J.*, *34*(1), 4.

Ghaemmaghami, S., Huh, W.-K., Bower, K., Howson, R. W., Belle, A., Dephoure, N., O'Shea, E. K., & Weissman, J. S. (2003). Global analysis of protein expression in yeast. *Nat. 2003 4256959*, *425*(6959), 737–741.

Gordon, D. E., Bond, L. M., Sahlender, D. A., & Peden, A. A. (2010). A Targeted siRNA Screen to Identify SNAREs Required for Constitutive Secretion in Mammalian Cells. *Traffic*, *11*(9), 1191–1204.

Graber, Z. T., Shi, Z., & Baumgart, T. (2017). Cations induce shape remodeling of negatively charged phospholipid membranes. *Phys. Chem. Chem. Phys.*, *19*(23), 15285–15295.

Graber, Z. T., Wang, W., Singh, G., Kuzmenko, I., Vaknin, D., & Kooijman, E. E. (2015). Competitive cation binding to phosphatidylinositol-4,5-bisphosphate domains revealed by X-ray fluorescence. *RSC Adv.*, *5*(129), 106536–106542.

Grice, D. M., Vetter, I., Faddy, H. M., Kenny, P. A., Roberts-Thomson, S. J., & Monteith, G. R. (2010). Golgi calcium pump secretory pathway calcium ATPase 1 (SPCA1) is a key regulator of Insulin-like Growth Factor Receptor (IGF1R) processing in the basal-like breast cancer cell line MDA-MB-231. *J. Biol. Chem.*, *285*(48), 37458–37466.

Hammond, A. T., & Glick, B. S. (2000). Dynamics of Transitional Endoplasmic Reticulum Sites in Vertebrate Cells. *Mol. Biol. Cell*, *11*(9), 3013.

Hay, J. C. (2007). Calcium: A fundamental regulator of intracellular membrane fusion? In *EMBO Reports* (Vol. 8, Issue 3, pp. 236–240). European Molecular Biology Organization.

Held, A., Sargeant, J., Hojanazarova, J., Madreiter-Sokolowski, C., Malli, R., Graier, W. F., & Hay, J. C. (2021). Steady-State Regulation of Secretory Cargo Export by Inositol Trisphosphate Receptors and Penta EF Hand Proteins. *BioRxiv*, 2020.06.13.150144.

Helm, J. R., Bentley, M., Thorsen, K. D., Wang, T., Foltz, L., Oorschot, V., Klumperman, J., & Hay, J. C. (2014). Apoptosis-linked gene-2 (ALG-2)/Sec31 interactions regulate endoplasmic reticulum (ER)-to-Golgi transport: A potential effector pathway for luminal calcium. *J. Biol. Chem.*, *289*(34), 23609–23628.

Henderson, M. J., Richie, C. T., Airavaara, M., Wang, Y., & Harvey, B. K. (2013). Mesencephalic Astrocyte-derived Neurotrophic Factor (MANF) Secretion and Cell Surface Binding Are Modulated by KDEL Receptors. *J. Biol. Chem.*, *288*(6), 4209–4225.

Henderson, M. J., Wires, E. S., Trychta, K. A., Richie, C. T., & Harvey, B. K. (2014). SERCaMP: a carboxy-terminal protein modification that enables monitoring of ER calcium homeostasis. *Mol. Biol. Cell*, *25*(18), 2828.

Hetz, C., Zhang, K., & Kaufman, R. J. (2020). Mechanisms, regulation and functions of the unfolded protein response. *Nat. Rev. Mol. Cell Biol. 2020 218*, *21*(8), 421–438.

Hu, H., Tian, M., Ding, C., & Yu, S. (2019). The C/EBP Homologous Protein (CHOP) Transcription Factor Functions in Endoplasmic Reticulum Stress-Induced Apoptosis and Microbial Infection. *Front. Immunol.*, *9*, 3083.

Hughes, H., & Stephens, D. J. (2008). Assembly, organization, and function of the COPII coat. *Histochem. Cell Biol.*, *129*(2), 129.

Hullin-Matsuda, F., Taguchi, T., Greimel, P., & Kobayashi, T. (2014). Lipid compartmentalization in the endosome system. *Semin. Cell Dev. Biol.*, *31*, 48–56.

Ireland, S., Ramnarayanan, S., Fu, M., Zhang, X., Zhang, J., Li, J., Emebo, D., & Wang, Y. (2020). Cytosolic Ca2+ Modulates Golgi Structure Through PKCα-Mediated GRASP55 Phosphorylation. *IScience*, *23*(3).

Jin, L., Pahuja, K. B., Wickliffe, K. E., Gorur, A., Baumgärtel, C., Schekman, R., & Rape, M. (2012).

Ubiquitin-dependent regulation of COPII coat size and function. *Nature*, *482*(7386), 495–500.
Kanadome, T., Shibata, H., Kuwata, K., Takahara, T., & Maki, M. (2017). The calcium-binding protein ALG-2 promotes endoplasmic reticulum exit site localization and polymerization of Trk-fused gene (TFG) protein. *FEBS J.*, *284*(1), 56–76.
Kanuru, M., & Aradhyam, G. K. (2017). Chaperone-like Activity of Calnuc Prevents Amyloid Aggregation. *Biochemistry*, *56*(1), 149–159.
Kitaura, Y., Matsumoto, S., Satoh, H., Hitomi, K., & Maki, M. (2001). Peflin and ALG-2, Members of the Penta-EF-Hand Protein Family, Form a Heterodimer That Dissociates in a Ca2+-dependent Manner. *J. Biol. Chem.*, *276*(17), 14053–14058.
Kitaura, Y., Satoh, H., Takahashi, H., Shibata, H., & Maki, M. (2002). Both ALG-2 and Peflin, Penta-EF-hand (PEF) Proteins, Are Stabilized by Dimerization through Their Fifth EF-Hand Regions. *Arch. Biochem. Biophys.*, *399*(1), 12–18.
Konopka-Postupolska, D., & Clark, G. (2017). Annexins as overlooked regulators of membrane trafficking in plant cells. In *International Journal of Molecular Sciences* (Vol. 18, Issue 4). MDPI AG.
la Cour, J. M., Mollerup, J., & Berchtold, M. (2007). ALG-2 oscillates in subcellular localization, unitemporally with calcium oscillations. *Biochem. Biophys. Res. Commun.*, *353*(4), 1063–1067.
la Cour, J. M., Schindler, A. J., Berchtold, M. W., & Schekman, R. (2013). ALG-2 Attenuates COPII Budding In Vitro and Stabilizes the Sec23/Sec31A Complex. *PLoS One*, *8*, e75309.
Larkin, H., Costantino, S., Seaman, M. N. J., & Lavoie, C. (2016). Calnuc Function in Endosomal Sorting of Lysosomal Receptors. *Traffic*, *17*(4), 416–432.
Lavender, V., Chong, S., Ralphs, K., Wolstenholme, A. J., & Reaves, B. J. (2008). Increasing the expression of calcium-permeable TRPC3 and TRPC7 channels enhances constitutive secretion. *Biochem. J.*, *413*(3), 437–446.
Lavoie, C., Meerloo, T., Lin, P., & Farquhar, M. (2002). Calnuc, an EF-hand Ca(2+)-binding protein, is stored and processed in the Golgi and secreted by the constitutive-like pathway in AtT20 cells. *Mol. Endocrinol.*, *16*(11), 2462–2474.
Le Corre, S., Eyre, D., & Drummond, I. A. (2014). Modulation of the secretory pathway rescues zebrafish polycystic kidney disease pathology. *J. Am. Soc. Nephrol.*, *25*(8), 1749–1759.
Lefrancois, L., & Lyles, D. S. (1982). The interaction of antibody with the major surface glycoprotein of vesicular stomatitis virus I. Analysis of neutralizing epitopes with monoclonal antibodies. *Virology*, *121*(1), 157–167.
Lennon, N. J., Kho, A., Bacskai, B. J., Perlmutter, S. L., Hyman, B. T., & Brown, R. H. (2003). Dysferlin Interacts with Annexins A1 and A2 and Mediates Sarcolemmal Wound-healing. *J. Biol. Chem.*, *278*(50), 50466–50473.
Li, G., Huang, D., Hong, J., Bhat, O. M., Yuan, X., & Li, P.-L. (2019). Control of lysosomal TRPML1 channel activity and exosome release by acid ceramidase in mouse podocytes. *Am. J. Physiol.*, *317*(3), C481–C494.
Li, X., Rydzewski, N., Hider, A., Zhang, X., Yang, J., Wang, W., Gao, Q., Cheng, X., & Xu, H. (2016). A Molecular Mechanism to Regulate Lysosome Motility for Lysosome Positioning and

Tubulation. *Nat. Cell Biol.*, *18*(4), 404.
Lin, P., Fischer, T., Lavoie, C., Huang, H., & Farquhar, M. G. (2009). Calnuc plays a role in dynamic distribution of Gαi but not Gβ subunits and modulates ACTH secretion in AtT-20 neuroendocrine secretory cells. *Mol. Neurodegener. 2009 41*, *4*(1), 1–16.
Lin, P., Le-Niculescu, H., Hofmeister, R., McCaffery, J., Jin, M., Hennemann, H., McQuistan, T., De Vries, L., & Farquhar, M. (1998). The mammalian calcium-binding protein, nucleobindin (CALNUC), is a Golgi resident protein. *J. Cell Biol.*, *141*(7), 1515–1527.
Lin, P., Li, F., Zhang, Y., Huang, H., Tong, G., Farquhar, M., & Xu, H. (2007). Calnuc binds to Alzheimer's beta-amyloid precursor protein and affects its biogenesis. *J. Neurochem.*, *100*(6), 1505–1514.
Lin, P., Yao, Y., Hofmeister, R., Tsien, R. Y., & Farquhar, M. G. (1999). Overexpression of CALNUC (Nucleobindin) Increases Agonist and Thapsigargin Releasable Ca2+ Storage in the Golgi. *J. Cell Biol.*, *145*(2), 279.
Lowe, M., Rabouille, C., Nakamura, N., Watson, R., Jackman, M., Jämsä, E., Rahman, D., Pappin, D. J. ., & Warren, G. (1998). Cdc2 Kinase Directly Phosphorylates the cis-Golgi Matrix Protein GM130 and Is Required for Golgi Fragmentation in Mitosis. *Cell*, *94*(6), 783–793.
Ludhiadch, A., Sharma, R., Muriki, A., & Munshi, A. (2021). Role of Calcium Homeostasis in Ischemic Stroke: A Review. *CNS Neurol. Disord. - Drug Targets*, *20*.
Luzio, J. P., Bright, N. A., & Pryor, P. R. (2007). The role of calcium and other ions in sorting and delivery in the late endocytic pathway. *Biochem. Soc. Trans.*, *35*(5), 1088–1091.
Ma, W., Goldberg, E., & Goldberg, J. (2017). ER retention is imposed by COPII protein sorting and attenuated by 4-phenylbutyrate. *Elife*, *6*, 213.
Madreiter-Sokolowski, C. T., Waldeck-Weiermair, M., Bourguignon, M. P., Villeneuve, N., Gottschalk, B., Klec, C., Stryeck, S., Radulovic, S., Parichatikanond, W., Frank, S., Madl, T., Malli, R., & Graier, W. F. (2019). Enhanced inter-compartmental Ca2+ flux modulates mitochondrial metabolism and apoptotic threshold during aging. *Redox Biol.*, *289*, 23609–23628.
Maki, M., Kitaura, Y., Satoh, H., Ohkouchi, S., & Shibata, H. (2002). Structures, functions and molecular evolution of the penta-EF-hand Ca2+-binding proteins. *Biochim. Biophys. Acta - Proteins Proteomics*, *1600*(1–2), 51–60.
Mao, Y., Du, Y., Cang, X., Wang, J., Chen, Z., Yang, H., & Jiang, H. (2013). Binding competition to the POPG lipid bilayer of Ca2+, Mg 2+, Na+, and K+ in different ion mixtures and biological implication. *J. Phys. Chem. B*, *117*(3), 850–858.
McCaughey, J., Miller, V. J., Stevenson, N. L., Brown, A. K., Budnik, A., Heesom, K. J., Alibhai, D., & Stephens, D. J. (2016). TFG Promotes Organization of Transitional ER and Efficient Collagen Secretion. *Cell Rep.*, *15*(8), 1648.
McGourty, C. A., Akopian, D., Walsh, C., Gorur, A., Werner, A., Schekman, R., Bautista, D., & Rape, M. (2016a). Regulation of the CUL3 Ubiquitin Ligase by a Calcium-Dependent Co-adaptor. *Cell*.
McGourty, C. A., Akopian, D., Walsh, C., Gorur, A., Werner, A., Schekman, R., Bautista, D., & Rape, M. (2016b). Regulation of the CUL3 Ubiquitin Ligase by a Calcium-Dependent Co-adaptor. *Cell*, *167*(2), 525-538.e14.

Micaroni, M. (2012). Calcium Around the Golgi Apparatus: Implications for Intracellular Membrane Trafficking. *Adv. Exp. Med. Biol.*, *740*, 439–460.

Micaroni, M., Perinetti, G., Di Giandomenico, D., Bianchi, K., Spaar, A., & Mironov, A. (2010). Synchronous intra-Golgi transport induces the release of Ca2+ from the Golgi apparatus. *Exp. Cell Res.*, *316*(13), 2071–2086.

Miller, E. A., & Barlowe, C. (2010). Regulation of coat assembly- sorting things out at the ER. *Curr. Opin. Cell Biol.*, *22*(4), 447.

Miller, M., Wu, M., Xu, J., Weaver, D., Li, M., & Zhu, M. X. (2011). High-Throughput Screening of TRPC Channel Ligands Using Cell-Based Assays. *TRP Channels*, 1–20.

Missiaen, L., Raeymaekers, L., Dode, L., Vanoevelen, J., Van Baelen, K., Parys, J. B., Callewaert, G., De Smedt, H., Segaert, S., & Wuytack, F. (2004). SPCA1 pumps and Hailey–Hailey disease. *Biochem. Biophys. Res. Commun.*, *322*(4), 1204–1213.

Mukherjee, I., & Barlowe, C. (2016). Overexpression of Sly41 suppresses COPII vesicle-tethering deficiencies by elevating intracellular calcium levels. *Mol. Biol. Cell*, *27*(10), 1635–1649.

Nyfeler, B., Reiterer, V., Wendeler, M. W., Stefan, E., Zhang, B., Michnick, S. W., & Hauri, H.-P. (2008). Identification of ERGIC-53 as an intracellular transport receptor of α1-antitrypsin. *J. Cell Biol.*, *180*(4), 705.

Nyfeler, B., Zhang, B., Ginsburg, D., Kaufman, R., & Hauri, H. (2006). Cargo selectivity of the ERGIC-53/MCFD2 transport receptor complex. *Traffic*, *7*(11), 1473–1481.

Omari, S., Makareeva, E., Roberts-Pilgrim, A., Mirigian, L., Jarnik, M., Ott, C., Lippincott-Schwartz, J., & Leikin, S. (2018). Noncanonical autophagy at ER exit sites regulates procollagen turnover. *Proc. Natl. Acad. Sci.*, *115*(43), E10099–E10108.

Pacheco-Fernandez, N., Pakdel, M., Blank, B., Sanchez-Gonzalez, I., Weber, K., Tran, M. L., Hecht, T. K. H., Gautsch, R., Beck, G., Perez, F., Hausser, A., Linder, S., & von Blume, J. (2020). Nucleobindin-1 regulates ECM degradation by promoting intra-Golgi trafficking of MMPs. *J. Cell Biol.*, *219*(8).

Patel, S. (2019). Getting close. Lysosome-ER contact sites tailor Ca2+ signals. *Cell Calcium*, *80*, 194–196.

Pedersen, U., Leidy, C., Westh, P., & Peters, G. (2006). The effect of calcium on the properties of charged phospholipid bilayers. *Biochim. Biophys. Acta*, *1758*(5), 573–582.

Peters, C., & Mayer, A. (1998). Ca2+/calmodulin signals the completion of docking and triggers a late step of vacuole fusion. *Nature*, *396*(6711), 575–580.

Petersson, U., Somogyi, E., Reinholt, F., Karlsson, T., Sugars, R., & Wendel, M. (2004). Nucleobindin is produced by bone cells and secreted into the osteoid, with a potential role as a modulator of matrix maturation. *Bone*, *34*(6), 949–960.

Pietro, E. S., Capestrano, M., Polishchuk, E. V., DiPentima, A., Trucco, A., Zizza, P., Mariggiò, S., Pulvirenti, T., Sallese, M., Tete, S., Mironov, A. A., Leslie, C. C., Corda, D., Luini, A., & Polishchuk, R. S. (2009). Group IV Phospholipase A2α Controls the Formation of Inter-Cisternal Continuities Involved in Intra-Golgi Transport. *PLOS Biol.*, *7*(9), e1000194.

Pizzo, P., Lissandron, V., Capitanio, P., & Pozzan, T. (2011). Ca(2+) signalling in the Golgi apparatus. *Cell Calcium*, *50*(2), 184–192.

Pryor, P. R., Mullock, B. M., Bright, N. A., Gray, S. R., & Luzio, J. P. (2000). The Role of

Intraorganellar Ca2+In Late Endosome–Lysosome Heterotypic Fusion and in the Reformation of Lysosomes from Hybrid Organelles. *J. Cell Biol.*, *149*(5), 1053.

Raote, I., Ortega-Bellido, M., Santos, A. J. M., Foresti, O., Zhang, C., Garcia-Parajo, M. F., Campelo, F., & Malhotra, V. (2018). TANGO1 builds a machine for collagen export by recruiting and spatially organizing COPII, tethers and membranes. *Elife*, *7*, 2639.

Rauter, T., Burgstaller, S., Gottschalk, B., Ramadani-Muja, J., Bischof, H., Hay, J. C., Graier, W. F., & Malli, R. (2020). ER-to-Golgi Transport in HeLa Cells Displays High Resilience to Ca2+ and Energy Stresses. *Cells*, *9*(10).

Rayl, M., Truitt, M., Held, A., Sargeant, J., Thorsen, K., & Hay, J. C. (2016). Penta-EF-hand protein peflin is a negative regulator of ER-to-Golgi transport. *PLoS One*, *11*(6).

Regan-Klapisz, E., Krouwer, V., Langelaar-Makkinje, M., Nallan, L., Gelb, M., Gerritsen, H., Verkleij, A. J., & Post, J. A. (2009). Golgi-associated cPLA2α Regulates Endothelial Cell–Cell Junction Integrity by Controlling the Trafficking of Transmembrane Junction Proteins. *Mol. Biol. Cell*, *20*(19), 4225.

Rivera, V. M., Wang, X., Wardwell, S., Courage, N. L., Volchuk, A., Keenan, T., Holt, D. A., Gilman, M., Orci, L., Cerasoli, F., Rothman, J. E., & Clackson, T. (2000). Regulation of protein secretion through controlled aggregation in the endoplasmic reticulum. *Science (80-.).*, *287*(5454), 826–830.

Rossi, A. H., Sears, P. R., & Davis, C. W. (2004). Ca2+ dependency of 'Ca2+-independent' exocytosis in SPOC1 airway goblet cells. *J. Physiol.*, *559*(Pt 2), 555.

Saito, K., Chen, M., Bard, F., Chen, S., Zhou, H., Woodley, D., Polischuk, R., Schekman, R., & Malhotra, V. (2009). TANGO1 facilitates cargo loading at endoplasmic reticulum exit sites. *Cell*, *136*(5), 891–902.

Sammels, E., Devogelaere, B., Mekahli, D., Bultynck, G., Missiaen, L., Parys, J. B., Cai, Y., Somlo, S., & Smedt, H. De. (2010). Polycystin-2 Activation by Inositol 1,4,5-Trisphosphate-induced Ca2+ Release Requires Its Direct Association with the Inositol 1,4,5-Trisphosphate Receptor in a Signaling Microdomain. *J. Biol. Chem.*, *285*(24), 18794.

Santella, L., Lim, D., & Moccia, F. (2004). Calcium and fertilization: the beginning of life. *Trends Biochem. Sci.*, *29*(8), 400–408.

Sargeant, J., Seiler, D., Costain, T., Madreiter-Sokolowski, C., Gordon, D. E., Peden, A. A., Malli, R., Graier, W. F., & Ray, J. C. (2021). ALG-2 and Peflin Stimulate or Inhibit COPII Targeting and Secretion in Response to Calcium Signaling. *J. Biol. Chem., 297*(6), 101393.

Sarmento, M. J., Coutinho, A., Fedorov, A., Prieto, M., & Fernandes, F. (2014). Ca2 + induces PI(4,5)P2 clusters on lipid bilayers at physiological PI(4,5)P2 and Ca2 + concentrations. *Biochim. Biophys. Acta - Biomembr.*, *1838*(3), 822–830.

Sasaki-Osugi, K., Imoto, C., Takahara, T., Shibata, H., & Maki, M. (2013). Nuclear ALG-2 Protein Interacts with Ca2+ Homeostasis Endoplasmic Reticulum Protein (CHERP) Ca2+-dependently and Participates in Regulation of Alternative Splicing of Inositol Trisphosphate Receptor Type 1 (IP3R1) Pre-mRNA. *J. Biol. Chem.*, *288*(46), 33361–33375.

Shibata, H., Inuzuka, T., Yoshida, H., Sugiura, H., Wada, I., & Maki, M. (2010). The ALG-2 Binding Site in Sec31A Influences the Retention Kinetics of Sec31A at the Endoplasmic Reticulum Exit Sites as Revealed by Live-Cell Time-Lapse Imaging. *Biosci. Biotechnol. Biochem.*, *74*(9),

1819–1826.
Shibata, H., Kanadome, T., Sugiura, H., Yokoyama, T., Yamamuro, M., Moss, S. E., & Maki, M. (2015). A new role for annexin A11 in the early secretory pathway via stabilizing Sec31A protein at the endoplasmic reticulum exit sites (ERES). *J. Biol. Chem.*, *290*(8), 4981–4993.
Shibata, H., Suzuki, H., Yoshida, H., & Maki, M. (2007). ALG-2 directly binds Sec31A and localizes at endoplasmic reticulum exit sites in a Ca2+-dependent manner. *Biochem. Biophys. Res. Commun.*, *353*(3), 756–763.
Sinn, C. G., Antonietti, M., & Dimova, R. (2006). Binding of calcium to phosphatidylcholine–phosphatidylserine membranes. *Colloids Surfaces A Physicochem. Eng. Asp.*, *282–283*, 410–419.
Sonnichsen, B., Fullekrug, J., Nguyen Van, P., Diekmann, W., Robinson, D. G., & Mieskes, G. (1994). Retention and retrieval: both mechanisms cooperate to maintain calreticulin in the endoplasmic reticulum. *J. Cell Sci.*, *107*(10), 2705–2717.
Stagg, S. M., LaPointe, P., Razvi, A., Gürkan, C., Potter, C. S., Carragher, B., & Balch, W. E. (2008). Structural Basis for Cargo Regulation of COPII Coat Assembly. *Cell*, *134*(3), 474.
Tabata, K. V, Sato, K., Ide, T., Nishizaka, T., Nakano, A., & Noji, H. (2009). Visualization of cargo concentration by COPII minimal machinery in a planar lipid membrane. *EMBO J.*, *28*(21), 3279–3289.
Takahara, T., Inoue, K., Arai, Y., Kuwata, K., Shibata, H., & Maki, M. (2017). The calcium-binding protein ALG-2 regulates protein secretion and trafficking via interactions with MISSL and MAP1B proteins. *J. Biol. Chem.*, *292*(41), 17057–17072.
Takeshi, T., Kojima, K., Zhang, W., Sasaki, K., Ito, M., Suzuki, H., Kawasaki, M., Wakatsuki, S., Takahara, T., Shibata, H., & Maki, M. (2015). Structural analysis of the complex between Penta-Ef-Hand Alg-2 protein and sec31a peptide reveals a novel target recognition mechanism of Alg-2. *Int. J. Mol. Sci.*, *16*, 3677–3699.
Tarabykina, S., Møller, A. L., Durussel, I., Cox, J., & Berchtold, M. W. (2000). Two Forms of the Apoptosis-linked Protein ALG-2 with Different Ca2+ Affinities and Target Recognition. *J. Biol. Chem.*, *275*(14), 10514–10518.
Tarafdar, P. K., Chakraborty, H., Dennison, S. M., & Lentz, B. R. (2012). Phosphatidylserine Inhibits and Calcium Promotes Model Membrane Fusion. *Biophys. J.*, *103*(9), 1880–1889.
Trychta, K. A., Bäck, S., Henderson, M. J., & Harvey, B. K. (2018). KDEL Receptors Are Differentially Regulated to Maintain the ER Proteome under Calcium Deficiency. *Cell Rep.*, *25*(7), 1829-1840.e6.
Van Anken, E., Romijn, E. P., Maggioni, C., Mezghrani, A., Sitia, R., Braakman, I., & Heck, A. J. R. (2003). Sequential Waves of Functionally Related Proteins Are Expressed When B Cells Prepare for Antibody Secretion. *Immunity*, *18*(2), 243–253.
Veglia, E., Grange, C., Pini, A., Moggio, A., Lanzi, C., Camussi, G., Chazot, P. L., & Rosa, A. C. (2015). Histamine receptor expression in human renal tubules: a comparative pharmacological evaluation. *Inflamm. Res. 2015 643*, *64*(3), 261–270.
Velloso, L. M., Svensson, K., Pettersson, R. F., & Lindqvist, Y. (2003). The Crystal Structure of the Carbohydrate-recognition Domain of the Glycoprotein Sorting Receptor p58/ERGIC-53 Reveals an Unpredicted Metal-binding Site and Conformational Changes Associated with

Calcium Ion Binding. *J. Mol. Biol.*, *334*(5), 845–851.
Vergarajauregui, S., Martina, J., & Puertollano, R. (2009). Identification of the penta-EF-hand protein ALG-2 as a Ca2+-dependent interactor of mucolipin-1. *J. Biol. Chem.*, *284*(52), 36357–36366.
Wegierski, T., Steffl, D., Kopp, C., Tauber, R., Buchholz, B., Nitschke, R., Kuehn, E. W., Walz, G., & Köttgen, M. (2009). TRPP2 channels regulate apoptosis through the Ca2+ concentration in the endoplasmic reticulum. *EMBO J.*, *28*(5), 490–499.
Wilson, D. G., Phamluong, K., Li, L., Sun, M., Cao, T. C., Liu, P. S., Modrusan, Z., Sandoval, W. N., Rangell, L., Carano, R. A. D., Peterson, A. S., & Solloway, M. J. (2011). Global defects in collagen secretion in a Mia3/TANGO1 knockout mouse. *J. Cell Biol.*, *193*(5), 935.
Wong, C., Li, R., Montell, C., & Venkatachalam, K. (2012). Drosophila TRPML is required for TORC1 activation. *Curr. Biol.*, *22*(17), 1616–1621.
Yamasaki, A., Tani, K., Yamamoto, A., Kitamura, N., & Komada, M. (2006). The Ca2+-binding Protein ALG-2 Is Recruited to Endoplasmic Reticulum Exit Sites by Sec31A and Stabilizes the Localization of Sec31A. *Mol. Biol. Cell*, *17*(11), 4876.
Yang, Y., Xu, M., Zhu, X., Yao, J., Shen, B., & Dong, X. (2019). Lysosomal Ca 2+ release channel TRPML1 regulates lysosome size by promoting mTORC1 activity. *Eur. J. Cell Biol.*, *98*(2–4), 116–123.
Yoshibori, M., Yorimitsu, T., & Sato, K. (2012). Involvement of the Penta-EF-hand protein Pef1p in the Ca2+-dependent regulation of COPII subunit assembly in Saccharomyces cerevisiae. *PLoS One*, *7*(7), 40765.
Zhang, B., Kaufman, R., & Ginsburg, D. (2005). LMAN1 and MCFD2 form a cargo receptor complex and interact with coagulation factor VIII in the early secretory pathway. *J. Biol. Chem.*, *280*(27), 25881–25886.
Zheng, C., Page, R. C., Das, V., Nix, J. C., Wigren, E., Misra, S., & Zhang, B. (2013). Structural Characterization of Carbohydrate Binding by LMAN1 Protein Provides New Insight into the Endoplasmic Reticulum Export of Factors V (FV) and VIII (FVIII). *J. Biol. Chem.*, *288*(28), 20499.
Zhu, Y., Abdullah, L. H., Doyle, S. P., Nguyen, K., Ribeiro, C. M. P., Vasquez, P. A., Forest, M. G., Lethem, M. I., Dickey, B. F., & Davis, C. W. (2015). Baseline goblet cell mucin secretion in the airways exceeds stimulated secretion over extended time periods, and is sensitive to shear stress and intracellular mucin stores. *PLoS One*, *10*(5), e0127267.